AD

USAAVLABS TECHNICAL REPORT 67-10

DYNAGYRO - A MECHANICAL STABILITY AUGMENTATION SYSTEM FOR HELICOPTERS

By

M. George
E. Kisielowski
A. A. Perlmutter

March 1967

U. S. ARMY AVIATION MATERIEL LABORATORIES
FORT EUSTIS, VIRGINIA

CONTRACT DA 44-177-AMC-286(T)
DYNASCIENCES CORPORATION
BLUE BELL, PENNSYLVANIA

Disclaimers

The findings in this report are not to be construed as an official Department of the Army position unless so designated by other authorized documents.

When Government drawings, specifications, or other data are used for any purpose other than in connection with a definitely related Government procurement operation, the United States Government thereby incurs no responsibility nor any obligation whatsoever; and the fact that the Government may have formulated, furnished, or in any way supplied the said drawings, specifications, or other data is not to be regarded by implication or otherwise as in any manner licensing the holder or any other person or corporation, or conveying any rights or permission, to manufacture, use, or sell any patented invention that may in any way be related thereto.

Trade names cited in this report do not constitute an official endorsement or approval of the use of such commercial hardware or software.

Disposition Instructions

Destroy this report when no longer needed. Do not return it to originator.

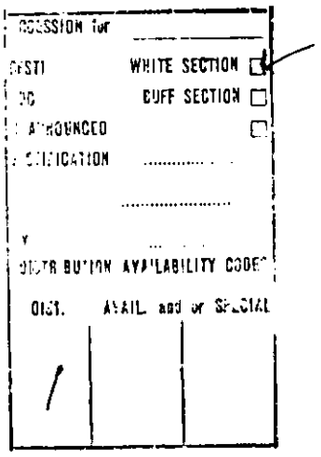

ERRATA

USAAVLABS TECHNICAL REPORT 67-10

DYNAGYRO - A MECHANICAL STABILITY AUGMENTATION SYSTEM FOR HELICOPTERS

Dynasciences Corporation
Contract DA 44-177-AMC-286(T)

Page 8, Equation 22 - Change to read:

$$\dot{B}_{1_S} = -B_{1_S}\left(0.5 + 56.2|B_{1_S}|\right) + k_1\dot{\theta}$$

Page 9, Equation 27 - Change to read:

$$\dot{A}_{1_S} = -A_{1_S}\left(0.5 + 56.2|A_{1_S}|\right) - k_2\dot{\phi}$$

Page 114, Figure 57, Test No. 19 - Change "N = 2685 grams" to "N = 2865 grams"

DEPARTMENT OF THE ARMY
U. S. ARMY AVIATION MATERIEL LABORATORIES
FORT EUSTIS, VIRGINIA 23604

This report has been reviewed by the U. S. Army Aviation Materiel Laboratories and is considered to be technically sound. The report is published for the exchange of information and the stimulation of ideas.

Task 1F125901A13905
Contract DA 44-177-AMC-286(T)
USAAVLABS Technical Report 67-10
March 1967

DYNAGYRO - A MECHANICAL STABILITY AUGMENTATION SYSTEM FOR HELICOPTERS

Dynasciences Report No. DCR-221

by

M. George
E. Kisielowski
A. A. Perlmutter

Prepared by

Dynasciences Corporation
Blue Bell, Pennsylvania

for

U. S. ARMY AVIATION MATERIEL LABORATORIES
FORT EUSTIS, VIRGINIA

SUMMARY

This report presents the results of an investigation of the design and performance characteristics of a compact and lightweight stability augmentation system for helicopters. This system, known as the DYNAGYRO, consists of a two-degree-of-freedom coulomb damped gyroscope which is mounted within the helicopter fuselage. The investigation includes an analog computer study, a comprehensive component test program, and a bench test performance evaluation of a laboratory test model.

The results obtained from this investigation showed that the DYNAGYRO provides stability augmentation characteristics which compare favorably with those of the much larger and heavier rotor hub-mounted devices.

FOREWORD

A theoretical and experimental program was conducted to determine the design and performance characteristics of a compact and lightweight mechanical stability augmentation system for helicopters. This work was performed for the U. S. Army Aviation Materiel Laboratories (USAAVLABS), Fort Eustis, Virginia, under Contract DA 44-177-AMC-286(T), during the period from 26 May 1965 through 30 October 1966.

Mr. G. Fosdick was the Army technical representative. His contributions to this work are gratefully acknowledged.
The following Dynasciences Corporation personnel authored or contributed to this report:

Mr. M. George - Project Engineer
Mr. E. Kisielowski - Manager, Aerodynamics
Dr. A. A. Perlmutter - Senior Vice President
Mr. R. R. Kenworthy - Senior Design Engineer
Mr. E. Fraundorf - Aeronautical Engineer

CONTENTS

ILLUSTRATIONS

TABLES

SYMBOLS

A_{1_S}	lateral cyclic control due to stabilizer input, radians
A_{1_C}	lateral cyclic control due to pilot input, radians
B_{1_S}	longitudinal cyclic control due to stabilizer input, radians
B_{1_C}	longitudinal cyclic control due to pilot input, radians
F	vertical component of applied normal force (Figure 46), lb.
F_1	control force due to actuator motion (see Figure 30), lb.
F_2	control force due to actuator and friction block (Figure 30), lb.
G	damper flexure force (Figure 46), grams (equation 28)
g	acceleration due to gravity, ft./sec.^{2}
I_X	mass moment of inertia about X-axis, slug-ft.^{2}
I_Y	mass moment of inertia about Y-axis, slug-ft.^{2}
I_Z	mass moment of inertia about Z-axis, slug-ft.^{2}
J_1	pilot's longitudinal cyclic control authority ratio, $1-k_1$
J_2	pilot's lateral cyclic control authority ratio, $1-k_2$
K	size factor based on DYNAGYRO geometry, ft.^{2}

k_1	gyro to pilot longitudinal control authority ratio
k_2	gyro to pilot lateral control authority ratio
L_c	lateral control power, deg./sec.^{2}/in.
L_u, L_v, L_w, etc.	aircraft rolling moment derivatives with respect to the variables written as subscripts
ℓ	damper test fixture geometry (Figure 46), ft.
M_c	longitudinal aircraft control power, deg./sec.^{2}/in.
m_d	mass of each damper, slugs
M_u, M_v, M_w, etc.	aircraft pitching moment derivatives with respect to the variables written as subscripts
N	normal force acting on damper contact point at $\beta' = 0$ (Figure 46)
N_u, N_v, N_w, etc.	aircraft yawing moment derivatives with respect to the variables written as subscripts
P	counterbalance weight generating simulated "g" loading on damper test fixture (Figure 46), grams
R	gyro damping rate, radians/sec.
r	damper test fixture geometry (Figure 46), ft.
S	gyro momentum factor (equation 29)
s	damper test fixture geometry (Figure 46), ft.
$(T_x)_A$	applied control torque to gyro about X-axis, ft.-lb.

$(T_Y)_A$	applied control torque to gyro about Y-axis, ft.-lb.
$\bar{T}_{x_\beta}$	average damper restoring torque about X-axis, ft.-lb.
$\bar{T}_{Y_\delta}$	average damper restoring torque about Y-axis, ft.-lb.
$T_{1/2}$	the time to half amplitude of aircraft motion, seconds
T_2	the time to double amplitude of aircraft motion, seconds
u	aircraft perturbation velocity along the body X-axis, positive forward, ft./sec.
V	aircraft free-stream forward speed, knots
v	aircraft perturbation velocity along the body Y-axis, positive to the right, ft./sec.
W	aircraft gross weight, pounds
w	aircraft perturbation velocity along the body Z-axis, positive down, ft./sec.
X,Y,Z	aircraft and gyro axes coordinate system defined in Figure 2
X_u, X_v, etc.	aircraft longitudinal force derivatives with respect to the variables written as subscripts
Y_u, Y_v, etc.	aircraft side force derivatives with respect to the variables written as subscripts
Z_u, Z_v, etc.	aircraft normal force derivatives with respect to the variables written as subscripts
β	angle between gyro spin axis and fixed reference axis in longitudinal plane (Figure 2), radians

β'	simulated gyro displacement used during damper material evaluation, degrees
δ	angle between gyro spin axis and fixed reference axis in lateral plane (Figure 2), radians
θ	aircraft or tilt table pitch attitude (Figure 2), radians
θ_c	main rotor collective pitch control, radians
θ_{ctr}	tail rotor collective pitch control, radians
$\overline{\mu}$	time averaged coefficient of friction
μ	coefficient of friction obtained at $\beta' = 0°$
μ_β	coefficient of friction as a function of β'
ϕ	aircraft roll attitude, radians
τ_u	time constant for aircraft longitudinal velocity response, sec.
τ_v	time constant for aircraft lateral velocity response, sec.
ψ	aircraft yaw attitude, radians
Ω	gyro rotational speed, radians/sec.
ω_x	angular velocity of gyro about X-axis (Figure 2), radians/sec.
ω_y	angular velocity of gyro about Y-axis (Figure 2), radians/sec.
ω_z	angular velocity of gyro about Z-axis (Figure 2), radians/sec.

I. INTRODUCTION

All helicopters are inherently unstable in some speed regimes. Modern design practices have brought the degree of instability within the pilot's control capability, but considerations of flight safety and pilot fatigue usually dictate the need for some sort of stability augmentation. Acceptable flying characteristics can be provided through the use of either mechanical or electronic stabilization systems. Although both types of these systems are presently in common use, they have marked advantages and disadvantages.

Electronic stabilization systems can be very light in weight. Also, the inherent flexibility of electronic circuitry permits the designer to closely tailor the system characteristics to the requirements of the helicopter or, if desired, to provide for the execution of pre-programmed maneuvers. On the other hand, the electronic system is highly complex and costly to produce, requires extensive maintenance by highly skilled personnel, and is relatively low in reliability.

Mechanical stabilization systems of the type utilized by Bell, Hiller, and Lockheed rely on a gyroscope to sense the attitude deviation rate of the helicopter and to provide stabilizing signal inputs to the helicopter control system. The gyroscope motion is damped by viscous or aerodynamic dampers which provide a restoring torque that continuously seeks to align the gyroscope axis with a fixed reference axis in the helicopter. The mechanical stabilization systems in current use require very little maintenance and are highly reliable, but they are heavy as compared to electronic systems.

It would, of course, be desirable to provide a stabilizing system that possesses the lightweight characteristics of current electronic systems and the high reliability characteristics of current mechanical systems. To achieve this, attempts have been made to reduce the size of the mechanical system. Previous attempts have not been fruitful for a two-degree-of-freedom system because of the problems encountered in providing either viscous or aerodynamic

dampers that possess damping characteristics compatible with the requirements of miniaturized mechanical gyros. Hence, the damper problem has been the primary stumbling block in attempts to miniaturize mechanical stabilizers.

The Dynasciences Corporation recently developed a stabilized Image Motion Compensator (DYNALENS) which utilized a coulomb damped and miniaturized gyroscope. As a result of this work, it was established that the same damping principle could also be applied to a stability augmentation device for helicopters.

In the present program, a bench test model of a coulomb damped gyroscopic stability augmentation system (DYNAGYRO) was constructed and its performance characteristics were evaluated.

II. DYNAGYRO CONCEPT

The DYNAGYRO, shown in Figure 1, consists of a gyroscope spinning at high rotational speeds. Within the gyro mass, and rotating with it, are friction dampers which are hinged to a rotating but nontilting reference plane. Any tilting of the gyro mass results in a friction force between the dampers and the gyro mass. This friction force causes a restoring torque which tends to return the gyro to its original equilibrium position. The gyro tilt results in a motion of control linkages which actuate the aircraft control through a hydraulic boost system. The control motion thus transmitted corresponds to a lagged rate feedback signal. Both pitch and roll stability augmentation is thus achieved. The DYNAGYRO control input is in series with the pilot input but utilizes only a small percentage of the total control travel available to the pilot. This ratio of gyro to pilot authority is dictated by the specific aircraft and is generally less than 30 percent.

The DYNAGYRO can be powered electrically, hydraulically, or by a direct drive from the aircraft transmission.

III. THEORETICAL ANALYSIS

Equations of motion for a frictionally damped gyroscope were derived, and the gyroscope's stability augmentation characteristics were determined for a typical helicopter by analog computer analysis.

A. DYNAGYRO EQUATIONS OF MOTION

The DYNAGYRO equations of motion are derived by equating the applied control and friction torques to the inertia torques about the DYNAGYRO longitudinal and lateral axes, respectively. Thus, using Reference 1, the DYNAGYRO equations of motion can be expressed as follows:

$$(T_X)_A + \bar{T}_{X\beta} = I_X \dot{\omega}_X + I_Z \omega_Z \omega_Y \tag{1}$$

$$(T_Y)_A + \bar{T}_{Y\delta} = I_Y \dot{\omega}_Y - I_Z \omega_Z \omega_X \tag{2}$$

From Figure 2, the angular velocities about the X and Y axes are obtained as follows:

$$\omega_X = -(\dot{\phi} - \dot{\delta}) \tag{3}$$

$$\omega_Y = -(\dot{\theta} - \dot{\beta}) \tag{4}$$

By substituting equations (3) and (4) into equations (1) and (2) and denoting the gyro spin velocity ω_Z as Ω, there results

$$(T_X)_A + \bar{T}_{X\beta} = -I_X(\ddot{\phi} - \ddot{\delta}) - I_Z \Omega(\dot{\theta} - \dot{\beta}) \tag{5}$$

$$(T_Y)_A + \bar{T}_{Y\delta} = -I_Y(\ddot{\theta} - \ddot{\beta}) + I_Z\Omega(\dot{\phi} - \dot{\delta}) \tag{6}$$

For a hydraulically boosted control system, the control torques $(T_X)_A$ and $(T_Y)_A$ are much smaller than the inertia torques and therefore can be neglected. The average values of the DYNAGYRO restoring friction torques $\bar{T}_{X\beta}$ and $\bar{T}_{Y\delta}$ can be expressed as follows:

$$\bar{T}_{X\beta} = -K\Omega^2\mu m_d \frac{\beta}{|\beta|} \tag{7}$$

$$\bar{T}_{Y\delta} = -K\Omega^2\mu m_d \frac{\delta}{|\delta|} \tag{8}$$

where K is a function of the DYNAGYRO geometry.

By substituting equations (7) and (8) into equations (5) and (6) and neglecting also the generally small acceleration terms, the DYNAGYRO equations of motion can be expressed as follows:

$$K\Omega^2\mu m_d \frac{\beta}{|\beta|} = I_Z\Omega(\dot{\theta} - \dot{\beta}) \tag{9}$$

$$K\Omega^2\mu m_d \frac{\delta}{|\delta|} = -I_Z\Omega(\dot{\phi} - \dot{\delta}) \tag{10}$$

By simplifying equations (9) and (10), there results

$$\dot{\beta} = \dot{\theta} - R\frac{\beta}{|\beta|} \tag{11}$$

$$\dot{\delta} = \dot{\phi} + R \frac{\delta}{|\delta|} \tag{12}$$

where R is defined as the gyro damping rate and is given by

$$R = \frac{K\Omega\mu m_d}{I_z} \tag{13}$$

Examination of equations (11) and (12) shows that, unlike a viscous damped gyro, the DYNAGYRO motion is independent of the gyro amplitude. Its angular tilt rates $\dot{\beta}$ or $\dot{\delta}$ are dependent only on the tilt direction and the damping or return rate, R. This rate, R, is the most important criterion of the DYNAGYRO design and is a function of the DYNAGYRO geometry, damper material friction coefficient, damper mass, and gyro spin velocity. It can be further noted from equation (13) that if a variable speed control is incorporated in the DYNAGYRO design system, the DYNAGYRO can provide a variable return rate and, therefore, variable stability augmentation.

The gyro is connected through linkages to the longitudinal and lateral cyclic control system. The equivalent control motion thus introduced is related to the gyro tilt angles as follows:

$$B_{1_S} = k_1 \beta \tag{14}$$

$$A_{1_S} = -k_2 \delta \tag{15}$$

where k_1 and k_2 are the gyro to pilot authority ratios for longitudinal and lateral cyclic control, respectively. Substitution of equations (14) and (15) into equations (11) and (12) results in

$$\dot{B}_{1_S} = -k_1 R \frac{B_{1_S}}{|B_{1_S}|} + k_1 \dot{\theta} \tag{16}$$

$$\dot{A}_{1_S} = -k_2 R \frac{A_{1_S}}{|A_{1_S}|} - k_2 \dot{\phi} \tag{17}$$

B. ANALOG COMPUTER ANALYSIS

The effect of the DYNAGYRO stability augmentation characteristics on a helicopter response was evaluated using an analog computer simulation program. This program was tailored to the UH-1B helicopter (with and without the Bell Bar) and was performed utilizing an Electronic Associates Analog Computer Model 231-R. The analysis involved two degrees of freedom of the DYNAGYRO equations of motion and six degrees of freedom of the aircraft motion (obtained from Reference 2). The Bell Bar equations of motions were also programmed for the purpose of comparing the aircraft response with the DYNAGYRO and the Bell Bar. The equations used in the analog simulation program are as follows:

Longitudinal Force Equation

$$X_u u + X_{\dot{u}} \dot{u} + X_v v + X_w w + X_\theta \theta + X_{\dot{\theta}} \dot{\theta} + X_{\dot{\phi}} \dot{\phi} + X_{\dot{\psi}} \dot{\psi} + J_1 X_{B_{1_C}} B_{1_C} + J_2 X_{A_{1_C}} A_{1_C} + X_{B_{1_S}} B_{1_S} = 0 \tag{18}$$

Vertical Force Equation

$$Z_u u + Z_v v + Z_w w + Z_{\dot{w}} \dot{w} + Z_\theta \theta + Z_{\dot{\theta}} \dot{\theta} + Z_{\dot{\phi}} \dot{\phi} + Z_{\dot{\psi}} \dot{\psi} + J_1 Z_{B_{1_C}} B_{1_C} + J_2 Z_{A_{1_C}} A_{1_C} + Z_{B_{1_S}} B_{1_S} = 0 \tag{19}$$

Pitching Moment Equation

$$M_u u + M_v v + M_w w + M_{\dot{\theta}} \dot{\theta} + M_{\ddot{\theta}} \ddot{\theta} + M_{\dot{\phi}} \dot{\phi} + M_{\dot{\psi}} \dot{\psi} +$$

$$J_1 M_{B_{1_c}} B_{1_c} + J_2 M_{A_{1_c}} A_{1_c} + M_{B_{1_s}} B_{1_s} = 0 \qquad (20)$$

DYNAGYRO Equation in Pitch

$$\dot{B}_{1_s} = -k_1 R \frac{B_{1_s}}{|B_{1_s}|} + k_1 \dot{\theta} \qquad (21)$$

Bell Bar Equation in Pitch

$$\dot{B}_{1_s} = -B_{1_s} (0.5 + 56.2\, B_{1_s}) + k_1 \dot{\theta} \qquad (22)$$

Side Force Equation

$$Y_u u + Y_v v + Y_{\dot{v}} \dot{v} + Y_w w + Y_{\dot{\theta}} \dot{\theta} + Y_{\phi} \phi + Y_{\dot{\phi}} \dot{\phi} +$$

$$Y_{\psi} \psi + Y_{\dot{\psi}} \dot{\psi} + J_1 Y_{B_{1_c}} B_{1_c} + J_2 Y_{A_{1_c}} A_{1_c} + Y_{A_{1_s}} A_{1_s} = 0 \qquad (23)$$

Rolling Moment Equation

$$L_u u + L_v v + L_w w + L_{\dot{\theta}} \dot{\theta} + L_{\dot{\phi}} \dot{\phi} + L_{\ddot{\phi}} \ddot{\phi} + L_{\dot{\psi}} \dot{\psi} +$$

$$L_{\ddot{\psi}} \ddot{\psi} + J_1 L_{B_{1_c}} B_{1_c} + J_2 L_{A_{1_c}} A_{1_c} + L_{A_{1_s}} A_{1_s} = 0 \qquad (24)$$

Yawing Moment Equation

$$N_u u + N_v v + N_w w + N_{\dot{\theta}}\dot{\theta} + N_{\dot{\phi}}\dot{\phi} + N_{\ddot{\phi}}\ddot{\phi} + N_{\dot{\psi}}\dot{\psi} +$$

$$N_{\ddot{\psi}}\ddot{\psi} + J_1 N_{B_{1_C}} B_{1_C} + J_2 N_{A_{1_C}} A_{1_C} + N_{A_{1_S}} A_{1_S} = 0 \qquad (25)$$

DYNAGYRO Equation in Roll

$$\dot{A}_{1_S} = -k_2 R \frac{A_{1_S}}{|A_{1_S}|} - k_2 \dot{\phi} \qquad (26)$$

Bell Bar Equation in Roll

$$\dot{A}_{1_S} = -A_{1_S}(0.5 + 56.2 A_{1_S}) - k_2 \dot{\phi} \qquad (27)$$

The helicopter stability derivatives in the above equations were evaluated using the theoretical methods of Reference 2. The numerical values of these derivatives for the UH-1B helicopter, together with the schematic of the computer program, are presented in Appendix I.

C. ANALOG COMPUTER RESULTS

1. Comparison of Analog Computer Results With Bell Bar Versus Flight Test Data

The analog computer program was checked out by comparing the analog results for the UH-1B helicopter equipped with the Bell Bar stabilization system against the flight test data of Reference 3. This comparison is shown in Figures 3 and 4 for the helicopter longitudinal response to a control pulse and step input, respectively. It can be noted that,

although the simulated and the actual flight test operating conditions are not identical, the analog simulation results compare well with the flight test response characteristics of the UH-1B helicopter.

2. Optimization of the DYNAGYRO Stability Parameters

A parametric study was performed to determine the DYNAGYRO optimum damping rate R and the pilot control authority ratio k for the UH-1B helicopter. The results are presented in Figures 5 through 10, which show plots of the periods and damping rates of the aircraft motion versus the DYNAGYRO damping rate R for constant values of the gyro authority ratio k. The corresponding Bell Bar results are also presented in these figures.

The aircraft damping rate is expressed in terms of the reciprocal of the time to half-amplitude of the aircrafts' pitch and roll rates. Hence, neutral aircraft stability is represented by $1/T_{\frac{1}{2}} = 0$. Also, a negative increase in $1/T_{\frac{1}{2}}$ indicates an increase in aircraft stability.

Figures 5 and 6 show the aircraft hovering stability characteristics for the longitudinal and lateral modes, respectively. Similar results are presented in Figures 7 and 8 and in Figures 9 and 10 for forward flight conditions at 44 knots and 88 knots, respectively.

From the above figures, it can be noted that the DYNAGYRO with appropriate damping rates and authority ratios provides stability augmentation characteristics which compare favorably with those of the Bell Bar. Examining the effects of damping rate R and authority ratios k on aircraft damping $(1/T_{\frac{1}{2}})$, the above figures indicate that, in general, for any constant value of R, the aircraft damping increases with an increase of the authority ratio k. However, excessive values of k (greater than 0.15) result in reduced control response, and therefore a compromise must be made between aircraft damping and control effectiveness. Also, for constant values of k, the increase in the aircraft damping $(1/T_{\frac{1}{2}})$ for values of $0.005 < R < 0.015$ is generally

insignificant. Therefore, the DYNAGYRO damping rate of $R = 0.005$ and the authority ratio of $k = 0.15$ were selected as optimum values for the conditions analyzed. The corresponding time histories of the aircraft motion are discussed below.

3. Aircraft Response Characteristics

The response characteristics of the UH-1B helicopter equipped with the DYNAGYRO (dotted lines) and the Bell Bar (solid lines) are shown in Figures 11 through 16 for the three speed conditions considered. These results were obtained with a gyro authority ratio $k = 0.15$ and the damping rate $R = 0.005$.

Figures 11 and 12 show the hovering response for the aircraft longitudinal and lateral modes due to a stick pulse disturbance B_{1_C} and A_{1_C}, respectively. The corresponding stabilizer response (B_{1_S} and A_{1_S}) for the DYNAGYRO and the Bell Bar is also presented.

Similar results are presented in Figures 13 and 14 and in Figures 15 and 16 for forward flight conditions of 44 knots and 88 knots, respectively.

By examining these figures, it can be noted that the DYNAGYRO equipped UH-1B helicopter exhibits stability characteristics which are substantially similar to those of the UH-1B with the Bell Bar.

D. HANDLING QUALITIES

In addition to the aircraft time history responses due to pulse control inputs discussed above, analog computer simulations were performed for control step inputs to determine the handling qualities of the aircraft equipped with the DYNAGYRO and the Bell Bar.

While the handling qualities required for VTOL aircraft are subject to considerable controversy at the present time, it was decided to use the data from References 4 and 5 for evaluating the stabilization system design parameters. The criteria on damping of Reference 4, shown here in Figures

17 and 18, are obtained from pilot's opinion data from a fixed-base simulator study. From Figure 17, the minimum aircraft damping ($1/T_{\frac{1}{2}}$) required to provide satisfactory damping requirements for the UH-1B helicopter in the longitudinal mode is 0.23. For the lateral case, as shown in Figure 18, the corresponding value is 0.38. In these figures, the points showing the aircraft damping rates obtainable with the DYNAGYRO and the Bell Bar were extracted from Figures 4 through 9. By examining the results of Figures 17 and 18, it can be seen that the aircraft damping provided by the DYNAGYRO is well within the range of the acceptable boundaries.

Since any stability augmentation system in series with the pilot control input tends to reduce the control response of the aircraft, the criteria of Reference 5 have been used to evaluate this effect. These criteria are that the control power when hovering in still air will be sufficient to produce an angular displacement of at least $45/(W + 1000)^{1/3}$ degrees in pitch at the end of 1 second, and $27/(W + 1000)^{1/3}$ in roll, at the end of 1/2 second, for 1 inch of control motion. In the above relationships, W is the maximum overload gross weight of the aircraft. The minimum requirements for hovering for the UH-1B are given in Table I, together with the optimum angles achieved from the analog response data.

In addition to the above criteria for hovering, an analysis was performed to evaluate the aircraft control response in forward flight. The results are presented in Figures 19 and 20, which show the variation of time constants for the aircraft longitudinal and lateral degrees of freedom, respectively, as a function of forward speed for constant values of the authority ratio k. These figures show a comparison of the time constants for the UH-1B helicopter equipped with the DYNAGYRO and the Bell Bar. The time constants τ_u and τ_v are herein defined as the time increments required to attain 62 percent of the new steady-state values of forward speed and side velocity after applying longitudinal and lateral control step inputs, respectively.

All of the above handling qualities criteria were used as a means of selecting the DYNAGYRO design parameters so as to achieve the best compromise between the required aircraft damping and the control sensitivity.

From the results of the above analysis, it can be concluded that the DYNAGYRO provides dynamic stability characteristics which meet the existing handling qualities criteria for the UH-1B helicopter.

IV. BENCH TEST PROGRAM

The next phase of the program consisted of an experimental study to determine the wear characteristics of various damper materials and the performance of the DYNAGYRO.

A. DAMPER MATERIAL EVALUATION

Since the most critical components of the DYNAGYRO system are the friction dampers, a complete laboratory evaluation was conducted to document fully the friction and wear characteristics of various damper materials.

Prior to the tests, a literature survey was made to determine the state of the art on friction materials. Although no data were found to be directly applicable to the operating conditions of the DYNAGYRO, References such as 6, 7, and 8 provided some information on testing procedures previously utilized and served as a basis for preliminary material selection. Ten different material combinations and two damper rod sizes were finally selected for evaluation. These are listed in Table II. This evaluation included the determination of the effects on wear and friction coefficients of variables such as

Damper normal force

Contact pressure

Simulated gyro displacement, β'

Simulated gyro rotational speed

Ambient temperature

The objective of this evaluation was to select materials exhibiting very low wear rates and friction coefficients that were insensitive to the variables listed above.

A description of the test program and a summary of the final results are presented below.

1. Description of Test Program

a. Test Apparatus

A photograph and a detailed sketch of the equipment used for these tests are shown in Figures 21 and 22, respectively. The test apparatus essentially consisted of a stationary damper rod with provisions for "g" load simulation by a counter-balance scale arrangement. Relative motion between rod and gyro was simulated by a flat track pivoting about a radius representative of the actual DYNAGYRO design. The track was driven by eccentric cams powered by an electric motor. Different cams provided variation in maximum simulated gyro displacement from $\pm 3.8°$ to $\pm 15.2°$.

A photograph of a sample rod and track specimen is given in Figure 23. The simulated damper rods consisted of a 1/16-inch-square rod specimen bonded to a thermoplastic base. The plastic base was used to reduce heat transfer from the rod material to the support arm of the test fixture, thereby simulating the actual installation where the transfer medium is air. The nylon damper rod specimens were fabricated as a one-piece unit. The contact width of the nylon was increased to 1/8 inch in anticipation of the actual rod design, which would necessarily be larger than one of steel due to the low specific gravity of the nylon. The flat track consisted of 1/2-inch-diameter disks 0.080 inch thick.

The damper test fixture assembly was instrumented to monitor and measure the following:

(i) Damper motion
(Sanborn Position Transducer 7DCDT-500)

(ii) Damper surface velocity
(Sanborn Linear Rate Transducer LVDT6LVA8)

(iii) Damper friction force (Strain Gage Beam)

(iv) Simulated gyro rotational speed. (Strobotac)

(v) Damper rod and track wear as a function of operating time and condition, by before and after weighings of the specimens

(vi) Damper pressure (applied weight)

(vii) Operating temperature (environmental chamber instrumentation)

The output from items (i), (ii), and (iii) were monitored on a Tektronix four-channel oscilloscope, Type 564. Periodic recording of data was done by photographing the traces of the oscilloscope on Polaroid film. A typical photograph of the data thus obtained is shown in Figure 24. A 300-c.p.s. cut-off filter was used for the friction force instrumentation to eliminate the high-frequency noise of the test assembly.

b. Test Conditions

The following test conditions were evaluated:

(1) Damper "g" Load Simulation

Damper loading up to 2865 g's was simulated. Since the damper rod weight ranged between 1 and 2 grams, these loadings were obtained by applying normal loads at the contact surfaces of 875, 1885, and 2865 grams.

(2) Contact Pressure

The effect of contact pressure was determined by varying the contact surface width of the damper rod. Sizes tested were 1/16-inch- and 1/8-inch-thick rectangular rods.

(3) Simulated Gyro Displacement

Simulated gyro displacements from ±3.8° to a maximum of ±15.2° were tested in the following cycling procedure:

±3.8° (75% of test period)

±7.6° (15% of test period)

±15.2° (10% of test period)

(4) Simulated Gyro Rotational Speed

The gyro rotational speeds simulated for these tests were 2000 and 3000 r.p.m.

(5) Ambient Temperature

Two material combinations which demonstrated the best friction characteristics under 70°F temperature conditions were further tested at temperatures of -55°F and 150°F.

c. Test Procedure

The test cycles performed are presented in Table III for the 70°F temperature tests and Table IV for the -55°F and 150°F tests. Each type of damper material combination was tested up to a maximum of 100 hours at 70°F. Selected materials were also tested at -55°F and 150°F for an additional 45 hours at each temperature. One test cycle consisted of runs for a specified period of time at each of three gyro simulated angles for a given normal load, gyro speed, and temperature. A new damper rod and a new track set were used for each test cycle.

d. Data Reduction

A detailed description of the data reduction and analysis utilized for this test program is given in Appendix II. Briefly, the two parameters of interest are the friction coefficient and the wear rates of each specimen.

(1) Friction Coefficient

The friction coefficient was obtained from the periodic recording of damper parameters (see Figure 24). The damper force G shown in Figure 24 is a summation of all horizontal forces. It consists of the friction force and the normal force component and is expressed as

$$G = F\mu - F\tan\beta' \qquad (28)$$

By measuring the damper force at β' of zero, the friction force and the corresponding friction coefficient are obtained for a given normal force F.

(2) Wear Rates

The specimen wear rates were determined by weighing before and after each test. The resulting material loss was converted to volumetric values using the appropriate density of each material and was presented as a wear rate in terms of the inches of travel between damper rod and track. It should be noted that all wear rate data are cumulative for each test and assume linear wear with time.

2. Summary of Damper Material Test Results

The complete details of the damper material results are given in Appendix II. A summary of these results is presented below.

All materials listed in Table II were tested in accordance with the procedure described previously. Typical wear and friction coefficients obtained for these materials are also given in Table II. As may be noted, several combinations exhibited very poor friction characteristics. These materials were eliminated early in the test program. Only two material combinations survived the complete evaluation program. These were the nylon rod on Oilite track, and the steel rod on Oilite track. The results obtained for these two material combinations are discussed below.

a. Damper Material Wear Rates

The wear rates of nylon on Oilite and steel on Oilite are presented in Figures 25 and 26, respectively. The wear rates, presented in cubic centimeters of material lost per inch of travel, are shown as a function of normal load applied to the damper rod. The data also include the effect of temperature and simulated gyro speed. Figure 25 shows that the wear rate of the nylon damper rod only slightly increases with an increase in the normal load, whereas it increases significantly with an increase in temperature. The high temperature data also show that an increase of simulated gyro speed increases the wear rate. Gyro speed, however, does not appear to affect the -65°F or 70°F temperature data. The Oilite track wear data show relative insensitivity to all variables with the exception of -65°F temperature and low gyro speed.

The steel on Oilite data, shown in Figure 26, indicate that the wear rate of the Oilite track is approximately ten times greater than the corresponding wear rate of the Oilite track for the nylon on Oilite combination. The wear also increases

radically with normal load at 70°F. In fact, during tests at 2.84 kilograms normal load, the test specimens seized. This resulted in failure of the force measuring instrumentation. It can be noted from Table II that the steel rod for this damper material combination had no appreciable wear.

In conclusion, the nylon on Oilite material was found to be the only combination which gave acceptable results for all conditions tested. By extrapolating the present test data, it is estimated that 1000 hours of operation would result in a damper material loss of 3.3 percent of the total damper weight of a practical DYNAGYRO damper design.

b. Damper Material Friction Coefficients

The complete friction coefficient data obtained during these tests are presented in Appendix II. These results are plotted versus cumulative inches of motion between the damper rod and track. As such, the data give an indication of the variation of friction coefficient with time. A typical time history of the nylon on Oilite material combination is given in Figure 27. From these data, a time-averaged friction coefficient was extracted; the results are presented in Figure 28. It can be noted from this figure that both damper rod materials, nylon on Oilite and steel on Oilite, exhibit a slight reduction in friction coefficient with an increase in normal load. However, the nylon on Oilite combination (Figure 28-a) shows a significant reduction of friction coefficient with an increase in temperature at low simulated gyro r.p.m. On the other hand, at high gyro rotational speed, this friction coefficient is practically independent of temperature. The steel on Oilite combination (Figure 28-b) shows an overall increase in friction coefficient over that of the nylon on Oilite. However, in contrast to nylon on Oilite characteristics, friction coefficient of this material is unaffected by temperature or simulated gyro r.p.m.

In conclusion, by evaluating both the wear and friction coefficients of both materials tested, the nylon on Oilite material combination was found to be the best possible combination of those evaluated. This combination was therefore used for the DYNAGYRO design.

B. DYNAGYRO PERFORMANCE EVALUATION

This part of the test program was conducted to determine the performance characteristics of the DYNAGYRO system under simulated aircraft operating conditions. Specifically, the test program was performed to evaluate the effects of the following design and operational parameters on the gyro damping rate:

Gyro mass moment of inertia

Gyro rotational speed

Actuator control force

Ambient temperature

Tilt table amplitude

1. Description of Test Program

a. Test Apparatus

The test equipment used for this program, as shown in Figure 29, consisted of the following components.

(1) The DYNAGYRO Model

The laboratory test model of the DYNAGYRO used for these tests is shown in Figure 1. The model was constructed so as to facilitate the use of different gyro masses and dampers. Two masses were tested corresponding to gyro moments of inertia of 0.0305 and 0.061 slug-feet^2, respectively. For each gyro moment of inertia, appropriate damper rod weights were used so as to maintain a constant gyro damping

rate as a function of gyro r.p.m. for each condition. Specifically, the damper rod weight for the lower gyro moment of inertia was 1.12 grams and that for the higher gyro moment of inertia was 1.8 grams.

The two damper materials chosen for the tests consisted of plain monocast nylon, and monocast nylon impregnated with 2 percent molybdenum disulphide (MoS_2), both operating on Oilite tracks. Both of these damper materials finally selected exhibited low wear characteristics with friction coefficients relatively unaffected by the test variables such as temperature, contact pressure, and surface velocity.

(2) Tilt Table

The DYNAGYRO was mounted on a tilt table which was used to simulate aircraft motion. Pulse, step, and sinusoidal motions of a maximum amplitude of $\pm 20°$ about one axis could be simulated. The table was driven by a hydraulic servo actuator which in turn was controlled by a function generator, Exact Electronics Inc. Model 301. The dynamics of the table for step excitations had a rise time of 0.15 second. For sinusoidal excitations, the table frequency up to 1.0 cycle per second was maintained without excessive table vibrations.

(3) Stick Boost Actuator

In order to obtain realistic control forces, the gyro control output was connected by a series of control linkages to a stick boost actuator. These linkages translated the angular gyro motions to linear motions in the plane of the tilt table. The stick boost actuator, Model 114 H 5600-3, which was a mechanical hydraulic servo unit presently used for tandem-rotor helicopters, is similar to that required for an actual flightworthy

DYNAGYRO model. By the use of this actuator, the effect of the control forces on the gyro performance could be determined. In addition to the forces generated by the stick boost actuator, friction blocks were incorporated in both the pitch and roll control systems to provide for adjustable control force inputs to the gyro. The magnitudes of the control forces utilized for these tests are shown in Figure 30.

(4) Environmental Test Chamber

The environmental test chamber installation, shown in Figure 31, was used to determine the effect of temperature on the DYNAGYRO performance. The test chamber was a Standard Model TAH 36 FS, which provided a maximum temperature range from -100°F to 300°F within ±2°F tolerance. The chamber internal dimensions were 4 feet x 4 feet x 3 feet.

(5) Instrumentation

The major components of the electronic instrumentation consisted of a function generator, gyro output sensors, and an oscillograph recorder.

The output of the function generator was fed into an amplifier which provided inputs to the servo controlled actuator driving the table. Pulse, step, and sinusoidal excitations were thus generated.

The gyro output sensors (transducers), which measured gyro tilt amplitudes and rates, were mechanically coupled in parallel with the gyro control linkages. Calibration checks of these transducers were made at the beginning and the end of each test series. The force flexures, consisting of 350-ohm four-gauge bridges, measured gyro control forces and were mounted in series with the gyro control linkages.

Calibration curves of these flexures, for pitch and roll forces, are presented in Figures 32 and 33, respectively.

All sensor output signals were passed through 10-c.p.s. cut-off filter networks to eliminate extraneous high-frequency noise. The signals were amplified and subsequently were recorded on a Consolidated Electrodynamics Oscillograph Model 5-114-P3-18.

A block diagram of the DYNAGYRO test schematic is shown in Figure 34, and a detailed list of the instrumentation described above is presented in Table V.

b. Test Procedure

The overall test program consisted of recording time history response characteristics of the DYNAGYRO as affected by the variations of gyro inertia, damper materials, actuator force, and ambient temperature. The DYNAGYRO test program is presented in Table VI.

For a given gyro inertia, damper material control force, and temperature, shown in Table VI, the test cycle consisted of selecting a desired gyro r.p.m. and a tilt table maximum amplitude and applying various types of gyro excitations such as pulse, step, or sinusoidal motion. Keeping the same gyro r.p.m., this test cycle was repeated for different values of maximum tilt table amplitudes. After completion of all required gyro excitations and tilt table amplitudes, the above procedure was repeated with different gyro r.p.m. setting. The test procedure for one complete test cycle, together with the actual test conditions, is presented in Table VII. This test cycle was then repeated for different values of gyro inertia, damper materials, control force inputs, and temperature, as shown in Table VI. The corresponding gyro response characteristics were recorded on the oscillograph recording system described in Section a(5).

A total time of 25 hours was used for the completion of all the test conditions discussed above. A complete breakdown of test time for each gyro configuration is given in Table VIII.

c. Data Reduction

Typical oscillograph traces of the DYNAGYRO response to pulse, step, and sinuosidal inputs obtained using the above test procedure are shown in Figures 35 through 37. The response data to a pulse input as shown in Figure 35 were primarily obtained for visual demonstration of gyro behavior. The step response data such as presented in Figure 36 were utilized to determine the gyro damping rate R. This parameter was obtained as a time rate of change of gyro pitch attitude (i.e., trace deflection slope). The response data for a sinusoidal excitation, Figure 37, were used to determine gyro control forces, attitudes, and the degree of cross-coupling between the gyro pitch and roll motions.

The above data were reduced by measuring the trace deflections for the required parameters and multiplying these deflections by appropriate calibration scales. A typical data reduction sheet, together with the actual calibration scales (Rcal) for each channel, is presented in Table IX.

2. Test Results

The principal parameters affecting the gyro response characteristics are the gyro damping rates and the degree of cross-coupling between the gyro pitch and roll motions.

a. Damping Rate

The DYNAGYRO damping rate R is defined as the angular rate at which the gyro, after a step disturbance, returns to its equilibrium position. This damping rate is directly proportional to the restoring torque generated by the friction dampers.

Figures 38 through 43 show the variation of the DYNAGYRO damping rates as a function of gyro angular speed and include the effects of the following test variables:

Gyro wheel inertia

Damper material

Control force

Temperature

Tilt table amplitude

These figures also show a correlation between the theoretical and the experimental results. The theoretical results for each test condition considered were computed utilizing equation (13).

Figures 38 and 39 show the variation of gyro damping versus gyro rotational speed for the two damper materials, nylon and molybdenum disulfide impregnated nylon, both acting on Oilite tracks. These results were obtained for a gyro mass moment of inertia of 0.061 slug-feet^2 and include the effects of control force, amplitude of disturbance, and ambient temperature.

Comparison of Figures 38 and 39 shows that both materials exhibit similar characteristics with the exception that MoS_2 impregnated nylon yields a slight increase in damping rate over the pure nylon material. It is also noted that the damping increases with gyro rotational speed. However, the rate of increase, although constant in theory, decreases slightly with increasing r.p.m. These figures further indicate that within the experimental scatter there is no significant effect of either tilt table amplitude (represented by clusters of points at the same r.p.m.) or control force output (F_1 and F_2) on the gyro damping rate.

On the other hand, the increase in ambient temperature results in an appreciable reduction of damping rates for the test conditions considered. Specifically, in the expected operating range of gyro rotational speeds, the increase in ambient temperature from 70°F to 150°F results in a reduction of damping rate of about 28 percent. This is caused by the fact that an increase in ambient temperature results in a decrease in the damper friction coefficients, thereby reducing the gyro damping rate.

No low-temperature test data are available for this gyro inertia (i.e., 0.061 slug-feet^2). However, by extrapolating from the trends of the low inertia tests as indicated by Figures 41 and 43, it can be inferred that the gyro damping rate will remain relatively constant for the temperature range from -15°F to 70°F.

Similar results as discussed above are presented in Figures 40 to 43 for the gyro mass moment of inertia of 0.0305 slug-feet^2. Specifically, Figures 40 and 41 show the data for one damper material, nylon on Oilite, and two control forces, F_1 and F_2, respectively. The corresponding results for nylon damper material impregnated with 2 percent MoS_2 are presented in Figures 42 and 43.

Examining the above figures, it can be noted that, in general, the low inertia data exhibit similar effects of gyro r.p.m., ambient temperature, and damper material on gyro damping as obtained with the high inertia results. However, comparing Figures 38 and 39, the low inertia results indicate an appreciable increase in damping rates. This effect of gyro inertia can be explained as follows:

As mentioned previously, the damper rod weight was reduced proportionally with the gyro mass moment of inertia so as to theoretically maintain constant damping rates. The reduced damper weight, however, results in a lower normal force on the dampers and,

hence, a lower contact pressure. This reduction in normal force (as shown in Figure 28) causes an increase in damper friction coefficient and, thus, an increase in damping rate.

Therefore, as shown in Figures 40 through 43, a friction coefficient of $\mu = 0.3$ was used for the correlation of the theoretical and experimental results for low inertia data.

Also, by comparing Figures 40 and 41 or 42 and 43, it can be noted that an increase in the control force causes an appreciable increase in the gyro damping rate. This effect is primarily caused by an increase in gyroscopic coupling associated with the comparatively lower angular momentum developed by the low inertia gyro mass.

From the above, it can be concluded that the theoretical predictions are in good agreement with those experimental results for which cross-coupling was negligible.

b. Gyroscopic Coupling

The results of gyroscopic coupling due to control forces applied to the gyro are summarized in Figure 44. These data were obtained from the sinusoidal excitation tests and include the effects of the test variables previously discussed. The data are presented in nondimensional form as the percent of maximum roll to pitch coupling, $\left(\frac{\delta}{\beta}\right)_{MAX}$, versus an empirical gyro momentum factor, S, where S is defined as

$$S = \frac{I_Z \Omega \omega_Y \beta_{MAX}}{(T_Y)_{A_{MAX}}} \qquad (29)$$

This factor can also be obtained from equation (2) by neglecting the relatively small acceleration and damping terms. Hence, equation (2) for a free gyro becomes

$$(T_Y)_A = -I_Z \Omega \omega_X \tag{30}$$

For a sinusoidal torque input, the maximum gyro precession angle δ_{max} is then obtained by integration as follows:

$$\delta_{MAX} = \frac{(T_Y)_{A_{MAX}}}{I_Z \Omega \omega_Y} \tag{31}$$

Hence, the theoretical precession ratio is given by

$$\left(\frac{\delta}{\beta}\right)_{MAX} = \frac{(T_Y)_{A_{MAX}}}{I_Z \Omega \omega_Y \beta_{MAX}} = \frac{1}{S} \tag{32}$$

From Figure 44 it is seen that the experimental data correlate well with the theory. It is also noted that the coupling is not affected by the test variables.

Figure 44 can therefore be used as an effective design tool for establishing the minimum gyro angular momentum requirements for a given gyro cross-coupling ratio.

c. DYNAGYRO Mechanical Reliability

During the DYNAGYRO bench test evaluation, the DYNAGYRO's mechanical integrity was monitored continuously. Prior to each test, visual inspections were conducted to determine if any evidence of wear existed. At the completion of each damper material test series, the wear of the dampers was determined and a thorough inspection of all other gyro components was conducted. This was also repeated during the gyro mass moment of inertia changeover.

At the completion of the test program, the following observations were made:

(i) Throughout the tests, the DYNAGYRO performed satisfactorily.

(ii) No visible wear was encountered on any bearing.

(iii) The universal joint driving the articulated components of the gyro, when initially installed, had $\pm 2°$ of backlash. This increased by 20 percent after the completion of the tests.

(iv) The damper assemblies showed no measurable wear during the test program.

V. CONCLUSIONS AND RECOMMENDATIONS

1. The results of the theoretical and experimental investigation conducted in this program prove the feasibility of a mechanical stability augmentation system which is compact, lightweight, and reliable and which can be mounted within the helicopter fuselage.

2. Analog computer analyses show that the use of this system, known as the DYNAGYRO, will provide a typical helicopter with stability characteristics which meet the existing handling qualities criteria.

3. These analyses also show that the DYNAGYRO stability augmentation capabilities compare favorably with those exhibited by the much larger and heavier rotor-mounted stability augmentation devices.

4. Laboratory tests conducted with an experimental model of the DYNAGYRO show that this device possesses good structural reliability.

5. A comprehensive component test program has resulted in the selection of gyro damper materials which meet the operational requirements of this minaturized mechanical system.

6. In view of the promising results obtained from this study, it is recommended that a flight test evaluation program of the DYNAGYRO be conducted.

TABLE I

COMPARISON OF UH-1B PITCH AND ROLL ATTITUDES WITH MINIMUM REQUIREMENTS OF REFERENCE 5

Description	Pitch Attitude After 1 sec., deg.	Roll Attitude After ½ sec., deg.
Minimum Angular Displacement Due to 1-Inch Stick Motion (Reference 5)	2.2	1.32
Angular Displacement of the UH-1 with Bell Bar Due to 1-Inch Step Input	3.8	2.86
Angular Displacement of the UH-1 with DYNAGYRO After 1 Second due to 1-Inch Step Input	3.2	2.86

TABLE II

SUMMARY OF WEAR RATES AND FRICTION COEFFICIENTS OF DAMPER MATERIALS EVALUATED AT 70°F AMBIENT TEMPERATURE

Material		Simulated Gyro r.p.m.	Normal Load, gms.	Damper Rod Thickness, in.	Running Hours	Wear Rate $cm.^3/in.$ travel		Friction Coefficient, $\bar{\mu}$
Track	Damper Rod					Track	Rod	
Oilite	Nylon	2000	875	0.125	21.9	0.10×10^{-9}	0	0.22
Oilite	Steel	2000	875	0.062	21.8	0.20×10^{-9}	0	0.26
Oilite	Alum.	2000	875	0.062	24.4	0.63×10^{-9}	0	0.34
Oilite	Alum.	2000	875	0.125	23.8	0.58×10^{-9}	0.25×10^{-9}	0.45
S. Steel	Steel	2000	875	0.062	17.7	0.50×10^{-9}	4.86×10^{-9}	0.52
S. Steel	Nylon	2000	875	0.125	16.0	0	18.6×10^{-9}	0.22
S. Steel	Brass	2000	875	0.062	5.25	0	28.8×10^{-9}	0.46
Teflon	Steel	2000	2865	0.062	16.3	7.50×15^{-9}	0	0.181
*Bakelite	Steel	2000	1885	0.062	0.67	-	-	-
*KEL-F	Steel	2000	2365	0.125	0.03	-	-	-
*KEL-F	Nylon	2000	2805	0.125	0.03	-	-	-

*Materials ablated prior to test completion.

TABLE III

70°F TEMPERATURE TEST CYCLE

Normal Load, gms.	Hours						Total Hours
	3000 r.p.m. Gyro Displacement			2000 r.p.m. Gyro Displacement			
	±3.8°	±7.6°	±15.2°	±3.8°	±7.6°	±15.2°	
875	8.32	1.67	1.11	16.64	3.33	2.22	
1885	8.32	1.67	1.11	16.64	3.33	2.22	
2865	8.32	1.67	1.11	16.64	3.33	2.22	
Sub-total, Hours	25	5	3.33	50	10	6.66	100

TABLE IV

HIGH AND LOW TEMPERATURE TEST CYCLE

Normal Load, gms.	Hours						Total Hours
	3000 r.p.m. Gyro Displacement			2000 r.p.m. Gyro Displacement			
	±3.8°	±7.6°	±15.2°	±3.8°	±7.6°	±15.2°	
1885	5.62	1.12	0.75	11.25	2.25	1.5	
2865	5.62	1.12	0.75	11.25	2.25	1.5	
Sub-total, Hours	11.25	2.25	1.50	22.5	4.50	3.0	45

TABLE V

LIST OF INSTRUMENTATION

Parameter	Sensor	Method of Recording
Rate Table Position	Helipot JSP-CT-RS 20k	Oscillograph
DYNAGYRO Pitch Velocity	Sanborn 6LV2	
DYNAGYRO Pitch Position	Sanborn 7DCDT-500	
DYNAGYRO Roll Velocity	Sanborn 6LV2	
DYNAGYRO Roll Position	Sanborn 7DCDT-500	
Pitch Control Force	Strain Gage Flexure	
Roll Control Force	Strain Gage Flexure	Oscillograph
DYNAGYRO Spin Velocity	Strobotac	Visual Monitor
Ambient Temperature	Thermometer	Visual Monitor
Rate Table Frequency	Function Generator	Visual Monitor

TABLE VI
DYNAGYRO Test Program

Test No.	Gyro Inertia slug-ft.^{2}		Damper Material				Control Force		Temperature, °F		
			Nylon/Oilite		Nylon + (MoS_2)/Oilite						
	.0305	.0610	1.800 gms.	1.120 gms.	1.800 gms.	1.120 gms.	F_1	F_2	-15	70	150
1	x			x			x		x		
2	x			x			x			x	
3	x			x			x				x
4	x			x				x	x		
5	x			x				x		x	
6	x			x				x			x
7	x					x	x		x		
8	x					x	x			x	
9	x					x	x				x
10	x					x		x	x		
11	x					x		x		x	
12	x					x		x			x
13		x	x				x				
14		x	x				x			x	
15		x	x				x				x
16		x	x					x			
17		x	x					x		x	
18		x	x					x			x
19		x			x		x				
20		x			x		x			x	
21		x			x		x				x
22		x			x			x			
23		x			x			x		x	
24		x			x			x			x

TABLE VII

TYPICAL TEST CYCLE

Test Number 1

Gyro Inertia: 0.0305 slug-ft.^{2} Temperature: 70°F
Damper Material: Nylon on Oilite Control Force: F1

Gyro Speed (r.p.m.)	Table Amplitude θ°	Excitation		
		Pulse (sec.)	Step (sec.)	Sine Function (c.p.s.)
1250	4	1	10	0.2
	4			0.5
	4			1.0
	8		10	0.2
	8			0.5
	8			1.0
	12		10	0.2
	12			0.5
↓	12			1.0
2500	4	1	10	0.2
	4			0.5
	4			1.0
	8		10	0.2
	8			0.5
	8			1.0
	12		10	0.2
	12			0.5
↓	12			1.0
4000	4	1	10	0.2
	4			0.5
	4			1.0
	8		10	0.2
	8			0.5
	8			1.0
	12		10	0.2
	12			0.5
	12			1.0
↓	12			

TABLE VIII

TEST DURATION SCHEDULE

Gyro Inertia (slug-ft.^{2})	Damper Material	Test Duration
0.0610	Monocast Nylon	8 hours
0.0305	Monocast Nylon	6 hours 5 minutes
0.0610	Nylon with 2% MoS_2	4 hours 13 minutes
0.0305	Nylon with 2% MoS_2	6 hours 40 minutes

TABLE IX

TYPICAL DATA REDUCTION SHEET

Gyro Mass Inertia = 0.0610 slug-ft.^{2} Damper Material = Monocast Nylon on Oilite Temperature = 70°F

Parameter	Resistance Calibration	Test Rcal, in.	Calibration Slope	Trace Deflection	Actual Magnitude	Trace Deflection	Actual Magnitude	Trace Deflection	Actual Magnitude
Record No.	-	-	-	9475	-	9475	-	9475	-
Gyro r.p.m.	-	-	-	1210	-	1200	-	1195	-
Gyro Excitation c.p.s.	-	-	-	0.2	-	0.5	-	1.0	-
Rate Table Displacement	9.7°	±1.00	9.7°/in.	0.42 in.	4.07°	0.42 in.	4.07°	0.42 in.	4.07°
Gyro Roll Torque	3.3 in.-lb.	±1.01	3.27 in.-lb./in.	0.09 in.	0.29 in.-lb.	0.10 in.	0.33 in.-lb.	0.08 in.	0.26 in.-lb.
Gyro Pitch Position	10.25°	±.95	10.79°/in.	0.35 in.	3.77°	0.36 in.	3.88°	0.36 in.	3.88°
Gyro Pitch Torque	2.6 in.-lb.	±1.05	2.47 in.-lb./in.	0.43 in.	1.06 in.-lb.	0.49 in.	1.21 in.-lb.	0.60 in.	1.49 in.-lb.
Gyro Roll Position	10.25°	±.95	10.79°/in.	0.0 in.	0.0	0.0	0.0	0.0	0.0
Max. Gyro Pitch Rate	-	-	*	0.54 in./sec.	0.099 rad./sec.	1.18 in./sec.	0.22 rad./sec.	2.41 in./sec.	0.438 rad./sec.
Max. Gyro Roll Rate	-	-	*	0.0	0.0	0.0	0.0	0.0	0.0

* Velocity was measured from time history of gyro position.

FIGURE 1. Photograph of the DYNAGYRO Laboratory Test Model.

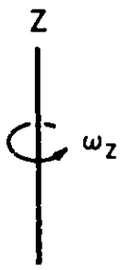

a. Gyro Axes Notation

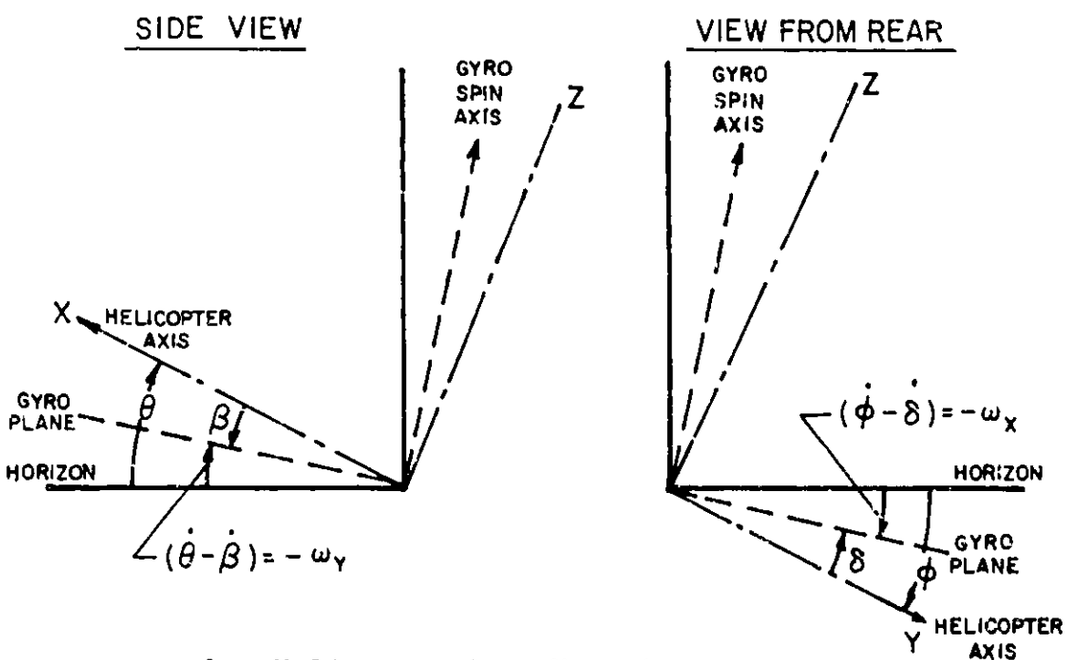

b. Helicopter Axes Notation

FIGURE 2. Definition of Axes System.

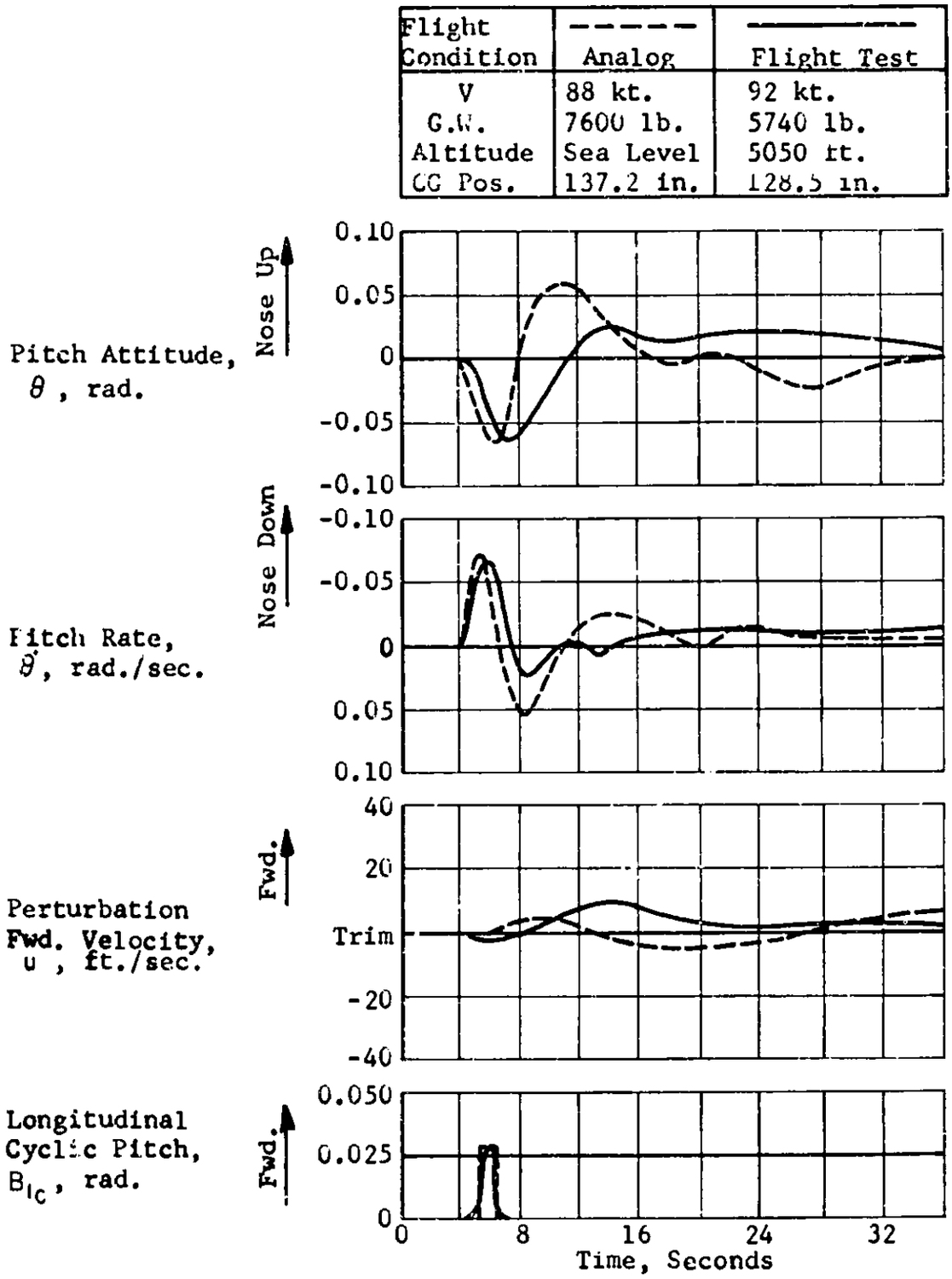

FIGURE 3. Comparison of Analog and Flight Test Results of the UH-1B Helicopter Longitudinal Response to a Control Pulse Input.

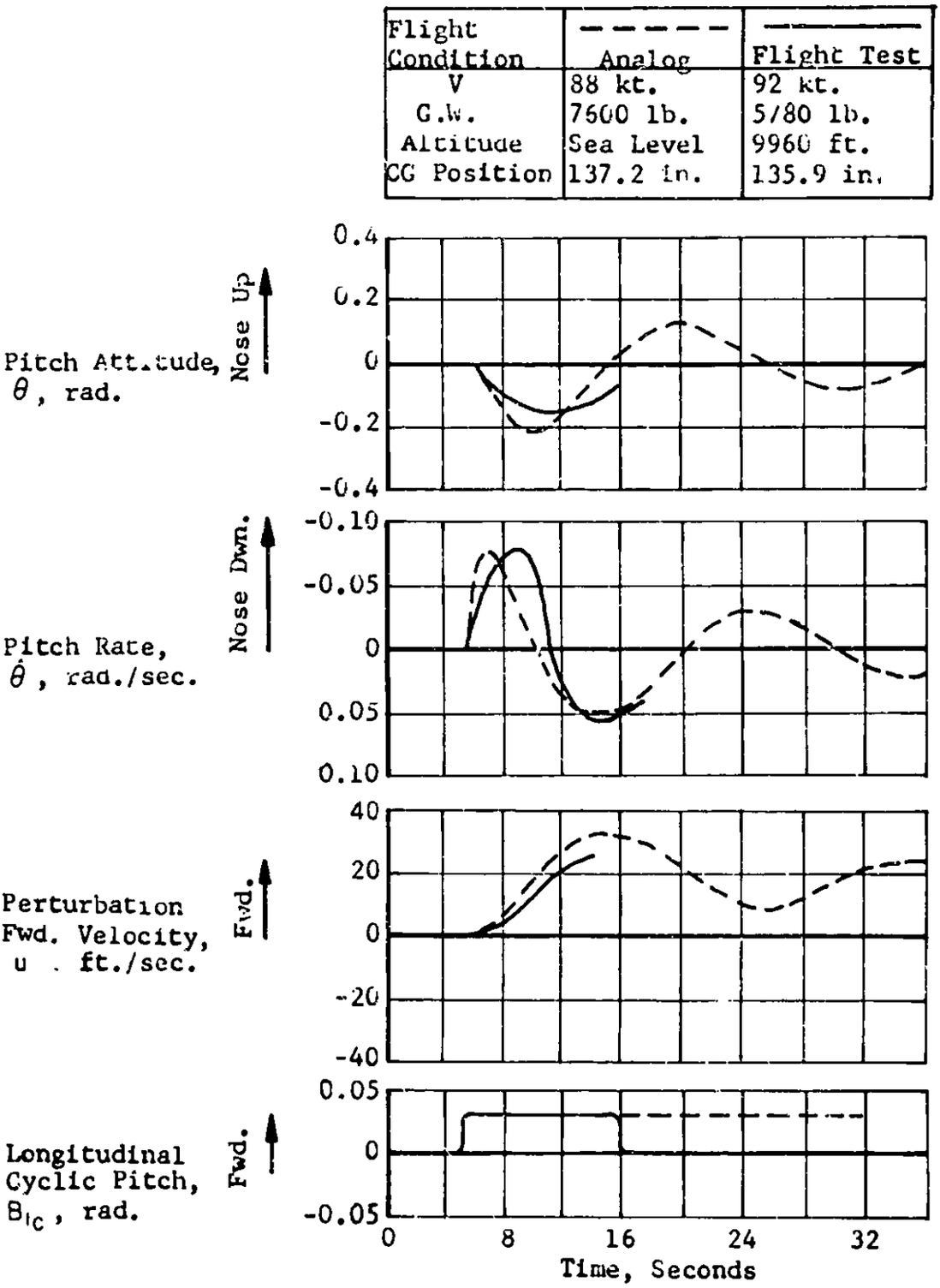

FIGURE 4. Comparison of Analog and Flight Test Results of the UH-1B Helicopter Longitudinal Response to a Control Step Input.

Symbol	k_L	Config.
○	0.05	DYNAGYRO
◇	0.10	DYNAGYRO
⬡	0.15	DYNAGYRO
------	0.16	Bell Bar

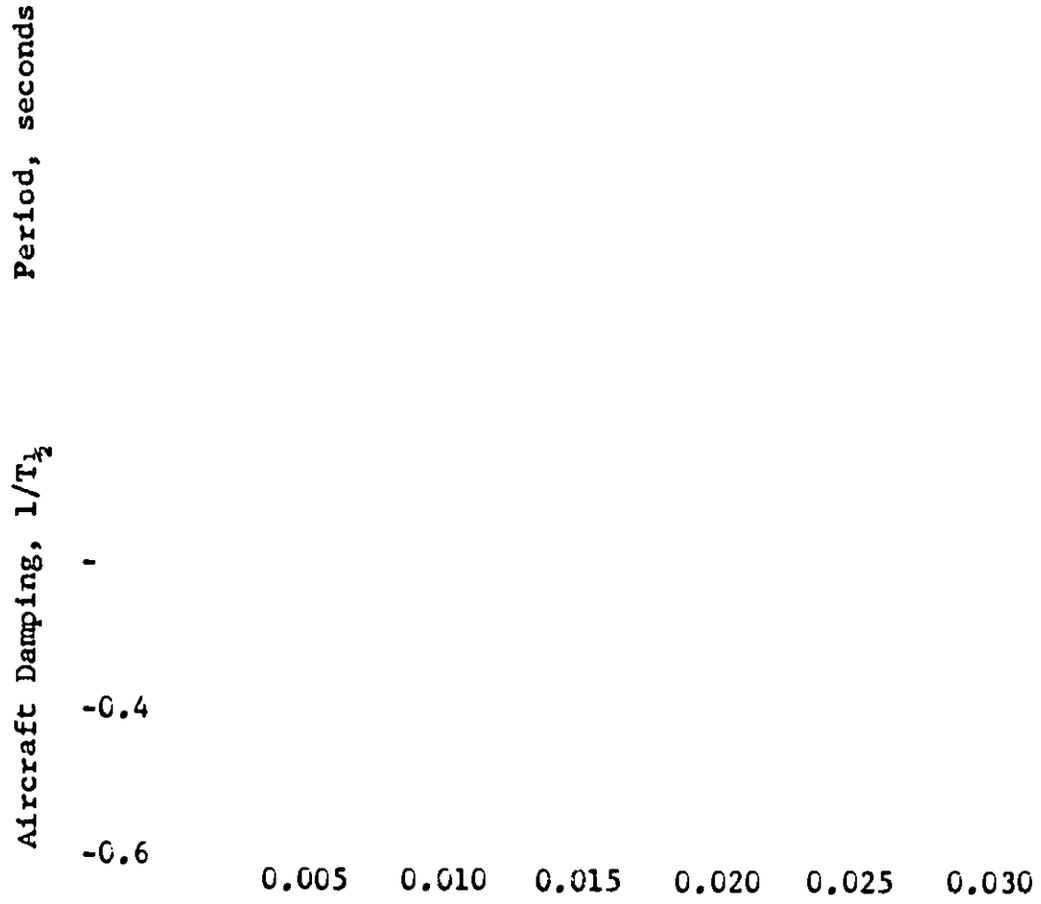

FIGURE 5. Effect of DYNAGYRO Stabilizer Parameters on the Longitudinal Dynamic Characteristics of the UH-1B Helicopter (Hover).

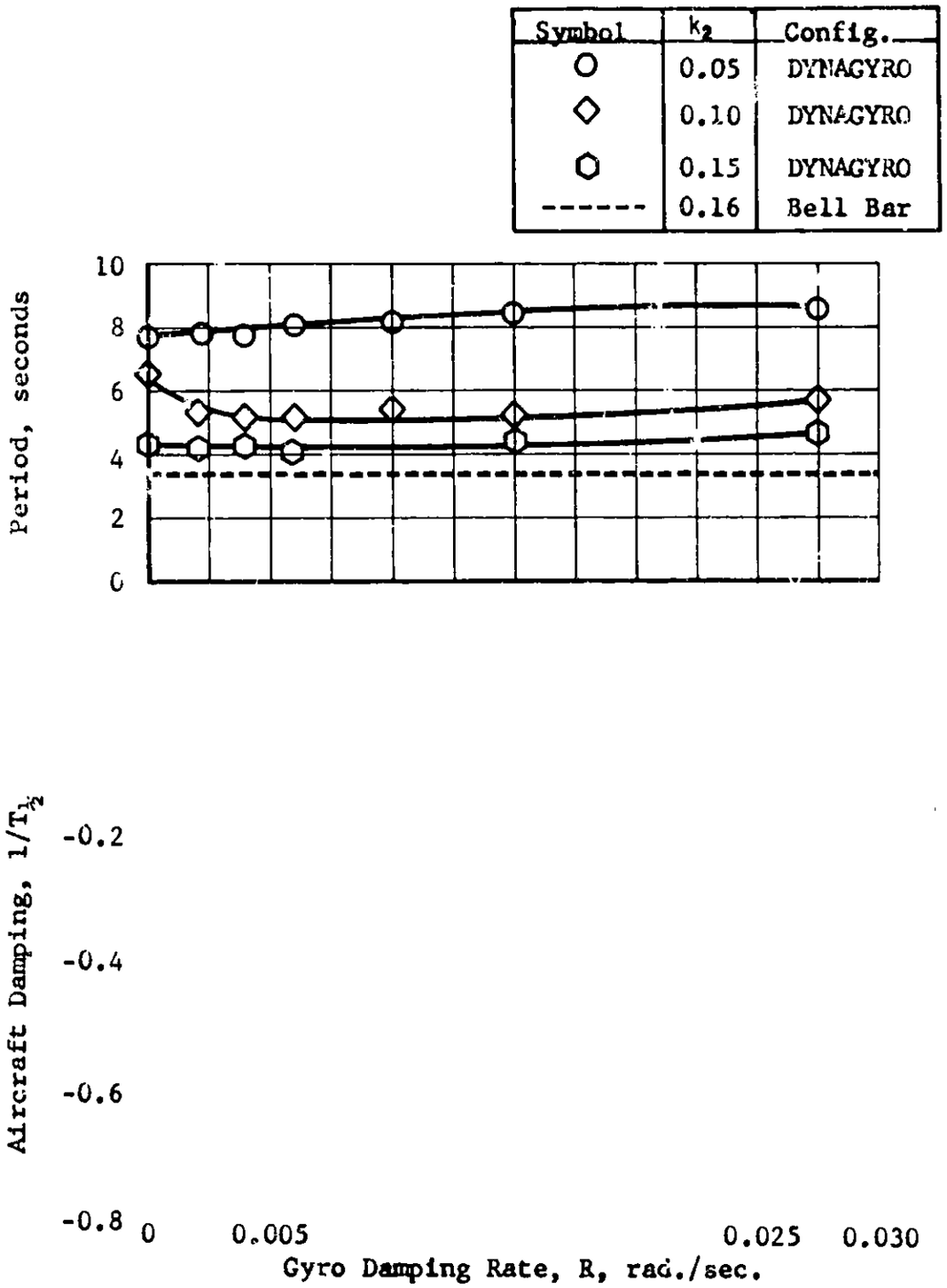

FIGURE 6. Effect of DYNAGYRO Stabilizer Parameters on the Lateral Dynamic Characteristics of the UH-1B Helicopter (Hover).

Symbol	k_1	Config.
○	0.05	DYNAGYRO
◇	0.10	DYNAGYRO
⬡	0.15	DYNAGYRO
-----	0.16	Bell Bar

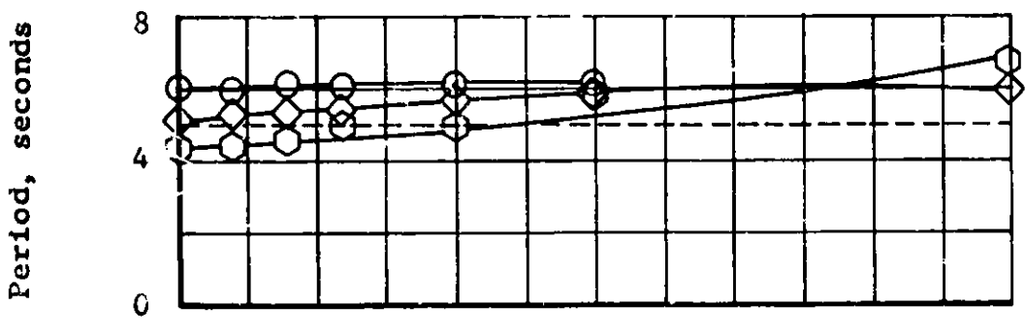

Aircraft Damping, $1/T_{\frac{1}{2}}$

0.005 0.010 0.015 0.020 0.025 0.030

Gyro Damping Rate, R, rad./sec.

FIGURE 7. Effect of DYNAGYRO Stabilizer Parameters on the Longitudinal Dynamic Characteristics of the UH-1B Helicopter (V = 44 knots).

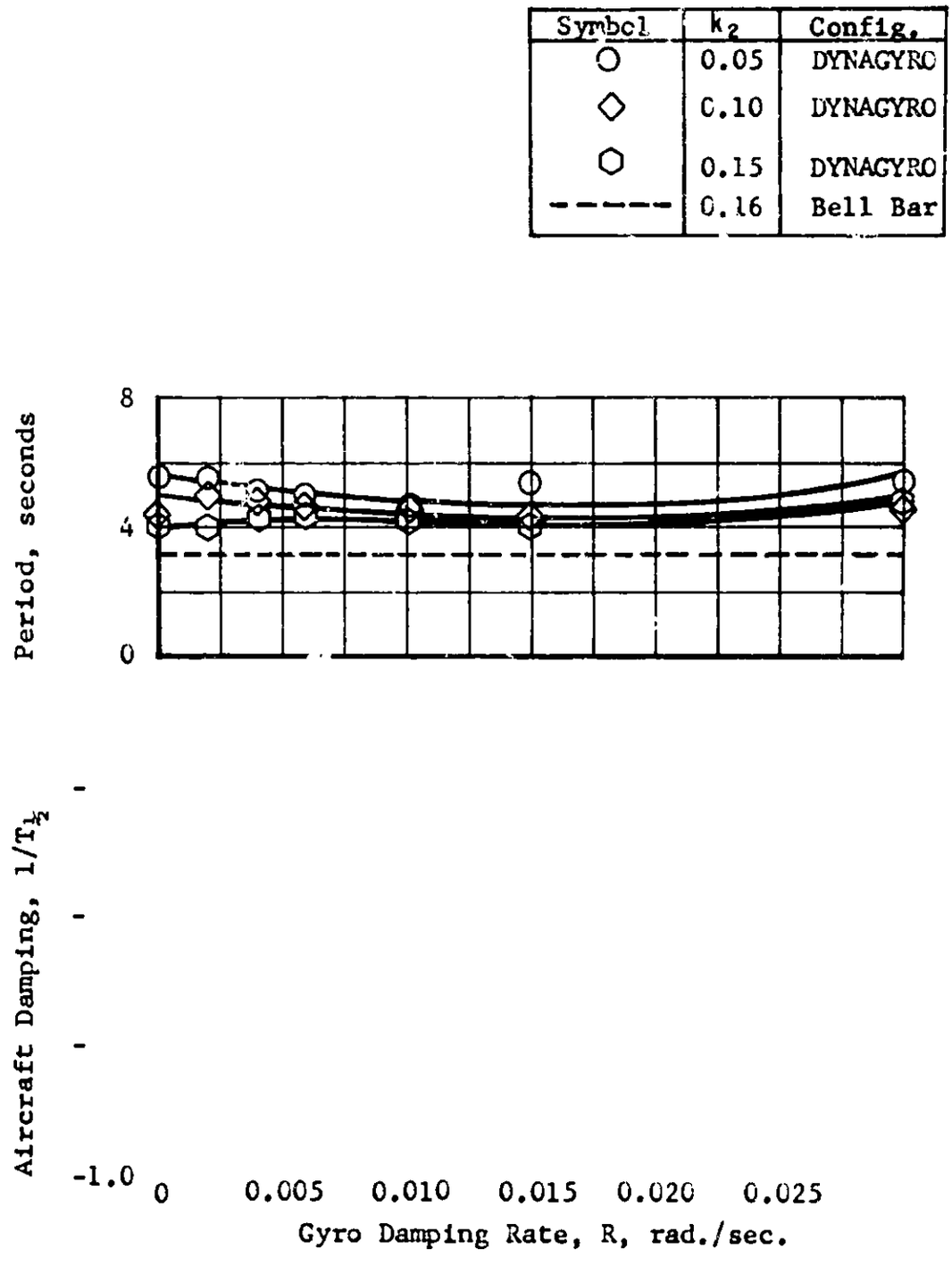

FIGURE 8. Effect of DYNAGYRO Stabilizer Parameters on the Lateral Dynamic Characteristics of the UH-1B Helicopter (V = 44 knots).

Symbol	k_I	Config.
□	0	DYNAGYRO
○	0.05	DYNAGYRO
◇	0.10	DYNAGYRO
⬡	0.15	DYNAGYRO
⬭	0.25	DYNAGYRO
— — —	0.16	Bell Bar
—·—·—	0.16	Bell Bar

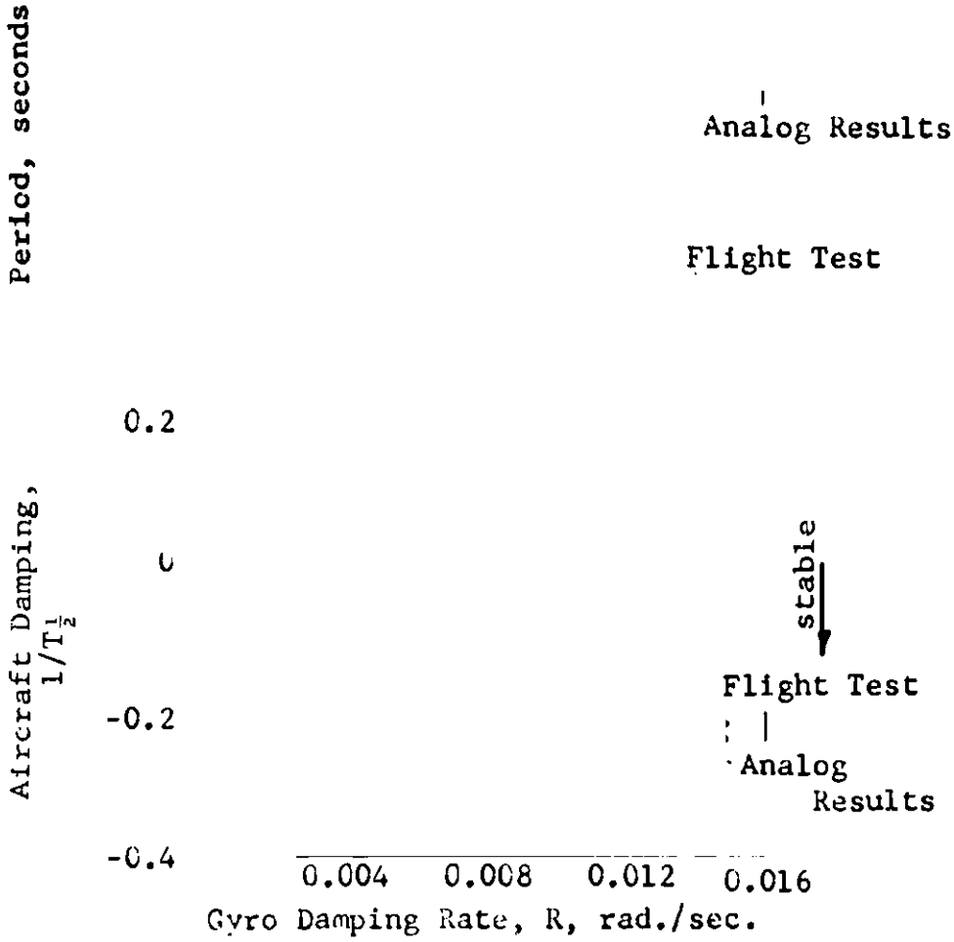

FIGURE 9. Effect of DYNAGYRO Stabilizer Parameters on the Longitudinal Dynamic Characteristics of the UH-1B Helocopter (V = 88 knots).

Symbol	k_2	Config.
○	0.05	DYNAGYRO
◇	0.10	DYNAGYRO
⬡	0.15	DYNAGYRO
———	0.16	Bell Bar

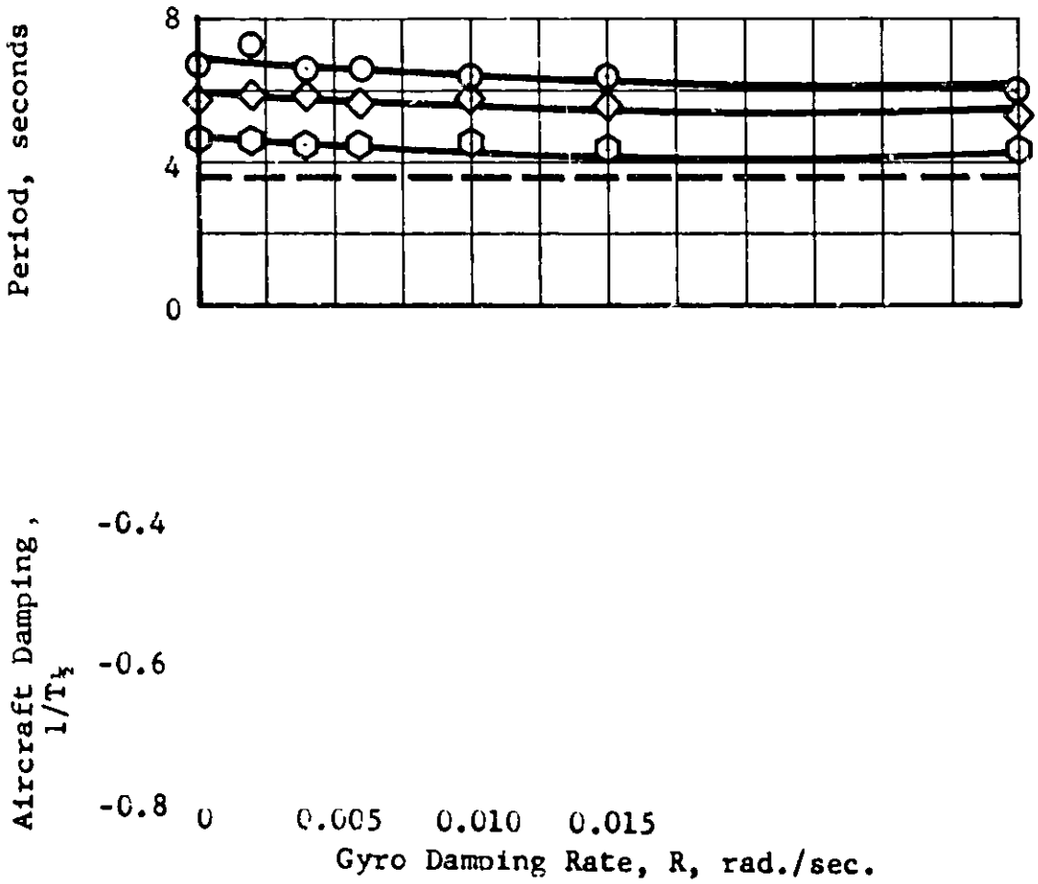

FIGURE 10. Effect of DYNAGYRO Stabilizer Parameters on the Lateral Dynamic Characteristics of the UH-1B Helicopter (V = 88 knots).

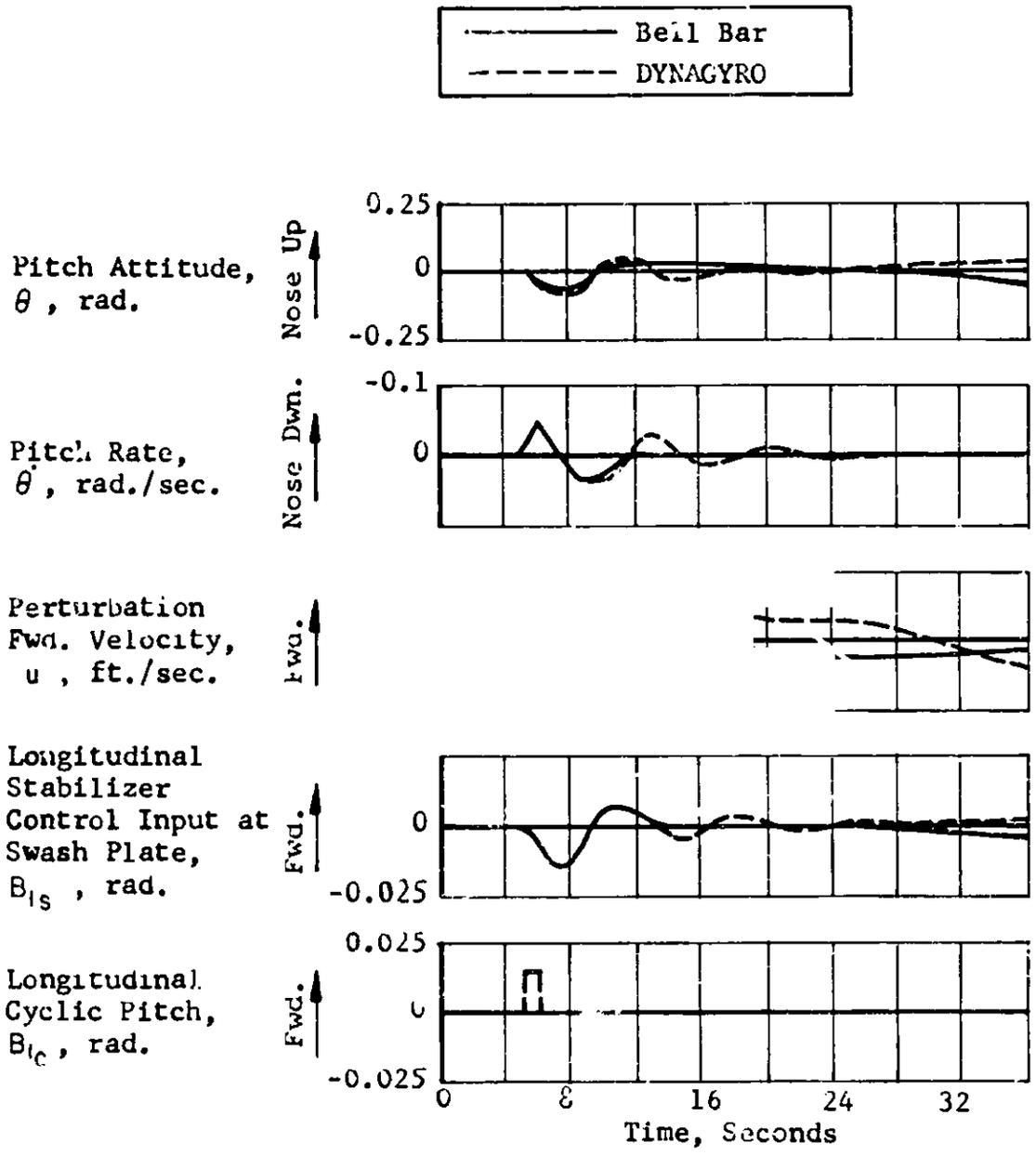

FIGURE 11. Comparison of the DYNAGYRO and Bell Bar Effectiveness on the Longitudinal Response of the UH-1B Helicopter at Hover.

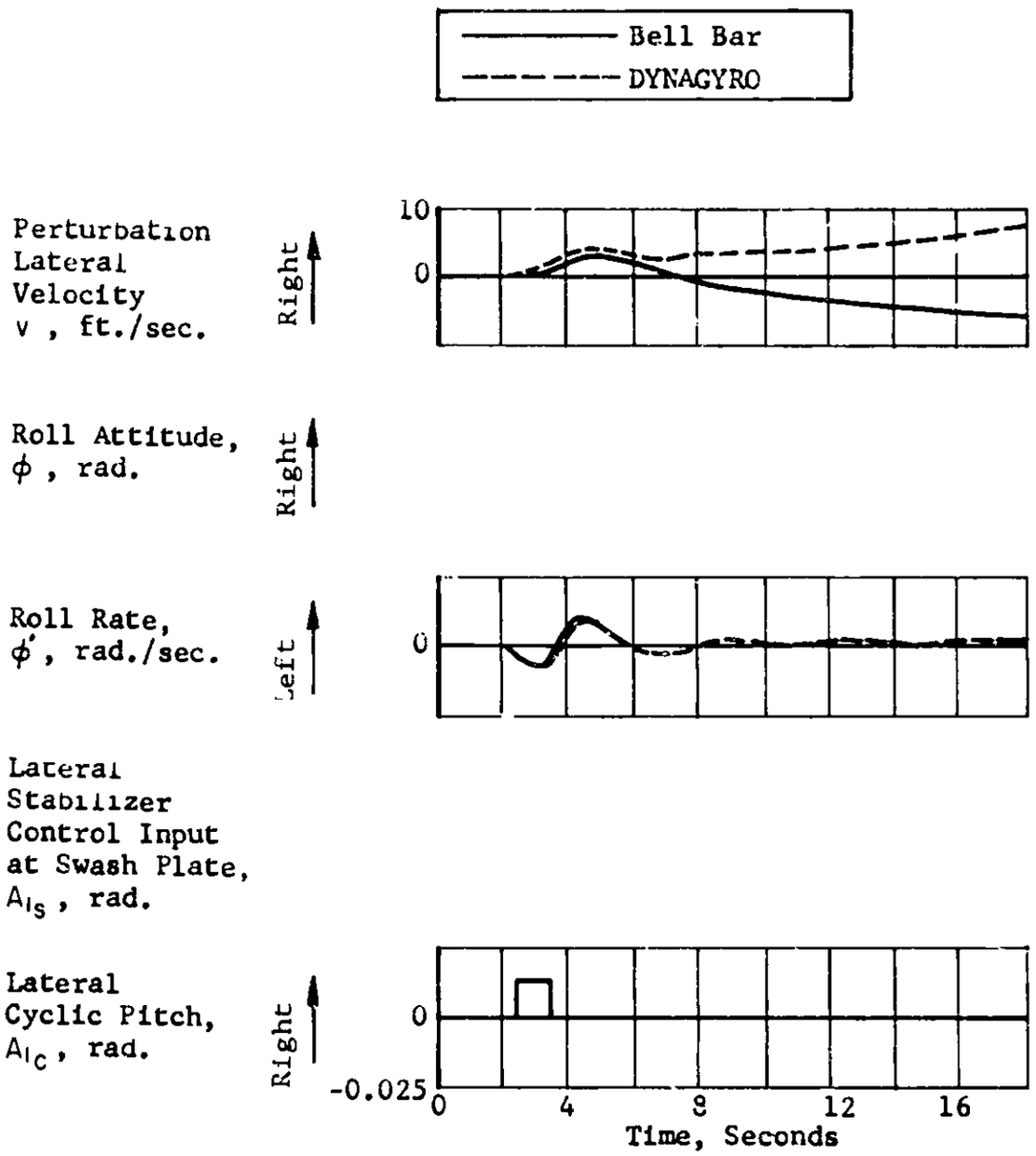

FIGURE 12. Comparison of the DYNAGYRO and Bell Bar Effectiveness on the Lateral Response of the UH-1B Helicopter at Hover.

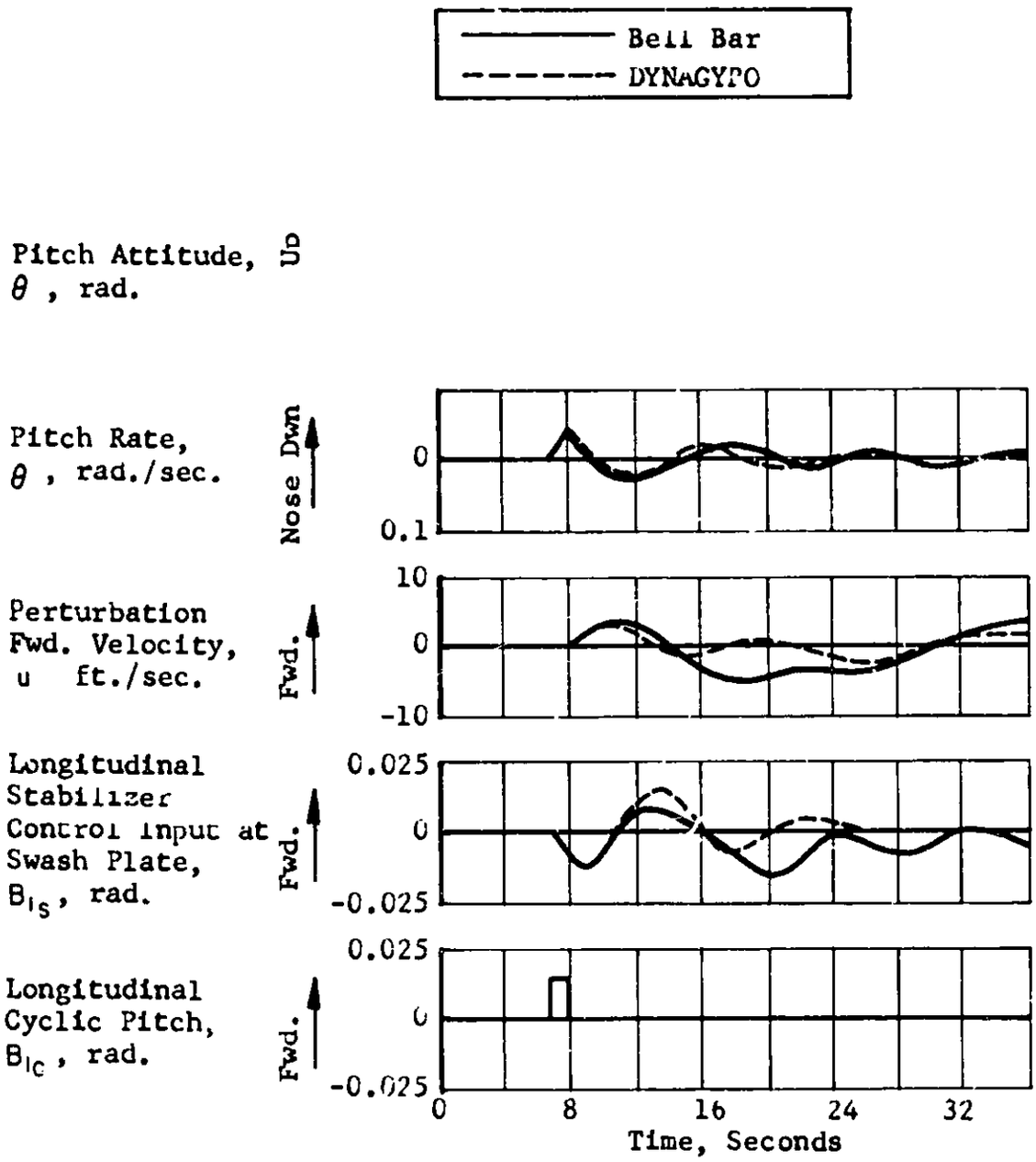

FIGURE 13. Comparison of the DYNAGYRO and Bell Bar Effectiveness on the Longitudinal Response of the UH-1B Helicopter at a Speed of 44 Knots.

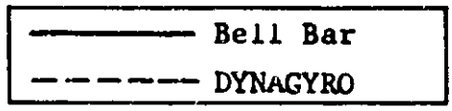

Perturbation
Lateral Velocity
v , ft./sec.

Right

Roll Attitude,
ϕ , rad.

Roll Rate,
$\dot{\phi}$, rad./sec.

Lateral Stabilizer
Control Input at
Swash Plate,
A_{ls} , rad.

Right

0.0125
0
-0.0125

Lateral
Cyclic Pitch,
A_{lc} , rad.

Right

0.025
0
-0.025

0 4 8 12 16
Time, Seconds

FIGURE 14. Comparison of the DYNAGYRO and Bell Bar Effectiveness on the Lateral Response of the UH-1B Helicopter at a Speed of 44 Knots.

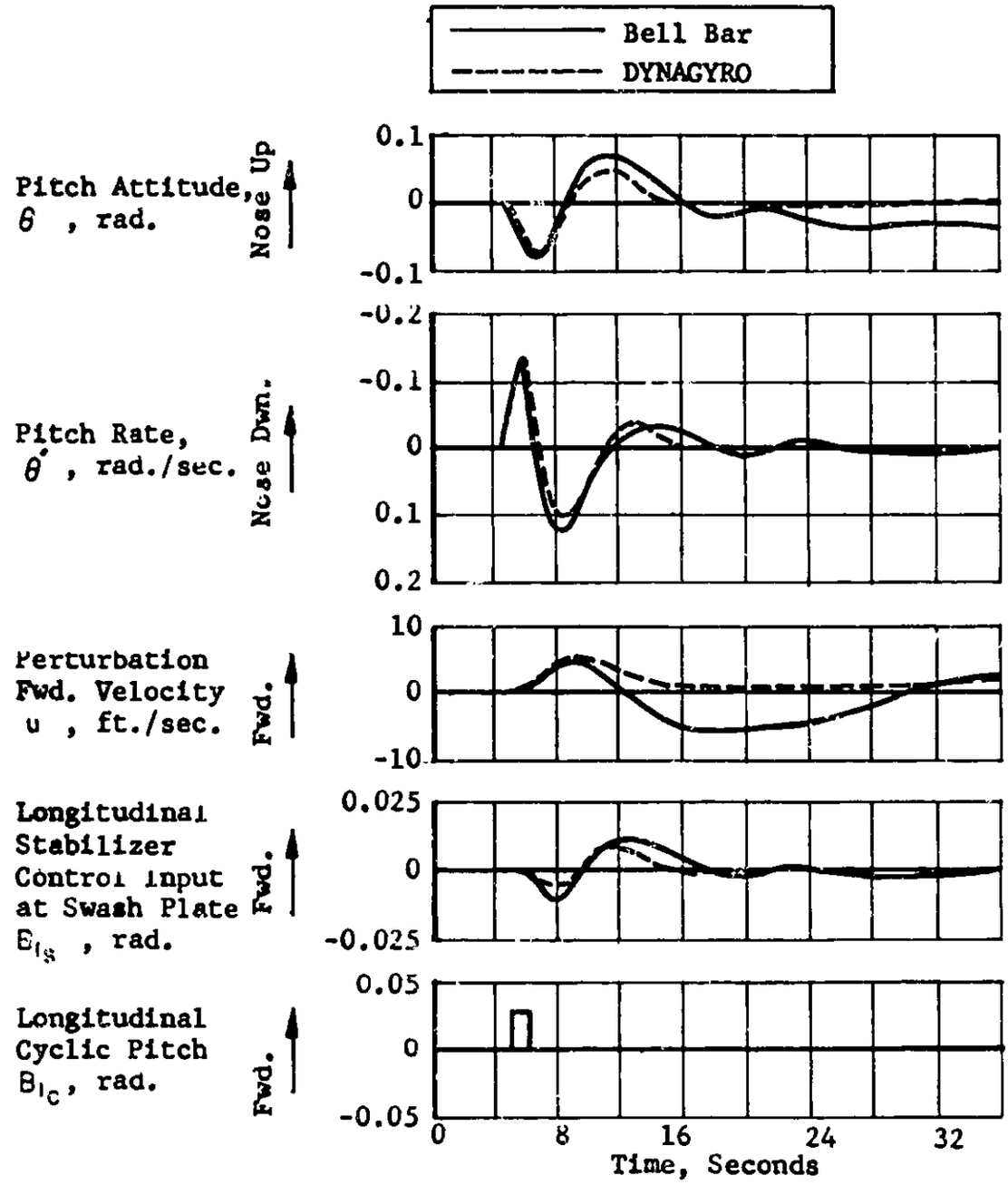

FIGURE 15. Comparison of the DYNAGYRO and Bell Bar Effectiveness on the Longitudinal Response of the UH-1B Helicopter at a Speed of 88 Knots.

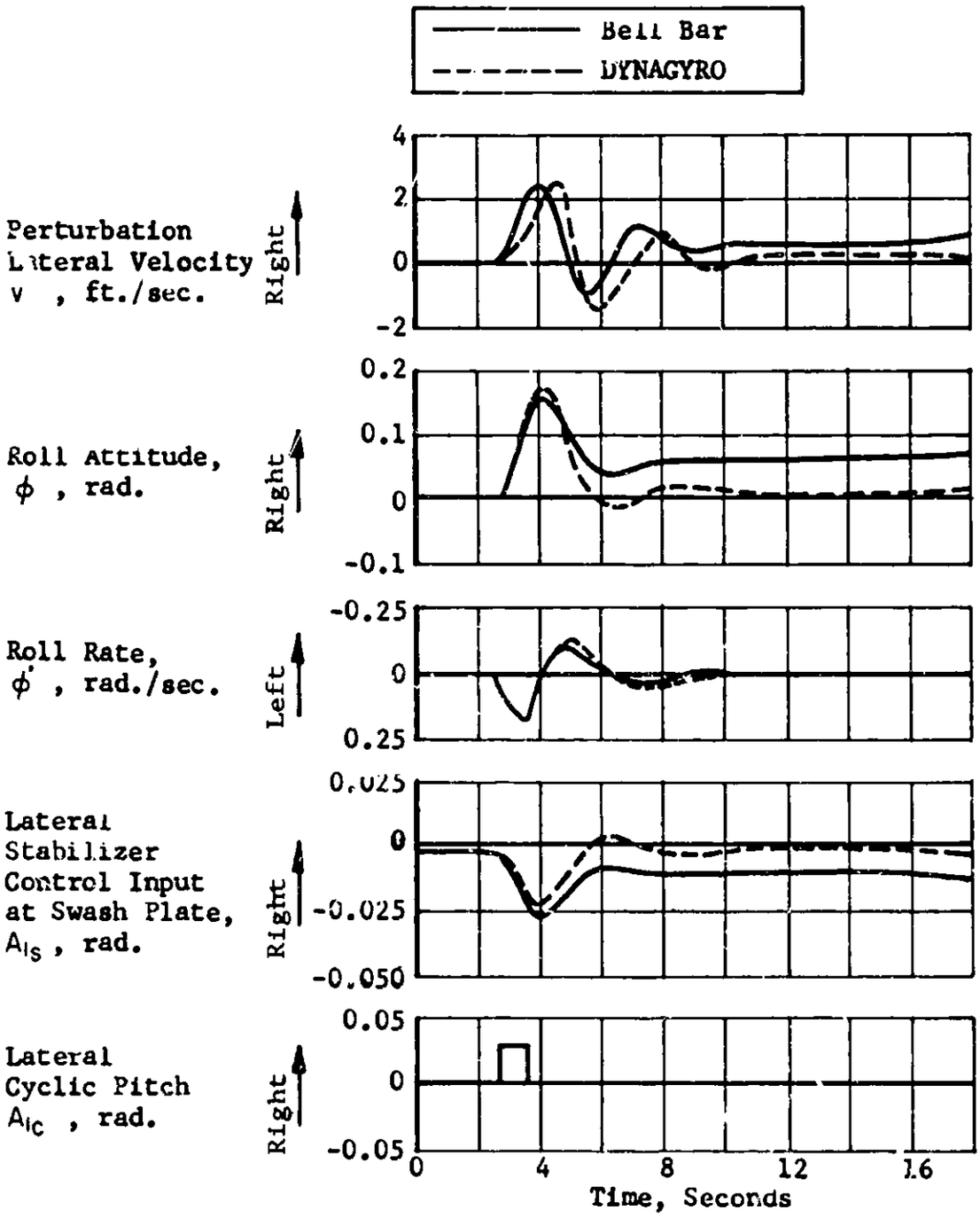

FIGURE 16. Comparison of the DYNAGYRO and Bell Bar Effectiveness on the Lateral Response of the UH-1B Helicopter at a Speed of 88 Knots.

Config.	Airspeed
Bell Bar	Hover
DYNAGYRO	Hover
Bell Bar	44 kt.
DYNAGYRO	44 kt.
Bell Bar	88 kt.
DYNAGYRO	88 kt.

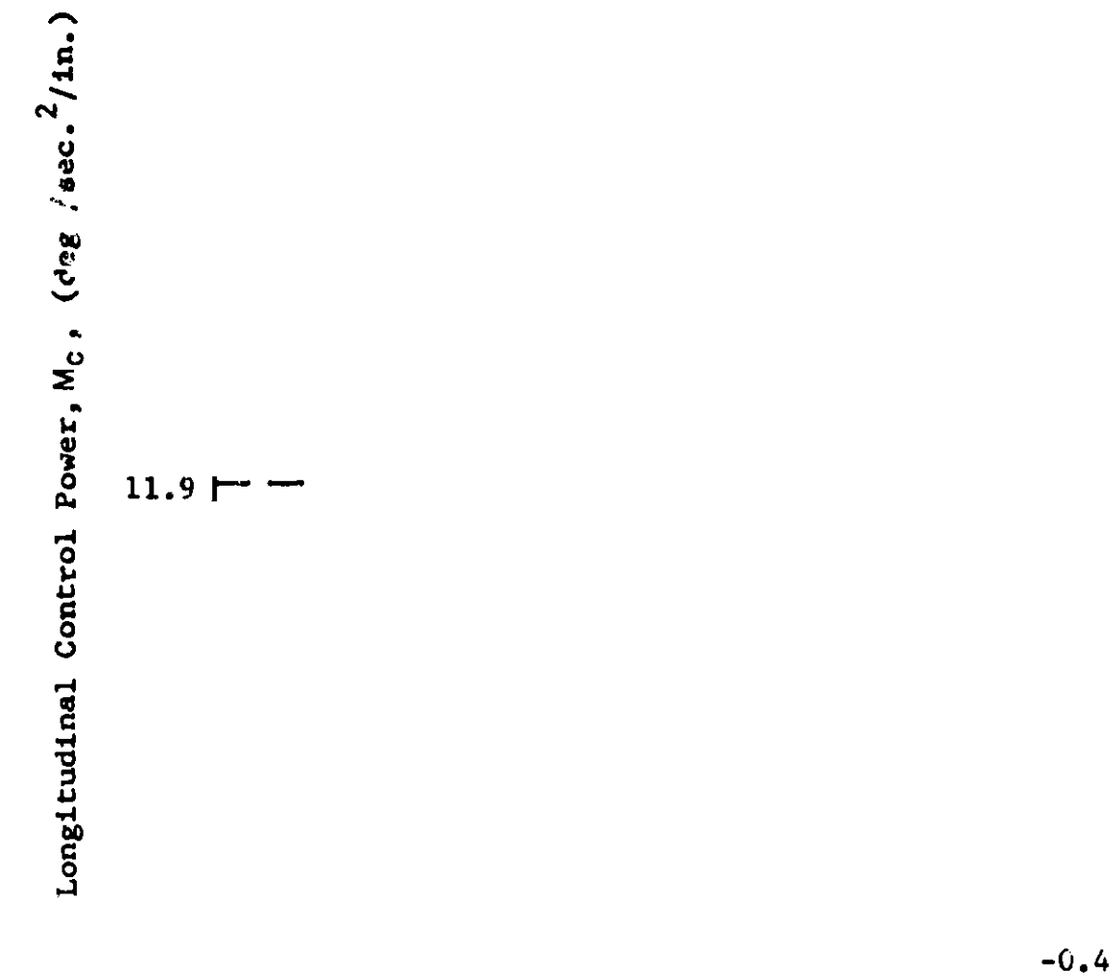

FIGURE 17. Comparison of Damping Requirements of the UH-1B Helicopter Equipped with the DYNAGYRO and the Bell Bar - Longitudinal Control.

Symbol	Config.	Airspeed
○	Bell Bar	Hover
◇	DYNAGYRO	Hover
△	Bell Bar	44 kt.
⬡	DYNAGYRO	44 kt.
□	Bell Bar	88 kt.
⬯	DYNAGYRO	88 kt.

Lateral Control Power, L_c, (deg./sec.^{2}/in.)

0.8 0.6 0.4 0.2 0.0 -0.2 -0.4 -0.6 -0.8 -1.0

Aircraft Damping, $1/T_{\frac{1}{2}}$, 1/sec.

FIGURE 18. Comparison of Damping Requirements of the UH-1B Helicopter Equipped with the DYNAGYRO and the Bell Bar - Lateral Control.

Symbol	k_1	Config.
○	0.05	DYNAGYRO
◇	0.10	DYNAGYRO
⬡	0.15	DYNAGYRO
△	0.16	Bell Bar

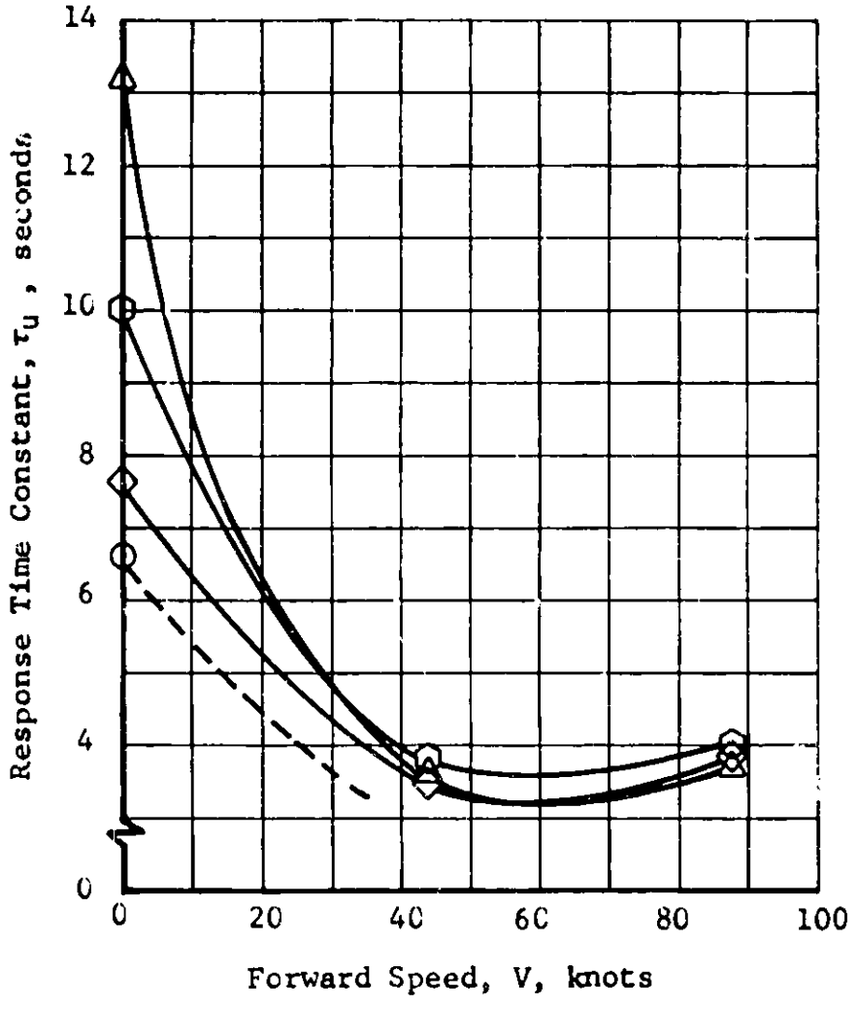

FIGURE 19. Effect of DYNAGYRO Stabilizer Parameters on the Aircraft Response After a Longitudinal Cyclic Control Step Input.

Symbol	k_2	Config.
○	0.05	DYNAGYRO
◇	0.10	DYNAGYRO
⬡	0.15	DYNAGYRO
△	0.16	Bell Bar

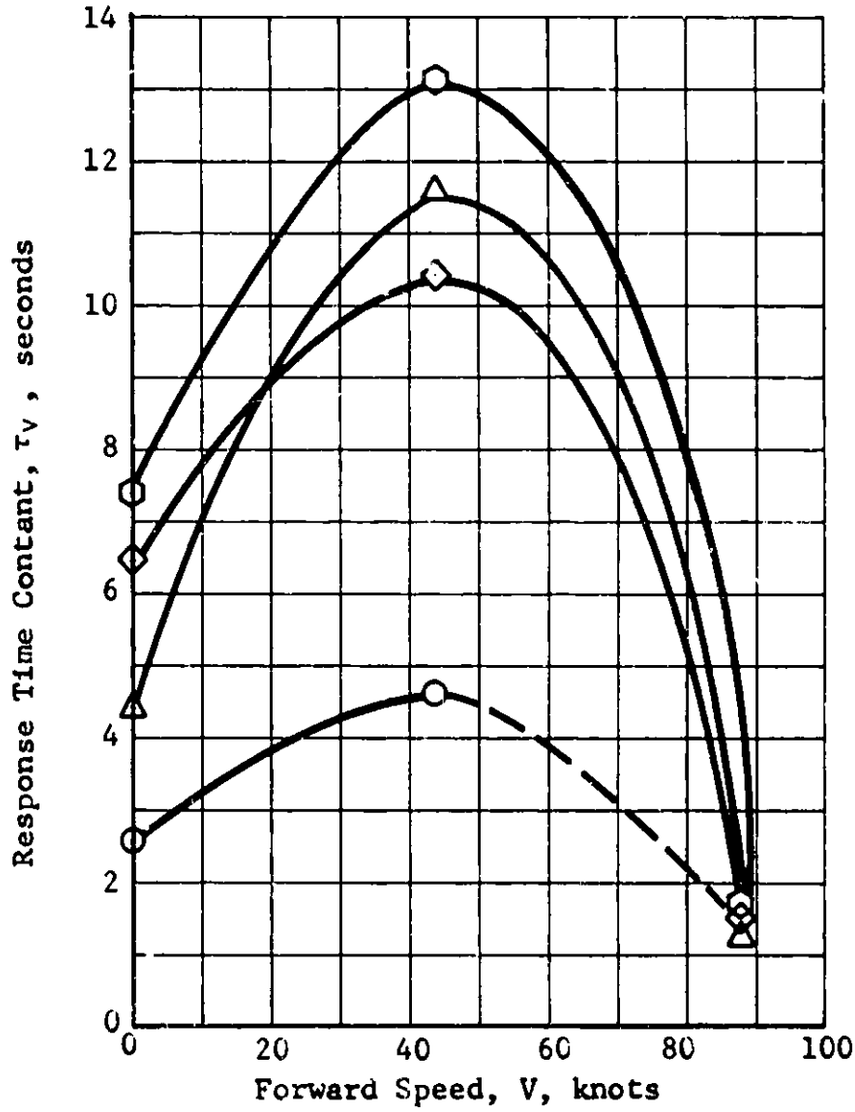

FIGURE 20. Effect of DYNAGYRO Stabilizer Parameters on the Aircraft Response After a Lateral Cyclic Control Step Input.

FIGURE 21. Damper Material Test Apparatus.

FIGURE 23. Damper Assembly Test Specimens.

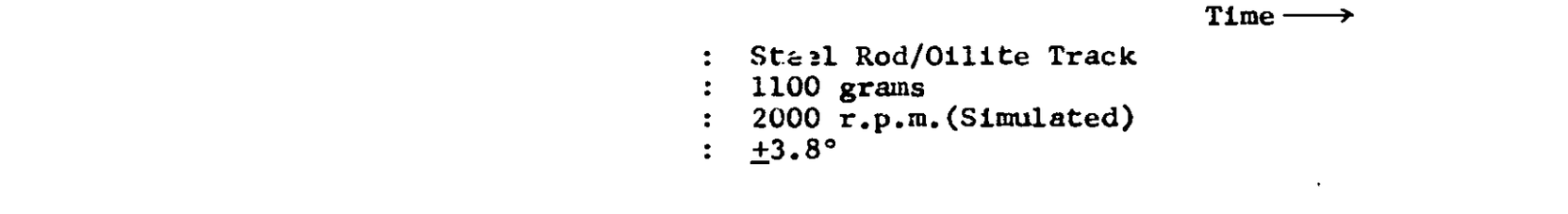

FIGURE 24. Typical Test Data Record.

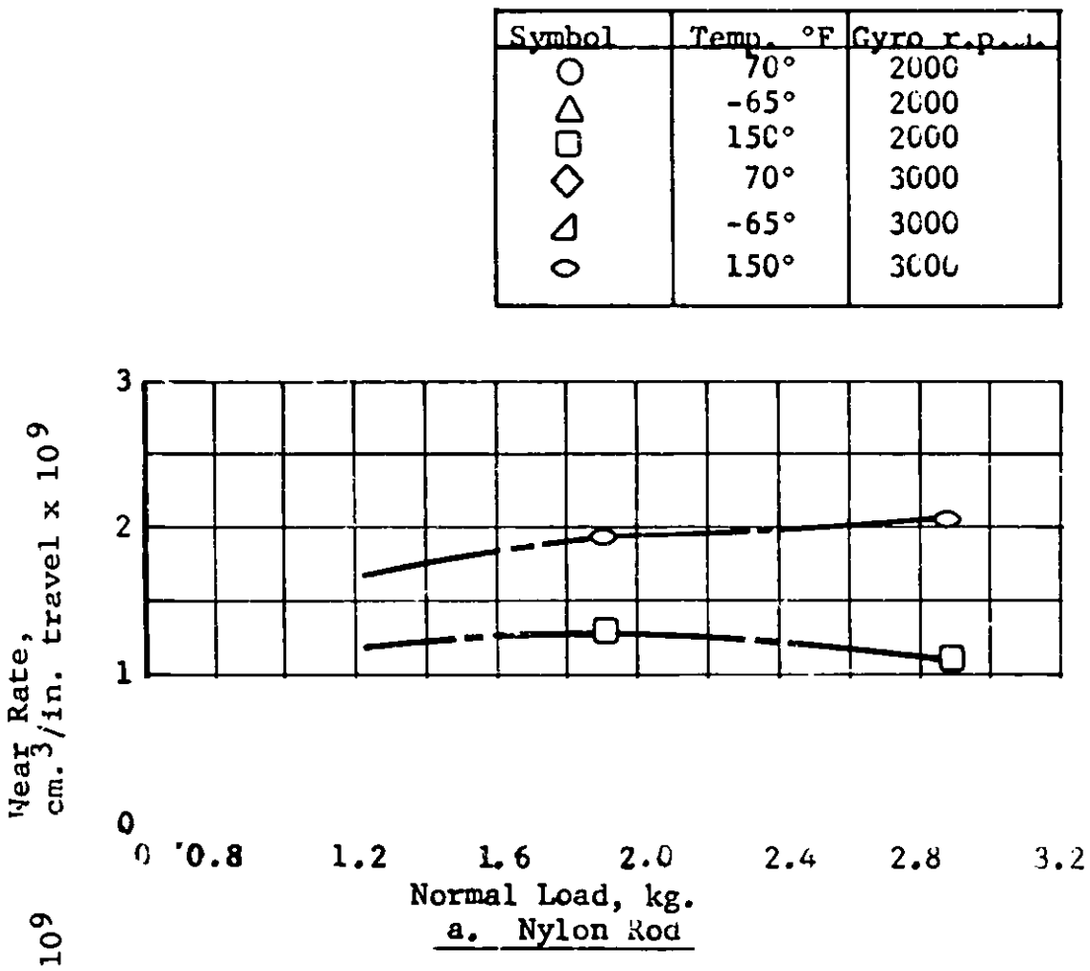

FIGURE 25. Effect of Normal Load, Gyro Speed, and Temperature on Wear Rates of Nylon Damper Rod and Oilite Track.

Symbol	Temp. °F	Gyro r.p.m.
○	70°	2000
□	150°	2000
◇	70°	3000
⬭	150°	3000

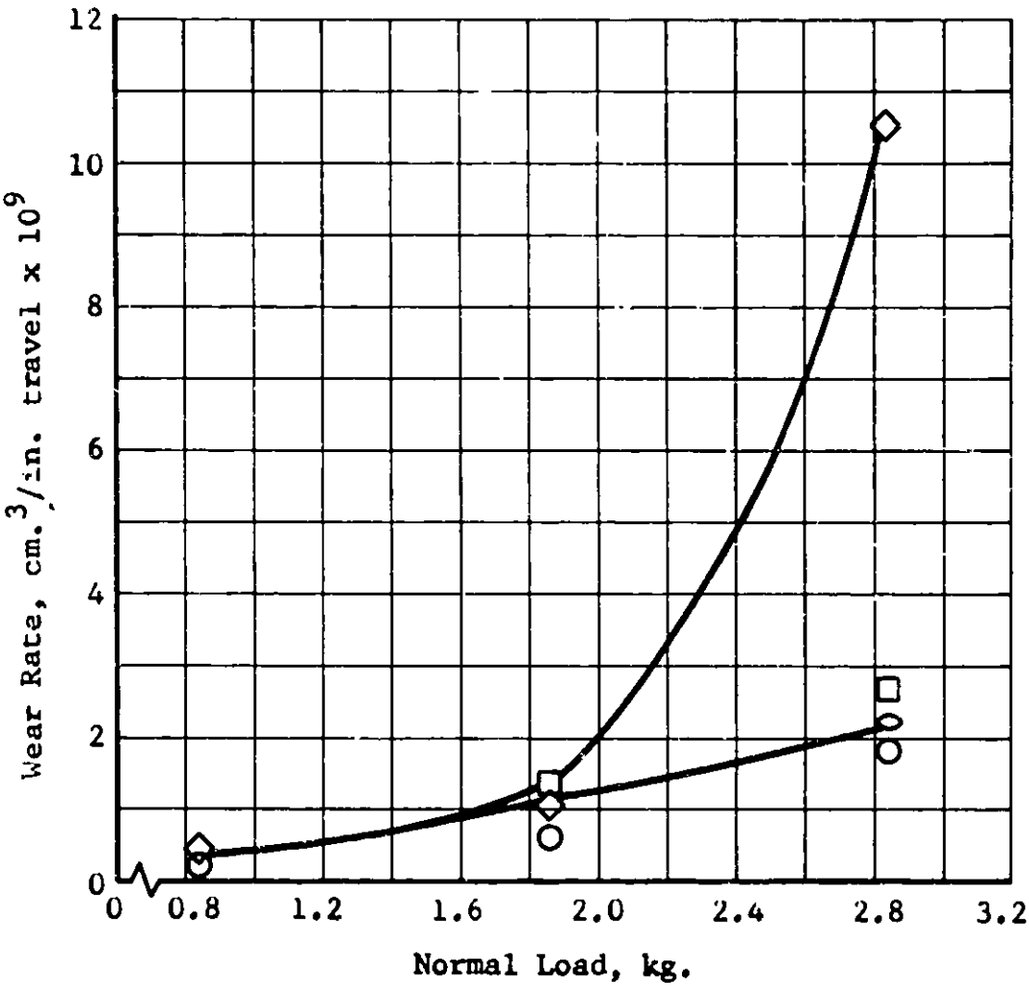

FIGURE 26. Effect of Normal Load, Gyro Speed, and Temperature on Wear Rate of Oilite Track (Steel Damper Rod on Oilite Track Combination).

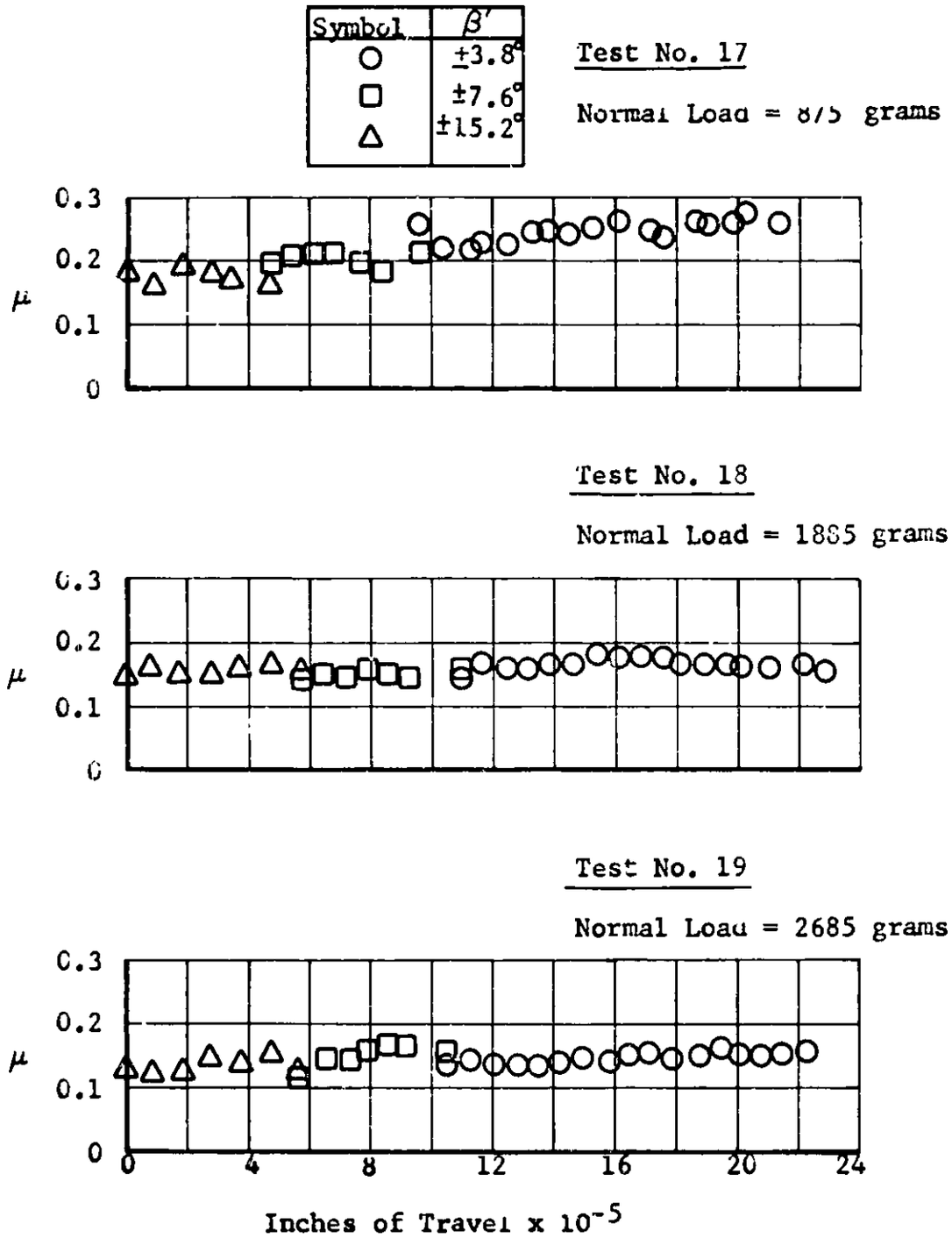

FIGURE 27. Effect of Normal Load on Friction Coefficient Time History of Nylon Rod on Oilite Track at 3000 r.p.m., 70°F.

Symbol	Temp. °F	Gyro r.p.m.
○	70	2000
△	-65	2000
□	150	2000
◇	70	3000
◁	-65	3000
⬭	150	3000

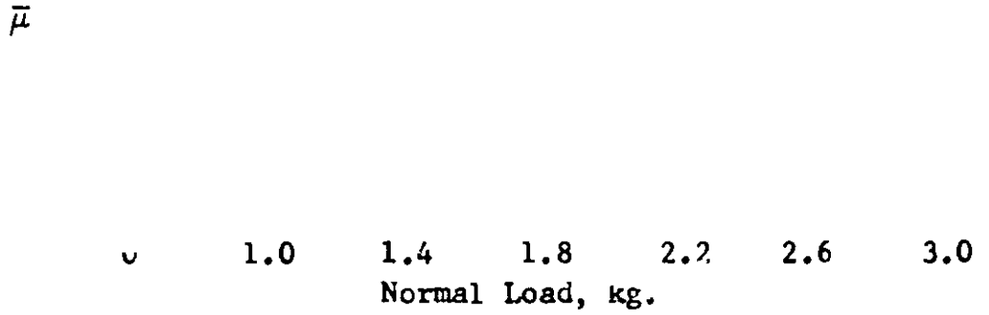

a. Nylon Rod on Oilite Track

b. Steel Rod on Oilite Track

FIGURE 28. Effect of Normal Load, Gyro Speed, and Temperature on Damper Material Friction Coefficients.

FIGURE 29. DYNAGYRO Bench Test Apparatus.

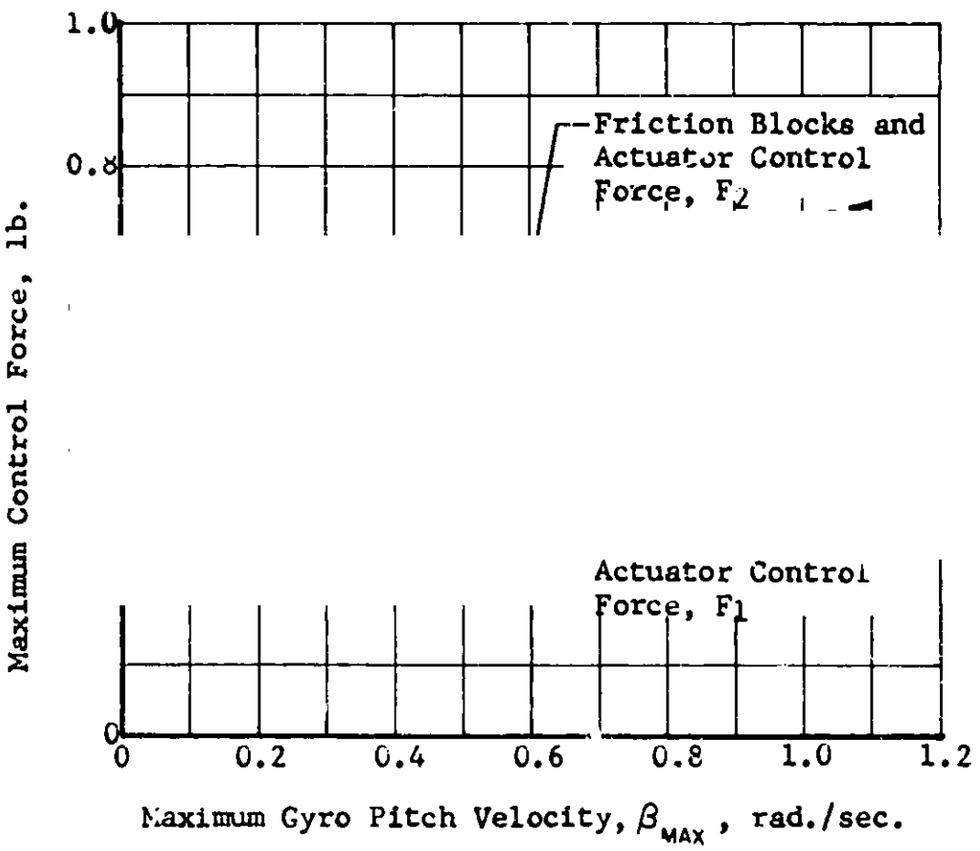

FIGURE 30. Variation of Stick Boost Actuator Control Force Requirements with Maximum Gyro Pitch Velocity.

FIGURE 31. Environmental Test Chamber Containing the Test Model.

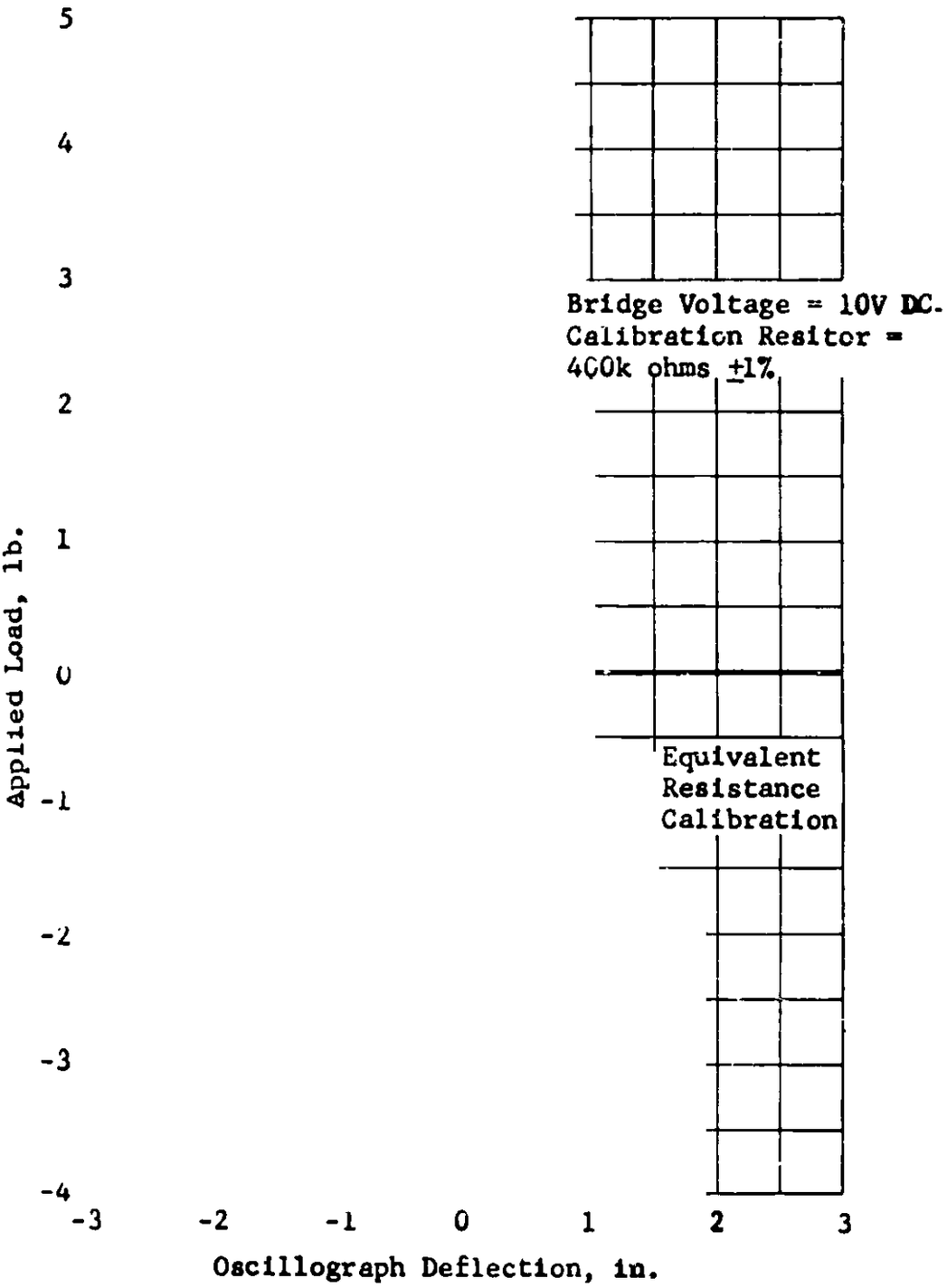

FIGURE 32. Force Flexure Calibration (Pitch Channel).

Applied Load, lb.

Bridge Voltage = 10V D.C.
Calibration Resistor =
400k ohms +1%

Oscillograph Deflection, in.

FIGURE 33. Force Flexure Calibration (Roll Channel).

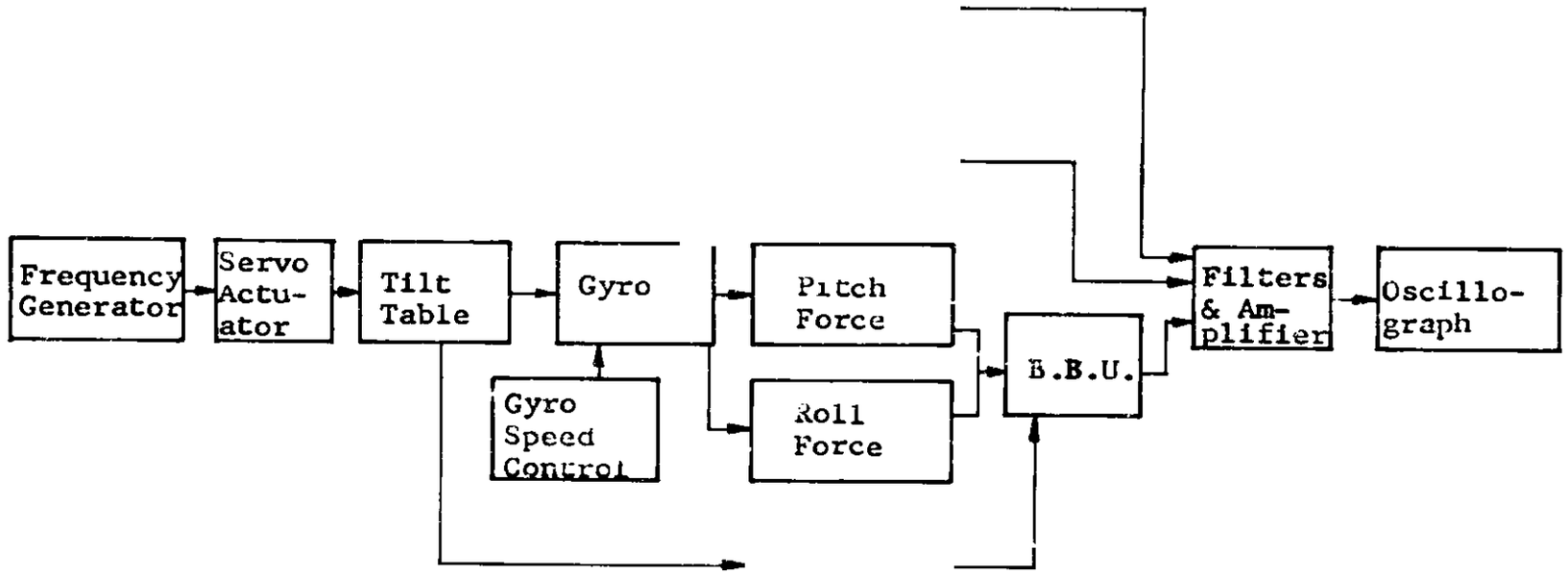

FIGURE 34. Block Diagram of DYNAGYRO Laboratory Test Instrumentation.

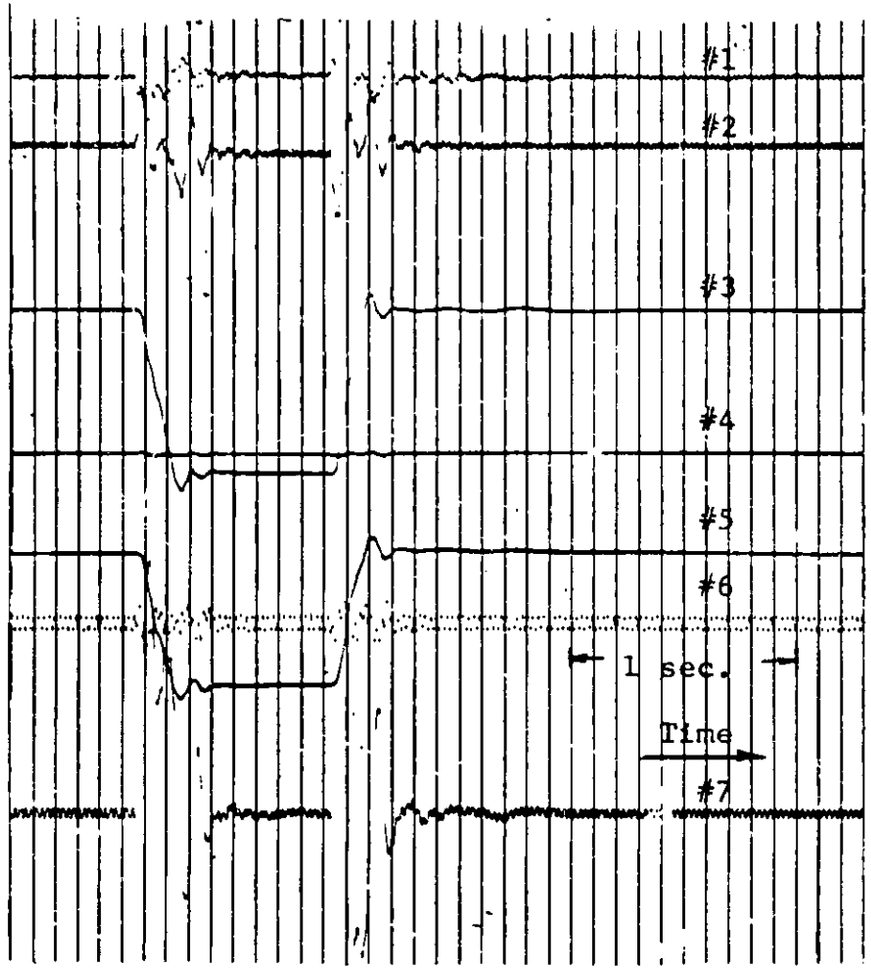

Ch. No.	Parameter	Scale Factor
1	Pitch Torque	2.53 $\frac{\text{in.-lb.}}{\text{in.}}$
2	Roll Torque	3.44 $\frac{\text{in.-lb.}}{\text{in.}}$
3	Table Angle	$\frac{\text{deg.}}{}$
4	Gyro Roll Angle	
5	Gyro Pitch Angle	10.5 $\frac{\text{deg.}}{\text{in.}}$
6	Gyro Roll Rate	0.71 $\frac{\text{rad./sec.}}{\text{in.}}$
7	Gyro Pitch Rate	0.71 $\frac{\text{rad./sec.}}{\text{in.}}$

FIGURE 35. DYNAGYRO Response to a Pulse Input (Gyro r.p.m.=2500).

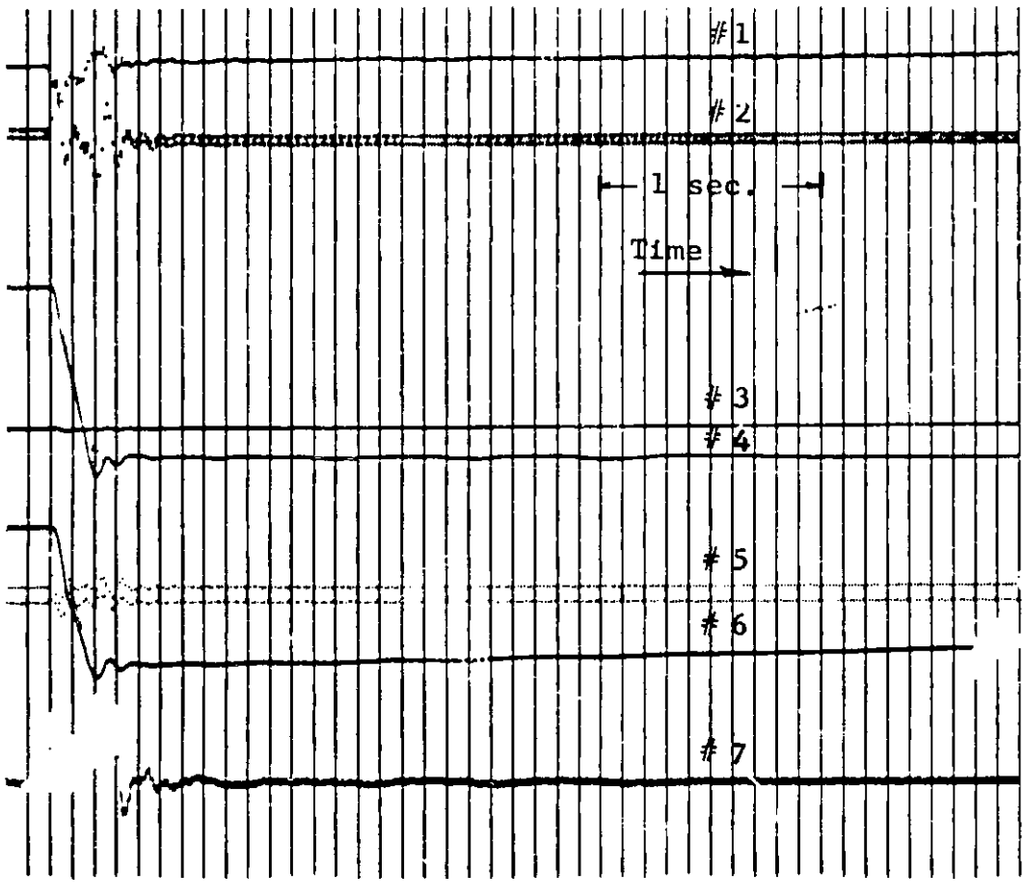

Ch. No.	Parameter	Scale Factor
1	Pitch Torque	2.53 $\frac{\text{in.-lb.}}{\text{in.}}$
2	Roll Torque	3.44 $\frac{\text{in.-lb.}}{\text{in.}}$
3	Gyro Roll Angle	9.0 $\frac{\text{deg.}}{\text{in.}}$
4	Table Angle	9.2 $\frac{\text{deg.}}{\text{in.}}$
5	Gyro Roll Rate	0.71 $\frac{\text{rad./sec.}}{\text{in.}}$
6	Gyro Pitch Angle	10.5 $\frac{\text{deg.}}{\text{in.}}$
7	Gyro Pitch Rate	0.71 $\frac{\text{rad./sec.}}{\text{in.}}$

FIGURE 36. DYNAGYRO Response to a Step Input (Gyro r.p.m. = 4200).

Ch. No.	Parameter	Scale Factor
1	Pitch Torque	2.53 $\frac{\text{in.-lb.}}{\text{in.}}$
2	Roll Torque	3.44 $\frac{\text{in.-lb.}}{\text{in.}}$
3	Table Angle	9.2 $\frac{\text{deg.}}{\text{in.}}$
4	Gyro Roll Angle	9.0 $\frac{\text{deg.}}{\text{in.}}$
5	Gyro Pitch Angle	10.5 $\frac{\text{deg.}}{\text{in.}}$
6	Gyro Roll Rate	0.71 $\frac{\text{rad./sec.}}{\text{in.}}$
7	Gyro Pitch Rate	0.71 $\frac{\text{rad./sec.}}{\text{in.}}$

FIGURE 37. DYNAGYRO Response to a $\frac{1}{2}$ c.p.s. Sinusoidal Input (Gyro r.p.m. = 4200).

Symbol	Control Force	Temp. °F
○	F_1	70
□	F_1	150
◇	F_2	70
⬯	F_2	150

Gyro Damping Rate, R, rad./sec.

Symbol	Control Force	Temp. °F
○	F_1	70
□	F_1	150
◇	F_2	70
◊	F_2	150

Rate
ft.^{2})

Gyro Damping Rate, R, rad./sec.

FIG

Symbol	Temp., °F
○	70
□	150

Gyro Damping Rate, R, rad./sec.

FIGURE 41. DYNAGYRO Damping Rate vs. Gyro r.p.m. for Nylon on Oilite Dampers. Control Force: F_2, Gyro Inertia: 0.0305 slug-ft.^{2}.

Gyro Damping Rate, R, rad./sec.

Symbol	Temp. °F
◇	70
△	-15
○	150

Gyro Damping Rate, R, rad./sec.

FIGURE 44. Gyro Coupling vs. Gyro Momentum.

VI. REFERENCES

1. Savet, Paul H., Gyroscopes, Theory and Design, McGraw-Hill Book Company, New York, 1961.

2. Kisielowski, E., Perlmutter, A. A., "Stability and Control Handbook for Helicopters", USAAVLABS Technical Report 66-66, U. S. Army Aviation Materiel Laboratories, Fort Eustis, Virginia, (To be Published).

3. Calderon, J. M., "HU-1 Stability and Control Evaluation", Airforce Flight Test Center, Edwards Air Force Base, California, AFFTL-TR-6-57, December 1960.

4. O'Harrah, R. C., Kwiatkowski, S. F., "A New Look at V/STO' Flying Qualities", IAS Paper No. 61-62, Presented at IAS 29th Annual Meeting, New York, January 1961.

5. Anonymous, Military Specification - Helicopter Flying Qualities, Requirements For. MIL H-8501A, April 1960.

6. Sauer, Fred M., "Fundamental Mechanism of Wear and Friction of Unlubricated Metallic Surfaces at High Sliding Speeds", U. S. Naval Ordnance Test Station, China Lake, California, NAVORD Report 5452, April 1957.

7. Shugarts, W. W., Jr., "New Instrumentation to Study Sliding Friction at High Speeds", Watertown Arsenal Laboratory WAL 760/452-21, April 1954 (AD No. 36867).

8. Kragel'skiy, I. V., et al., Dry and Boundary Friction, Frictional Materials (Selected Articles), FTD-TT-61-449/1 + 2, Foreign Technical Division, Air Force Systems Command, Wright-Patterson Air Force Base, Ohio, June 1962.

APPENDIX I

ANALOG COMPUTER PROGRAM

An analog computer program was developed to simulate the UH-1B helicopter response as affected by the DYNAGYRO and the Bell Bar stabilizing inputs. This program was utilized to optimize the DYNAGYRO damping rate R and the pilot control authority ratio k suitable for the UH-1B helicopter. The analog solution of the governing equations of motion presented in Section III-B is shown in the analog computer schematic, Figure 45. The numerical values of the helicopter stability derivatives for hover, 44 knots, and 88 knots speed regimes are presented in Table X. These derivatives were evaluated at the aircraft aft most c.g. position (Station 137.2) to demonstrate the DYNAGYRO stabilizing effects at the most unstable aircraft mode.

The analog computer simulation consisted of applying a step or pulse input to aircraft control (stick) and recording time histories of aircraft response in pitch, roll, yaw, forward and vertical velocities, etc., and their respective rates. Although the analog computer results were initially obtained utilizing the coupled six degrees of freedom of aircraft motion, it was subsequently found that the coupling effects between the aircraft longitudinal and lateral modes were small and therefore could be neglected. A sample run sheet for the decoupled longitudinal aircraft motion is presented in Table XI.

The numerical results obtained from this program are presented and discussed in Section III-C.

TABLE X

TOTAL STABILITY DERIVATIVES

(a) Hovering

Variable	X	Y	M	L	N
θ	-7980	0	0	0	0
$\dot{\theta}$	7.62	0	-40.79	0	0
$\ddot{\theta}$	0	0	-9100	0	0
u	-1.25	0	6.7	0	0
$\dot{u}$	-236	0	0	0	0
v	0	-5.08	0	-24.84	34.72
$\dot{v}$	0	-236.0	0	0	0
ϕ	0	7600	0	0	0
$\dot{\phi}$	0	0	0	-2240	317.7
$\ddot{\phi}$	0	0	0	-2685	0
ψ	0	708.0	0	0	0
$\dot{\psi}$	0	34.72	0	-99.29	-1786
$\ddot{\psi}$	0	0	0	0	-7565
B_{l_C}, B_{l_S}	7980	0	-42,700	0	0
$\dot{B}_{l_C}, \dot{B}_{l_S}$	-1.39	0	7.45	0	0
A_{l_C}, A_{l_S}	0	-7980	0	42,700	3990
$\dot{A}_{l_C}, \dot{A}_{l_S}$	0	+1.39	0	+7.45	0

TABLE X (Continued)

(b) 44 Knots

Variable	X	Y	Z	M	N	L
θ	-7600	0	-660	0	0	0
$\dot{\theta}$	-904.3	-246.4	17,640	-4992	-134.2	-1320
$\ddot{\theta}$	0	0	0	-9100	0	0
ϕ	0	7600	0	0	0	0
$\dot{\phi}$	-246	937.8	-12.64	1247	413.1	-3052.8
$\ddot{\phi}$	0	0	0	0	937.7	-2685
ψ	0	660.4	0	0	0	0
$\dot{\psi}$	70.70	-17,350	-1.50	-362	-5862	+733.5
$\ddot{\psi}$	0	0	0	0	-7565	938
u	-6.616	4.21	-21.76	44.07	-51.0	21.64
$\dot{u}$	-236	0	0	0	0	0
v	-1.62	6.78	0.054	1.428	131.7	16.62
$\dot{v}$	0	-236	0	0	0	0
w	7.56	-2.82	-149.5	43.22	-87.34	-10.67
$\dot{w}$	0	0	-236.0	0	0	0
B_{1c} , B_{1s}	6974	177.9	10,880	-42,140	6422	952
$\dot{B}_{1c}$, $\dot{B}_{1s}$	-627	244.2	-266	3480	+122.3	1306
A_{1c} , A_{1s}	11.18	7730	-218.7	4.51	3865	41,350
$\dot{A}_{1c}$, $\dot{A}_{1s}$	-234.0	-555.0	-12.64	1261	-277.5	-2969
θ_c	3915	-609.9	-69,080	13,590	65,470	-3263
θ_{ctr}	-102	3740	12.81	700	-104,700	12,170

TABLE X (Concluded)

(c) 88 Knots

Variable	X	Y	Z	M	N	L
θ	-7600	0	-623	0	0	0
$\dot{\theta}$	-2210	-246	34,900	-6930	-154.4	-1305
$\ddot{\theta}$	0	0	0	-9100	0	0
ϕ	0	7600	0	0	0	0
$\dot{\phi}$	-248.1	2258	-19.0	1280	632.2	-3290
$\ddot{\phi}$	0	0	0	0	932	-2685
ψ	0	622.4	0	0	0	0
$\dot{\psi}$	-7.90	34840	2.03	-243	-7673	+987.9
$\ddot{\psi}$	0	0	0	0	-7576	932
u	-10.68	6.00	-0.15	50.61	-15.34	23.44
$\dot{u}$	-236	0	0	0	0	0
v	-1.95	-12.50	-0.013	2.118	225.2	-1.625
$\dot{v}$	0	-236	0	0	0	0
w	14 67	-3.38	-188.5	6.389	-148.5	-18.41
$\dot{w}$	0	0	-236	0	0	0
B_{lc}, B_{ls}	5644	582.2	24,620	-42,610	20,180	3115
$\dot{B}_{lc}, \dot{B}_{ls}$	-641.7	243.9	-170	3536	122.0	1301
A_{lc}, A_{ls}	14.58	7723	-178.0	11.0	3862	41,320
$\dot{A}_{lc}, \dot{A}_{ls}$	-236.2	-570.2	-18.84	1250	-285.0	-3,049
θ_c	4325	-846	-80,080	16,935	43,750	-4526
θ_{ctr}	-207	4800	-8.68	450	-134,550	16,320

TABLE XI

DYNAGYRO ANALOG PROGRAM RUN SCHEDULE

Date = 30 November 1965 Mode = Longitudinal Speed = 44 knots

μ	Run No.	R	k	B_{1c}	Δt	Configurations
0.10	301	0	0	.03	1.0	Unstabilized
	302				0.5	
	303				0.1	
	304				Step	
	306		.16		1.0	Bell Bar
	307				Step	
	309	0	.05		1.0	DYNAGYRO
	310	.002				
	311	.004				
	312	.006				
	313	.010				
	314	.015				
	315	.030				
	316	.006			Step	
	317	0	.10		1.0	
	318	.002				
	319	.004				
	320	.006				
	321	.010				
	322	.015				
	323	.030				
	324	.006			Step	
	325	0	.15		1.0	
	326	.002				
	327	.004				
	328	.006				
	329	.010				
	330	.015				
	331	.030				
	332	.006			Step	
	335	.002	.20		1.0	
	336	.004				
	337	.006				
	338	.006			Step	

LEGEND

SYMB.	POT.
◌	P
○	Q

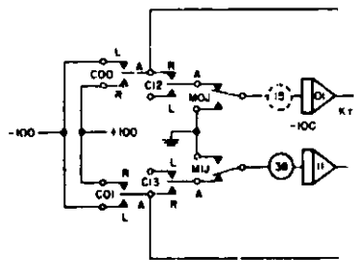

FIGURE 45. ANALOG COMPUTER SCHEMATIC

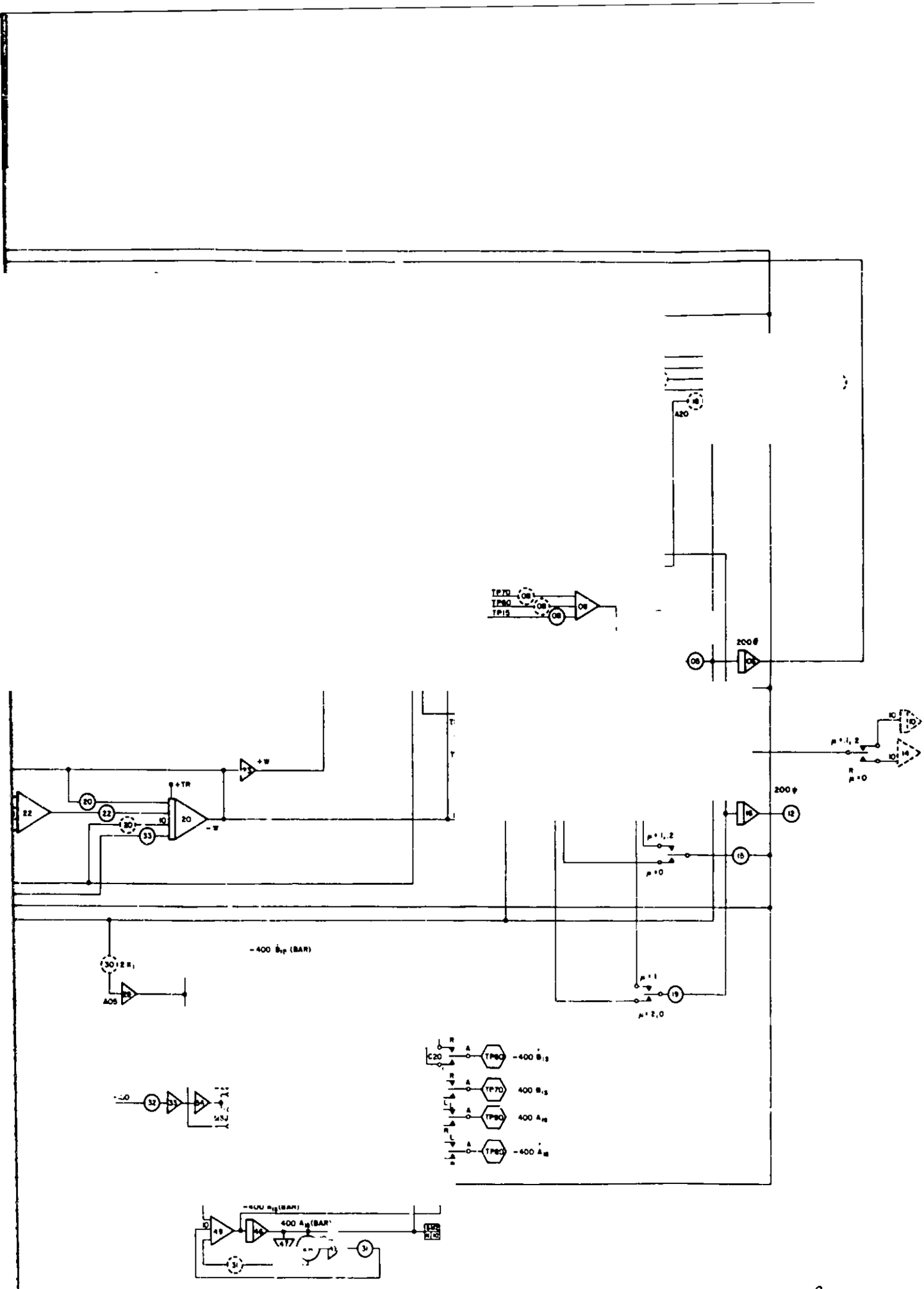
TP70
TP80
TP15
420
200 Φ
+W
-W
+TR
-400 $\dot{B}_{1P}$ (BAR)
400 $\dot{B}_{1S}$
400 $\dot{A}_{1S}$
-400 $\dot{A}_{1S}$
400 A_{1S} (BAR)
B

BLANK PAGE

APPENDIX II

SUPPLEMENTARY DATA ON FRICTION COEFFICIENTS OF DAMPER MATERIALS

In this appendix, additional detailed information is presented on the damper material evaluation program. A summary of the results and also a description of the test apparatus and program are presented in Section IV-A of the main text.

A total of thirty-seven tests were made, representing approximately 524 test hours. These tests and the resulting data are presented in Table XII.

A. VARIATION OF FRICTION COEFFICIENT WITH AMPLITUDE

The damper material friction coefficients obtained from these tests were first examined to establish to what extent they were affected by the simulated gyro tilt angle. All friction force data were extracted from the oscilloscope photographs, a sample of which is shown in Figure 24. The method utilized to reduce the data is described below.

Using a schematic of the forces acting on the damper assembly, presented in Figure 46, the normal force N and friction force $N\mu$ are resolved into horizontal and vertical components at the damper and track contact point. By taking moments about point "A", the force F is obtained:

$$\Sigma M_A = 0 = F(1+\mu \tan\beta')(s + r \sin\beta') - F(\mu - \tan\beta')\, r\,(1-\cos\beta') - P\ell$$

$$F = \frac{P\ell}{(1+\mu \tan\beta')(s + r \sin\beta') - r\,(\mu - \tan\beta')(1-\cos\beta')} \qquad (33)$$

Summing horizontal forces, the flexure force G is obtained:

$$G = F\mu - F \tan\beta' \qquad (34)$$

Solving equations 33 and 34 simultaneously for the instantaneous coefficient of friction, there results

$$\mu_\beta = \frac{P\ell \tan\beta' + G(a + r\ b \tan\beta')}{P\ell - G(a \tan\beta' - r\ b)} \qquad (35)$$

where

$$a = s + r \sin\beta'$$

$$b = 1 - \cos\beta'$$

In examining the flexure force G given in equation 34, it is seen that it is a composite of the friction force $F\mu$ and the horizontal component of the normal load F tan β'. Although both of these forces exist in the actual DYNAGYRO configuration, the one of interest is the friction force, since this is the only force affecting the gyro motion. The force F tan β' is reacted at the damper pivot point and does not in any way affect the gyro response. The two parts of the flexure force G are plotted separately, and are combined in Figure 47 as a function of simulated gyro displacement β'. It should be noted that the combined flexure force shows a distinct variation with β', which is also in agreement with the recorded force data shown in Figure 24. On the other hand, the friction force $F\mu$, which is the force acting on the gyro, very closely approximates the square wave assumed in the DYNAGYRO analysis.

The effect of β' on the friction coefficient μ_β was also determined by substituting the applied load P and the measured flexure force G at any β' into equation 35. The results for typical test conditions are plotted in Figure 48 for three normal loads. It can be seen from Figure 48 that the friction coefficient for the samples analyzed is independent of gyro displacement within the experimental scatter expected of friction testing.

Based on the above results, and to facilitate data reduction, all subsequent friction coefficients were measured at β' of 0°.

B. TIME HISTORIES OF FRICTION COEFFICIENTS

The friction coefficients measured for each of the tests conducted are presented in Figures 49 through 61. These data were obtained at periodic intervals during each test and are plotted as a function of cumulative inches of travel. A detailed discussion of each figure is given below:

1. Steel Rod on Teflon Track

The friction coefficient for this material combination was relatively constant with time, as shown in Figure 49. A comparison of tests 1 and 2 shows a decrease in the friction coefficient with increasing normal load. Further testing of this material was discontinued due to excessively high wear rates encountered on the Teflon track.

2. Nylon, Brass, and Steel on Stainless Steel Track

Figure 50 presents the results of several damper rod materials combined with a stainless steel track. Testing of the combinations of steel and brass damper rods on stainless steel tracks was discontinued after several hours of running due to the high wear and inconsistent friction coefficients obtained. The material combination of nylon on stainless steel (test 13, Table XII) was discontinued due to the erratic friction coefficients and the high wear rate of the nylon.

3. Aluminum on Oilite Track

Two widths of aluminum damper rods, 1/16 and 1/8 inch wide, were tested at similar gyro tilt angles and r.p.m. to determine the effects of reduced contact pressure. The results are shown in Figure 51. The friction coefficients for the narrow damper rod, although erratic, indicate that μ remains relatively constant with time, while the friction coefficients for the wider rod specimen increased with time. This is attributed to the decrease in bearing pressure of the wider specimen, which has the effect of releasing less lubricant from the Oilite. No further testing was conducted

for this material combination, since the friction coefficients were higher in magnitude than the design values required for the intended application and also since this material did not exhibit constant coefficient with time.

4. Steel on Oilite

Figures 52 through 55 present the friction coefficients for this material combination with variations in normal load, β', gyro r.p.m., and temperature. Each figure represents a constant temperature and r.p.m. test cycle.

The 70°F temperature tests are shown in Figures 52 and 53. At 2000 r.p.m. and 875-gram normal load given in Figure 52, the friction coefficient averages approximately 0.25. Only limited friction coefficient data were obtained for the 1885- and 2865-gram normal loads due to a transducer failure.

At 3000 r.p.m., Figure 53, the friction coefficient decreases with increasing normal load. The resulting friction coefficients at low normal load vary widely with time, ranging from 0.2 to 0.5. For the 1885-gram load, the friction coefficient is approximately 0.23 and that for the 2865-gram load is about 0.2. The test with 2865-gram load, shown in Figure 53, was terminated after 7.50×10^5 inches of travel due to seizure of the test specimen.

Figures 54 and 55 present the effects of high temperature, 150°F, on the friction coefficient for the 1885- and 2865-gram normal loads at 2000 and 3000 r.p.m., respectively. The trend in μ noted previously, i.e., a decrease in μ with increasing normal load at 2000 r.p.m. and 70°F, is apparent at the high temperature tests shown in Figure 54. This trend, however, is reversed at 3000 r.p.m. and 150°F, as shown in Figure 55.

In general, by examining the data of Figures 52 through 55, it can be concluded that the friction coefficient of the steel on Oilite damper material combination is relatively independent of gyro r.p.m. and temperature. On the other hand, the friction coefficient is significantly affected by normal load.

5. Nylon on Oilite

The friction coefficients for the nylon on Oilite material combination are given in Figures 56 through 61 as a function of normal load, β', gyro r.p.m., and temperature.

Figures 56 and 57 represent the 70°F test condition at 2000 r.p.m. and 3000 r.p.m., respectively. It should be noted that the friction coefficient μ is not significantly affected by variation in β' nor operating time, particularly at the higher normal load and for higher r.p.m. test conditions.

Test results at the 150°F condition are given in Figures 58 and 59 for 2000 and 3000 r.p.m., respectively. The data indicate a reduction of μ as compared to the 70°F tests. This is mainly attributed to increased lubrication characteristics of Oilite at high temperature.

For the low temperature tests, -65°F, the friction coefficients shown in Figures 59 and 60 are not as consistent as those at the higher temperatures. A comparison of these figures shows a lower friction coefficient at the higher r.p.m. for a given normal load. This is attributed to local heating of the contact area of the damper materials, thereby allowing lubricant to flow from the Oilite in spite of the low ambient temperature.

A comparison of the test data presented in Figures 56 through 61 indicates a general trend of decreasing friction coefficient with increasing temperature and r.p.m. at a constant normal load. Furthermore, the friction coefficient also reduces with increase of normal load at constant temperature and r.p.m.

SUMMARY

Test No.	Material		Simulated Gyro r.p.m.	β' deg.	N gms.	Running Hours	Total Travel, in.	Track Wear	
	Track	Damper Rod						mg.	$cm.^3 x10^3$
1	Teflon	Steel	2000	± 3.8	440	10.3	$490x10^3$	3.7	1.735
2	Teflon	Steel	2000	± 3.8	2865	16.3	$775x10^3$	12.4	5.81
3	Oilite	Steel	2000	± 3.8-± 15	875	21.8	$1510x10^3$	2.0	0.31
4	Oilite	Steel	2000	± 3.8-± 15	1885	22.0	$1520x10^3$	8.0	1.2
5	Oilite	Steel	2000	± 3.8-± 15	2865	21.3	$1266x10^3$	26.7	4.11
6	Oilite	Steel	2000	± 15	1885	2.20	$420x10^3$	6.0	0.92
6A	Oilite	Steel	2000	± 3.8	2865	2.5	$120x10^3$	5.0	0.77
7	S. Steel	Brass	2000	± 3.8	875	5.25	$250x10^3$	35.0*	4.08
8	S. Steel	Steel	2000	± 3.8	875	17.67	$840x10^3$	3.3	0.43
9	Oilite	Nylon	2000	± 3.8-± 15	2865	22.9	$1580x10^3$	1.7	0.26
10	S. Steel	Nylon	2000	± 15	2865	0.17	-	(Gage failure - te	
11	KEL-F	Nylon	2000	± 15	2865	0.03	-	(Extremely high we	
12	KEL-F	Steel	2000	± 15	2865	0.03	-	(Extremely high we	
13	S. Steel	Nylon	2000	± 3.8	875	16.0	$870x10^3$	0.8*	0.69
14	Oilite	Aluminum	2000	± 3.8-± 7.6	875	24.4	$1540x10^3$	6.3	0.97
15	Oilite	Nylon	2000	± 3.82-± 15	1885	21.7	$1490x10^3$	4.7	0.723
16	Oilite	Nylon	2000	± 3.8-± 15	875	21.86	$1497x10^3$	1.0	0.154
17	Oilite	Nylon	3000	± 3.8-± 15	875	21.73	$2215x10^3$	0.5	0.0769
18	Oilite	Nylon	3000	± 3.8-± 15	1885	22.17	$2270x10^3$	1.30	2.0

* Denoces increase in weight due to material transfer

A

TABLE XII

MARY - DAMPER MATERIAL TESTS

r	Rod Wear		Wear Rate x 10^9 $cm.^3/in.travel$		Friction Coefficient			Comments
0^3	mg.	$cm.^3 x 10^3$	Track	Rod	μ_{MAX}	μ_{MIN}	$\bar{\mu}$	
5	0	-	3.52	0	0.260	0.216	0.245	Consistent μ excessive wear, flaking.
	0	-	7.50	0	0.192	0.163	0.178	
	0	-	0.20	0	0.331	0.187	0.26	Variation in start-up friction coefficient.
	0	-	0.811	0	0.196	0.143	-	Force inst. failure, no $\bar{\mu}$ available.
	0	-	3.25	0	-	-	-	No friction coefficient data.
	0	-	2.2	0	0.197	0.144	0.175	Friction force inst. repaired.
	0	-	6.4	0	0.210	0.157	0.020	Variation of friction force coefficient.
	61.6	7.2	N/A	28.8	0.535	0.40	0.46	Large material transfer, variation of μ with β'.
	30.7	4.1	0.51	4.86	0.54	0.48	0.52	Rapid oxidation and flaking.
	0.4	0.34	0.166	0.218	0.19	0.13	0.15	Increased rod thickness from 0.062 to 0.125 for nylon rods.
- test discontinued)								
gh wear - test discontinued)								
gh wear - test discontinued)								Force instrument failure.
	18.8	16.2	N/A	18.6	0.26	0.156	0.22	Material transfer, variation of μ with β'
	0	-	0.63	0	0.43	0.19	0.34	
3	2.5	2.15	0.485	1.44	0.22	0.07	0.18	Contact surface reduced due to misalignment.
4	0	-	0.103	-	0.24	0.11	0.18	
69	0	-	0.035	-	0.27	0.16	0.23	
	0.7	0.602	0.088	0.265	0.18	0.14	0.16	

B

TABI

Test No.	Material		Simulated Gyro r.p.m.	β' deg.	N gms.	Running Hours	Total Travel, in.	Track Wear	
	Track	Damper Rod						mg.	$cm.^3 \times 10^3$
19	Oilite	Nylon	3000	± 3.8-± 15	2865	21.58	2200×10^3	2.4	0.369
20	Oilite	1/8" Al.	2000	± 3.8-± 15	875	23.75	1511×10^3	5.7	0.88
21	Oilite	Steel	3000	± 3.8-± 15	875	13.92	1581×10^3	1.6	0.246
22	Oilite	Steel	3000	± 3.8-± 15	1885	14.92	1544.5×10^3	12.9	1.98
23	Oilite	Steel	3000	± 3.8	2865	10.5	750×10^3	45.3	6.98
24	S. Steel	Bakelite	2000	± 15	1885	Bakelite Melted		Running time less	
25	Oilite	Nylon	2000	± 3.8-± 15	1885	15.16	1027×10^3	0.1	0.0154
26	Oilite	Nylon	2000	± 3.8-± 15	2865	15.33	1080×10^3	1.7	0.268
27	Oilite	Steel	2000	± 3.8-± 15	1885	15.1	1015×10^3	7.9	1.215
28	Oilite	Steel	2000	± 3.8-± 15	2865	14.83	1002×10^3	20.0	3.08
29	Oilite	Nylon	3000	± 3.8-± 15	1885	11.5	1257×10^3	0.6	0.0922
30	Oilite	Nylon	3000	± 3.8-± 15	2865	11.16	1150×10^3	1.02	1.57
31	Oilite	Steel	3000	± 3.8-± 15	2865	11.41	1168×10^3	19.2	2.95
32	Oilite	Steel	3000	± 3.8-± 15	1885	12.35	1213×10^3	1.2	0.1846
33	Oilite	Nylon	3000	± 3.8-± 15	1885	11.33	1175×10^3	0.5	0.0769
34	Oilite	Nylon	2000	± 3.8-± 15	1885	16.83	1127×10^3	2.7	0.415
35	Oilite	Nylon	3000	± 3.8-± 15	2865	15.25	988×10^3	4.8	2.59
36	Oilite	Nylon	2000	± 3.8-± 15	2865	11.25	1189×10^3	2.4	0.369
37	Oilite	Nylon	2000	± 3.32	2865	7.92	358×10^3	1.0	0.154

ABLE XII (Continued)

Rod Wear		Wear Rate x 10^9 $cm.^3$/in. travel		Friction Coefficient			Comments
mg.	$cm.^3 \times 10^3$	Track	Rod	μ_{MAX}	μ_{MIN}	$\bar{\mu}$	
0.7	0.602	0.168	0.278	0.17	0.12	0.14	
1.1	0.397	0.582	0.249	0.62	0.20	0.45	
0.7	0.093	0.156	0.059	0.496	0.156	0.30	
1.3	0.173	1.28	0.112	0.276	0.185	0.23	
1.6	0.213	10.7	0.284	0.58	0.144	0.20	Materials siezed, test was terminated.
s chan 20 minutes							Gage failure - bakelite melted.
1.4	1.19	0.016	1.16	0.13	0.10	0.11	150°F Temperature tests.
1.5	1.29	0.242	1.19	0.13	0.08	0.09	150°F
0.8	0.1057	1.2	0.104	0.26	0.11	0.22	150°F
3.2	0.427	3.08	0.427	0.26	0.11	0.19	150°F
2.8	1.21	0.0734	1.926	0.22	0.11	0.17	150°F
2.3	2.67	1.365	2.32	0.14	0.08	0.10	150°F
2.2	0.294	2.52	0.252	0.28	0.12	0.24	150°F
1.1	0.940	0.152	0.782	0.37	0.14	0.20	150°F
0.6	0.517	0.065	0.44	0.21	0.12	0.17	-65°F Temperature tests.
27.4	23.6	0.327	18.6	0.47	0.18	0.30	-65°F
0.4	0.346	0.747	0.350	0.25	0.17	0.19	-65°F
1.2	1.035	0.31	0.871	0.20	0.10	0.14	-65°F
0	0	0.43	0	0.16	0.11	0.15	0°F Temperature tests.

B

BLANK PAGE

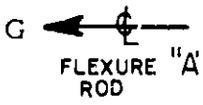

NOTE: All forces and angles as shown are positive.

$\mu_\beta \tan \beta'$

$F \tan \beta'$

Loads acting at Point "B"

FIGURE 46. Damper Test Fixture Force Notation.

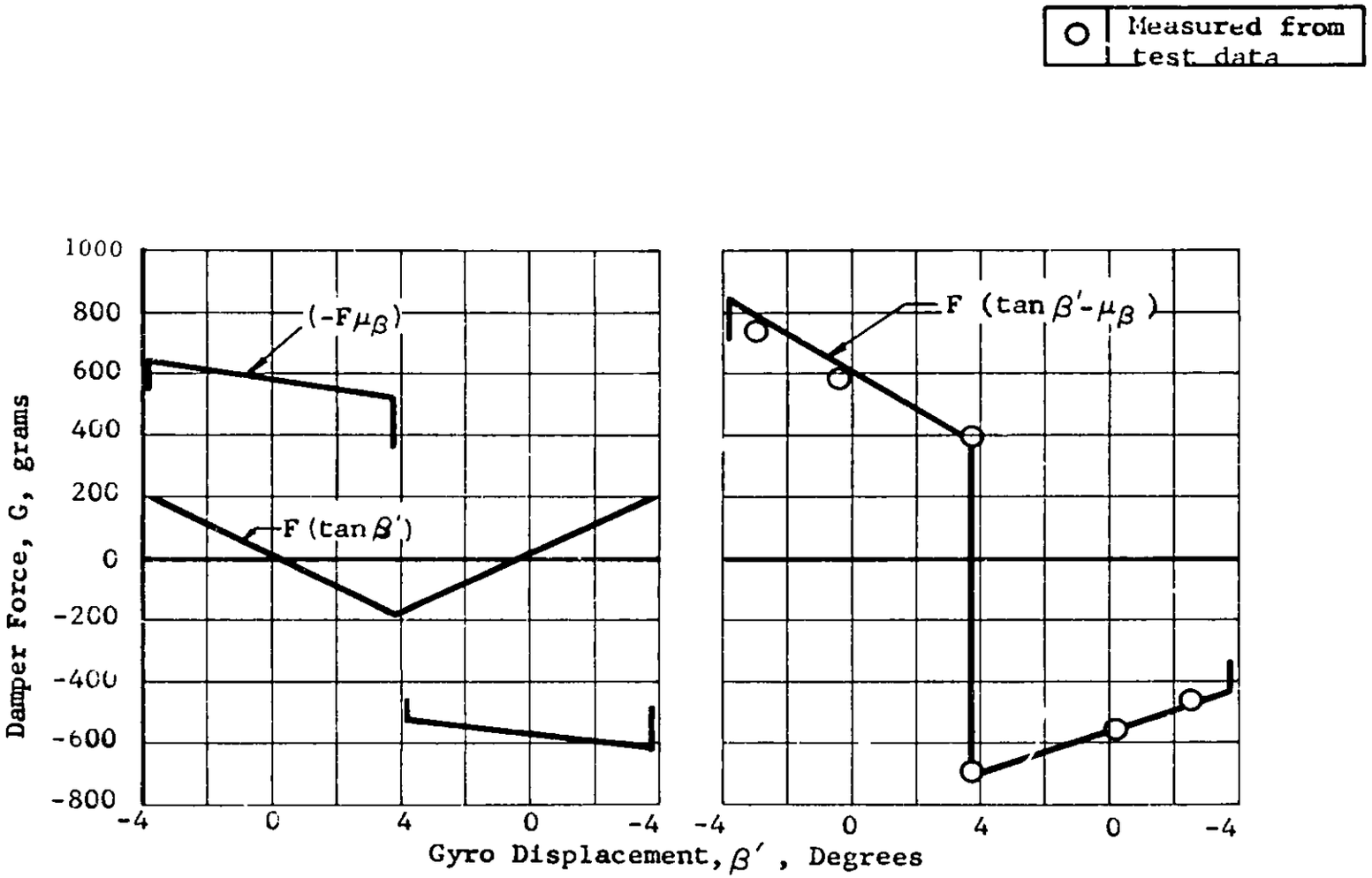

FIGURE 47. Flexure Force Variation with Simulated Gyro Displacement, β'.

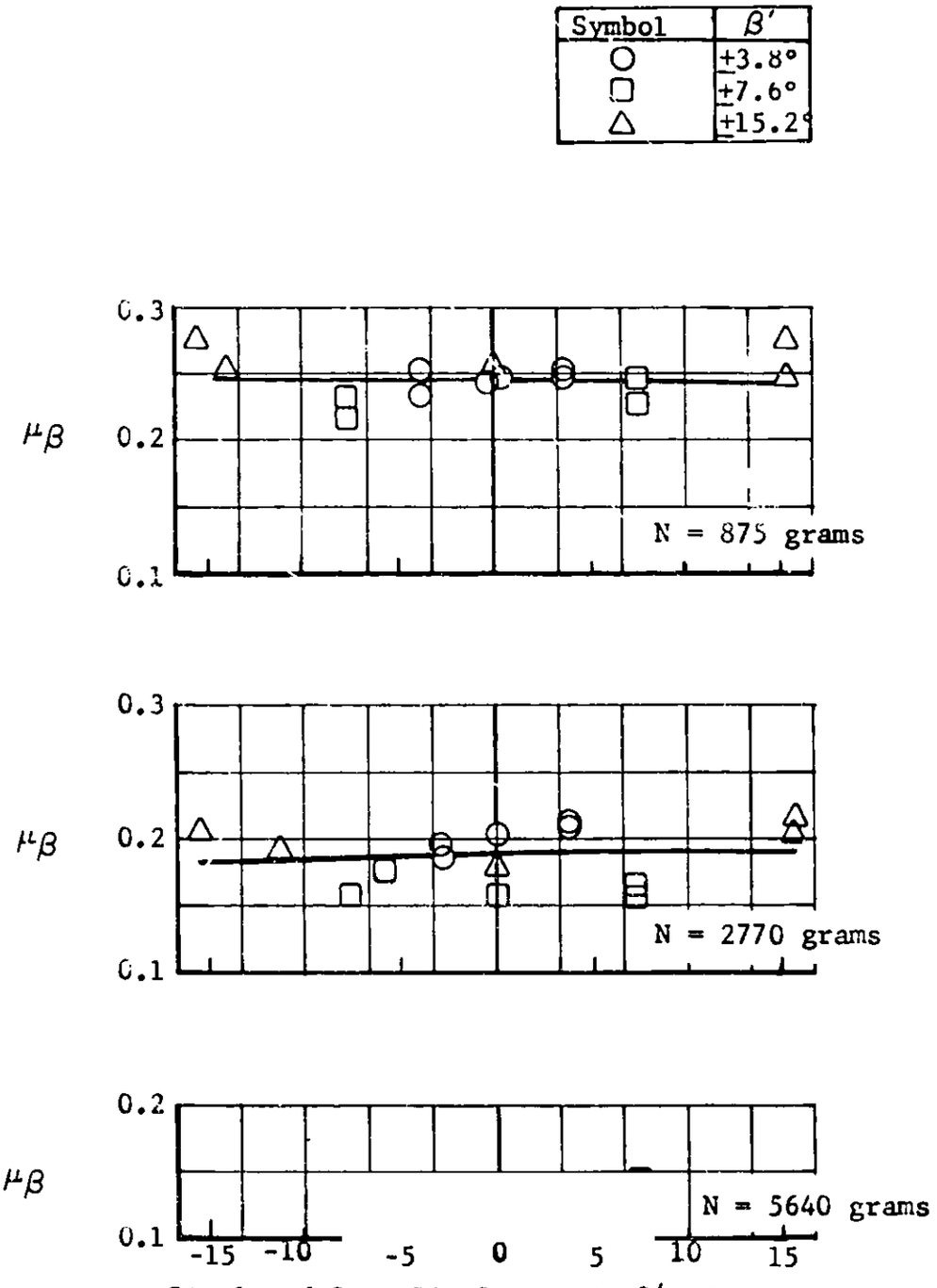

FIGURE 48. Variation of μ_β with Gyro Displacement, β', Damper Material: Steel Rod on Oilite Track, 2000 r.p.m.

Symbol	β'
O	$\pm 3.8°$

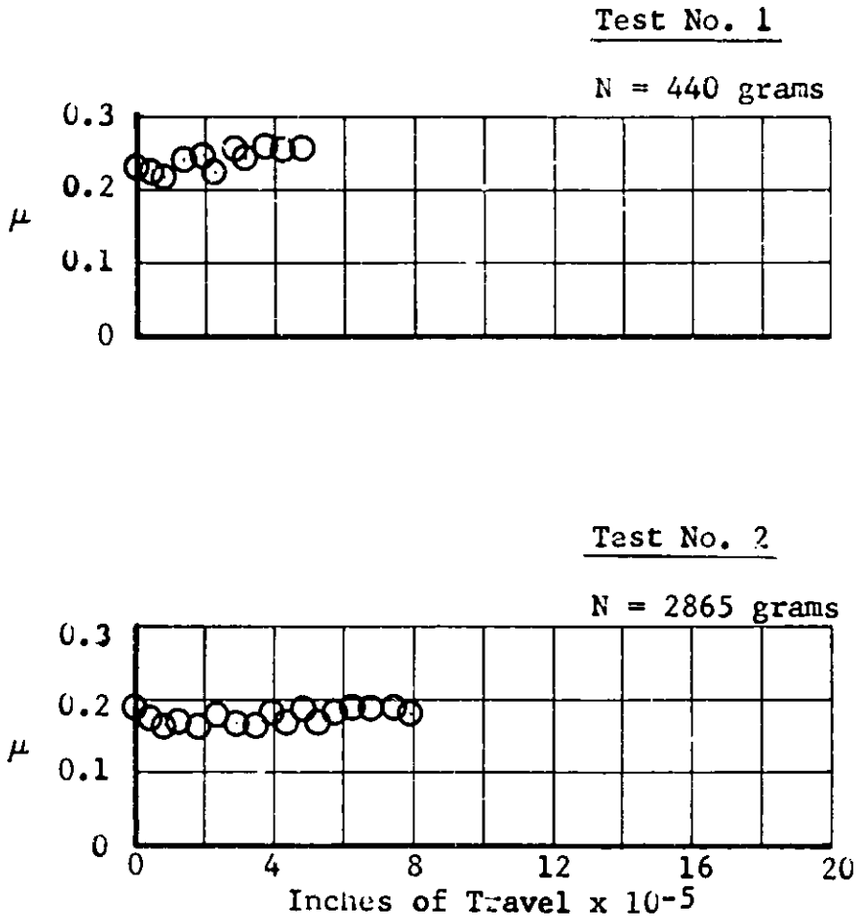

FICURE 49. Friction Coefficient Variation with Cumulative Inches of Travel for Steel Rod on Teflon Track at 2000 r.p.m., 70°F.

Symbol	β'
O	$\pm 3.8°$

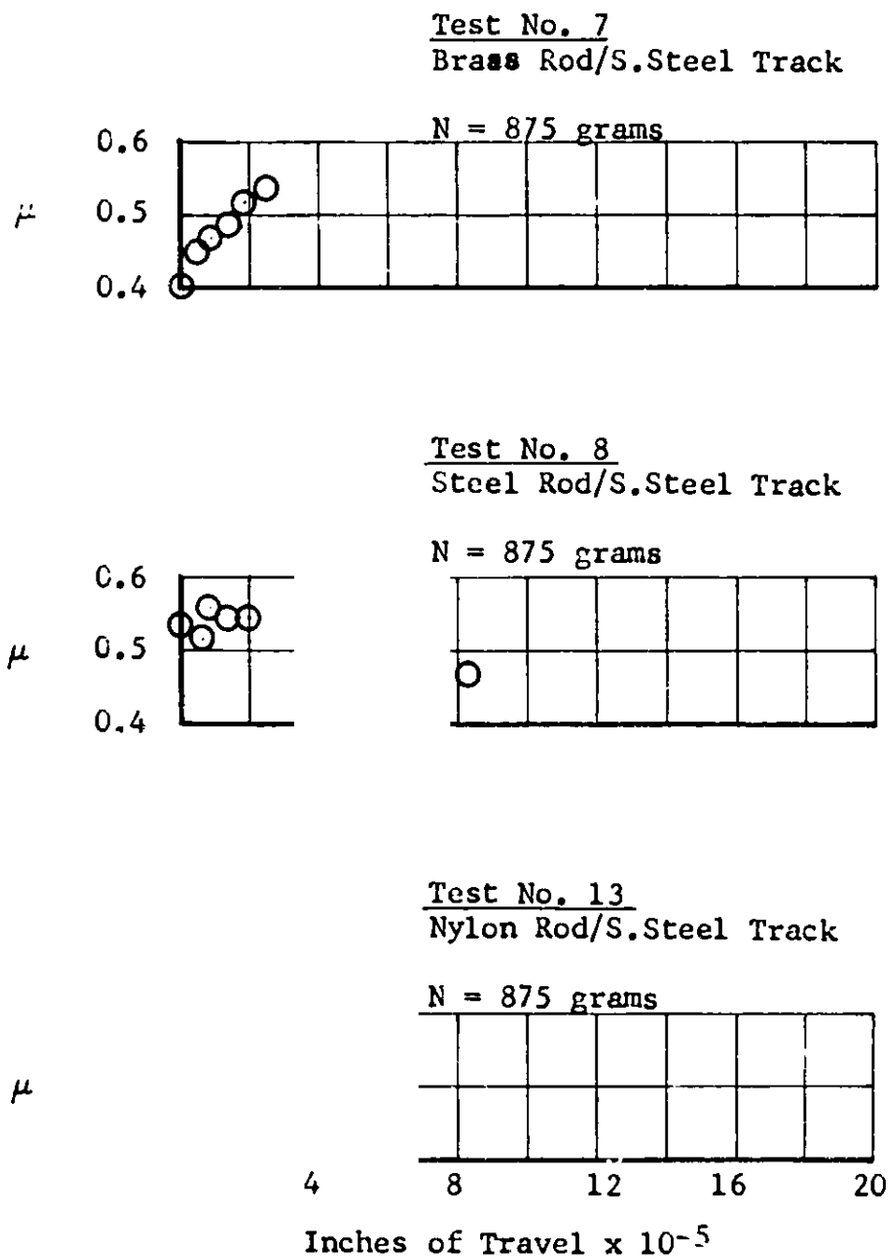

FIGURE 50. Friction Coefficient Variation with Cumulative Inches of Travel for Brass, Steel, and Nylon Rods on Stainless Steel Track at 2000 r.p.m., 70°F.

Symbol	β'
○	±3.8°
□	±7.6°

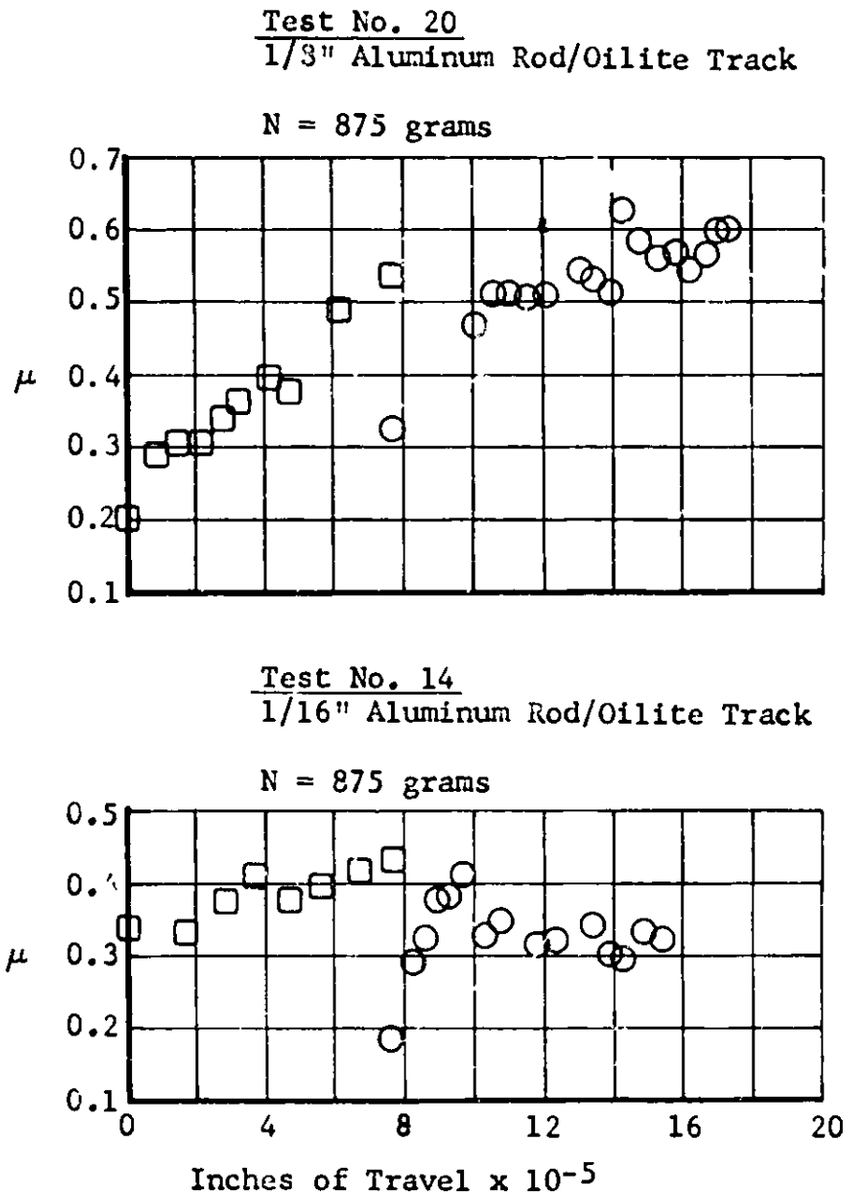

FIGURE 51. Effect of Contact Pressure on Friction Coefficient Time History for Aluminum Rod on Oilite Track at 2000 r.p.m., 70°F.

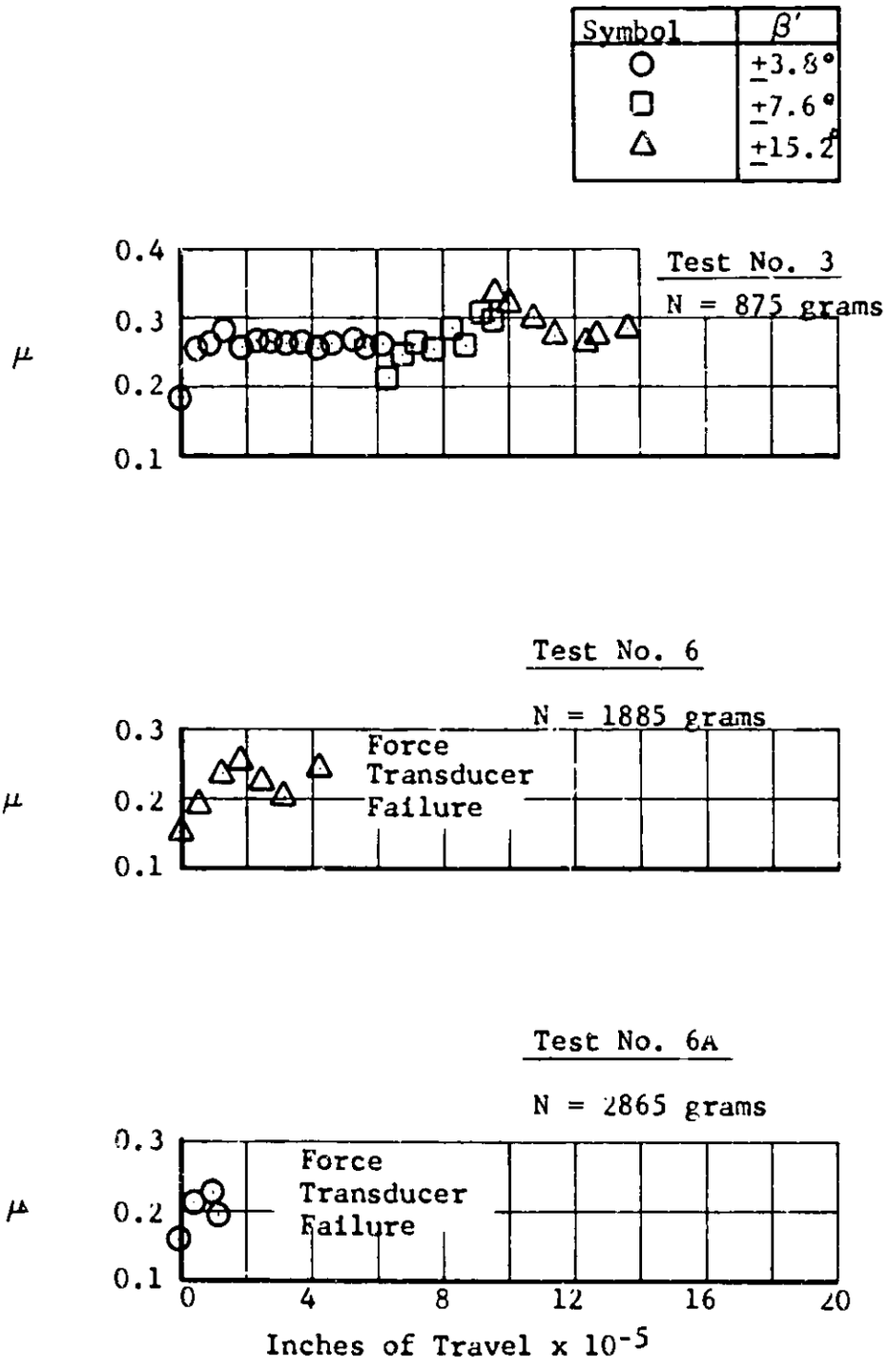

FIGURE 52. Effect of Normal Load on Friction Coefficient Time History of Steel Rod on Oilite Track at 2000 r.p.m., 70°F.

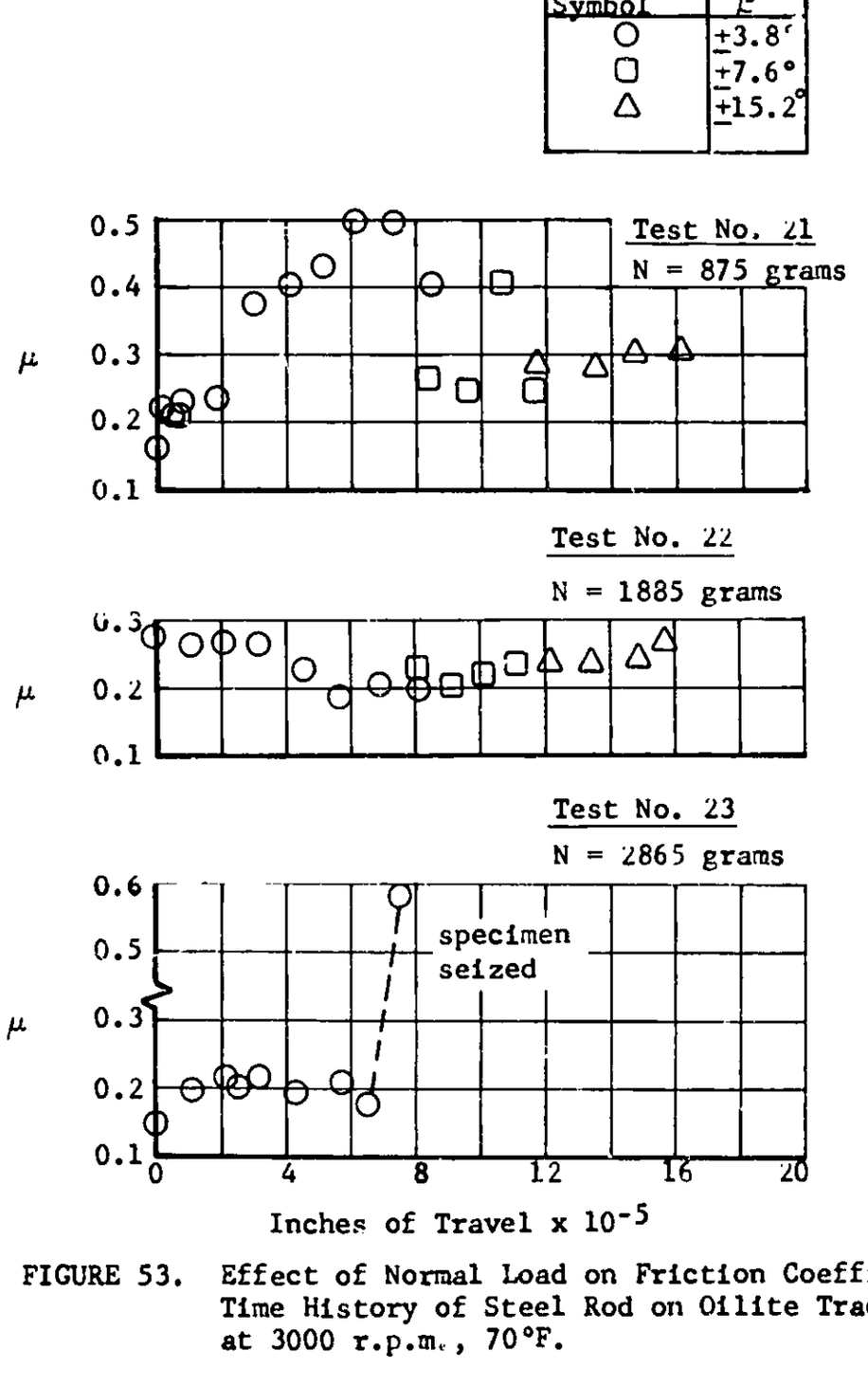

FIGURE 53. Effect of Normal Load on Friction Coefficient Time History of Steel Rod on Oilite Track at 3000 r.p.m., 70°F.

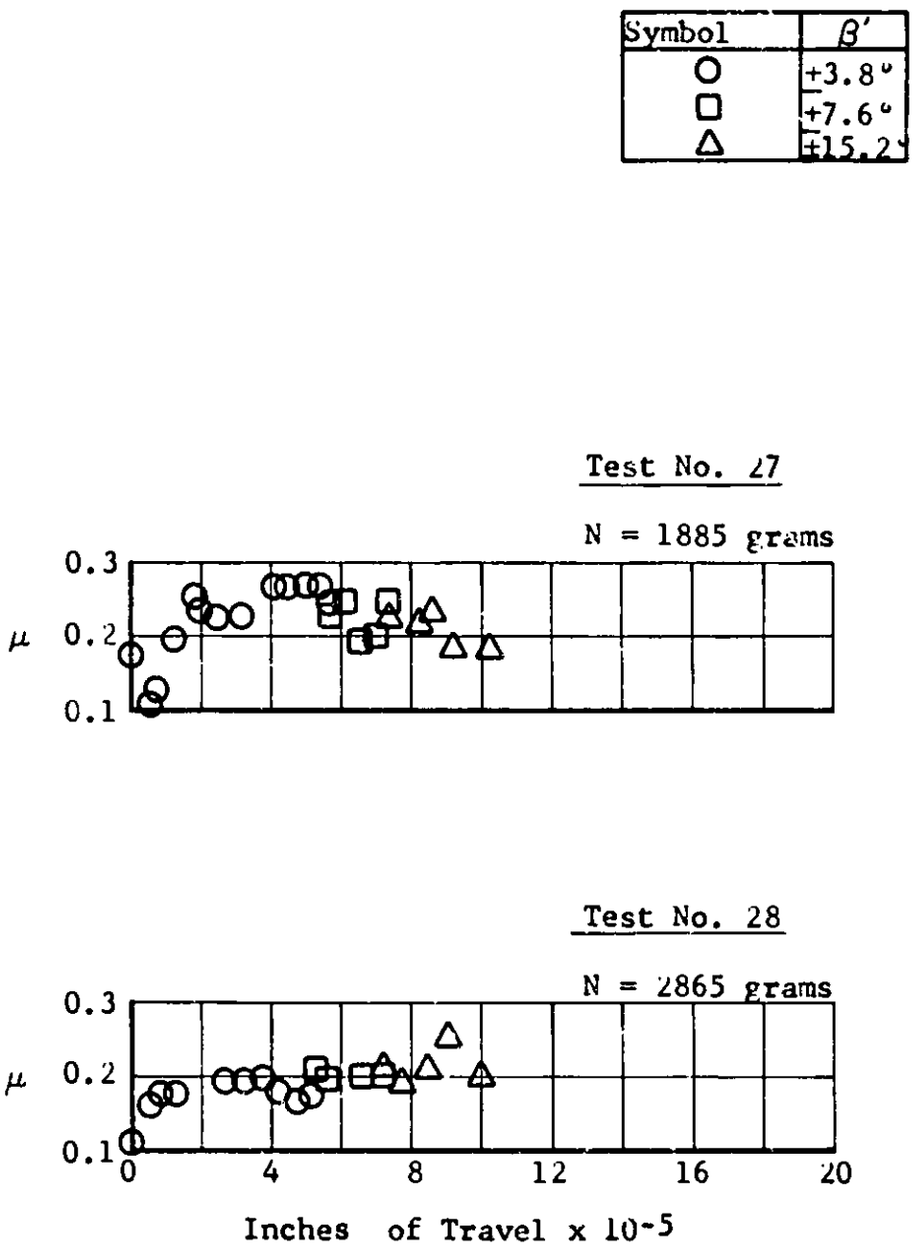

FIGURE 54. Effect of Normal Load on Friction Coefficient Time History of Steel Rod on Oilite Track at 2000 r.p.m., 150°F.

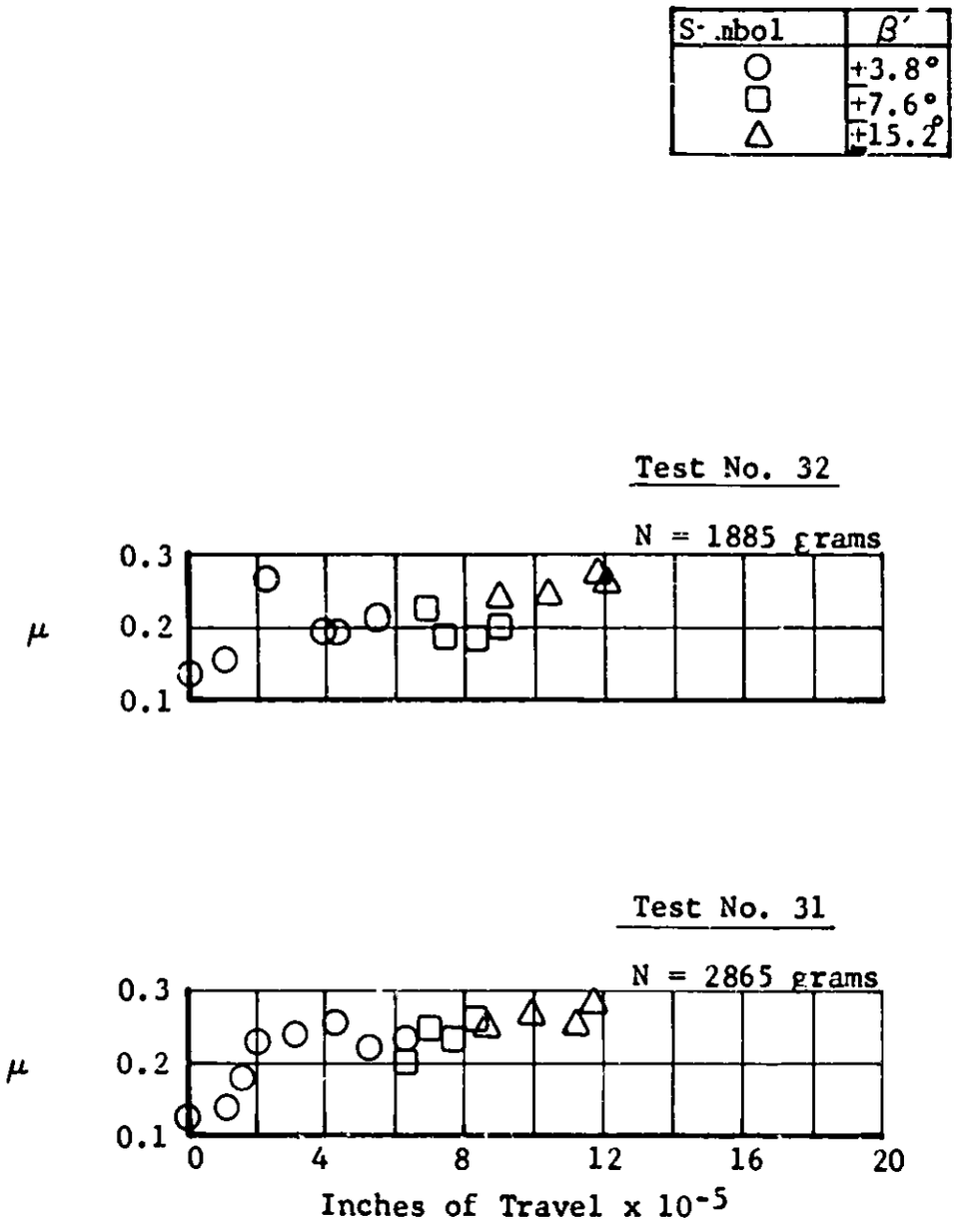

FIGURE 55. Effect of Normal Load on Friction Coefficient Time History of Steel Rod on Oilite Track at 3000 r.p.m., 150°F.

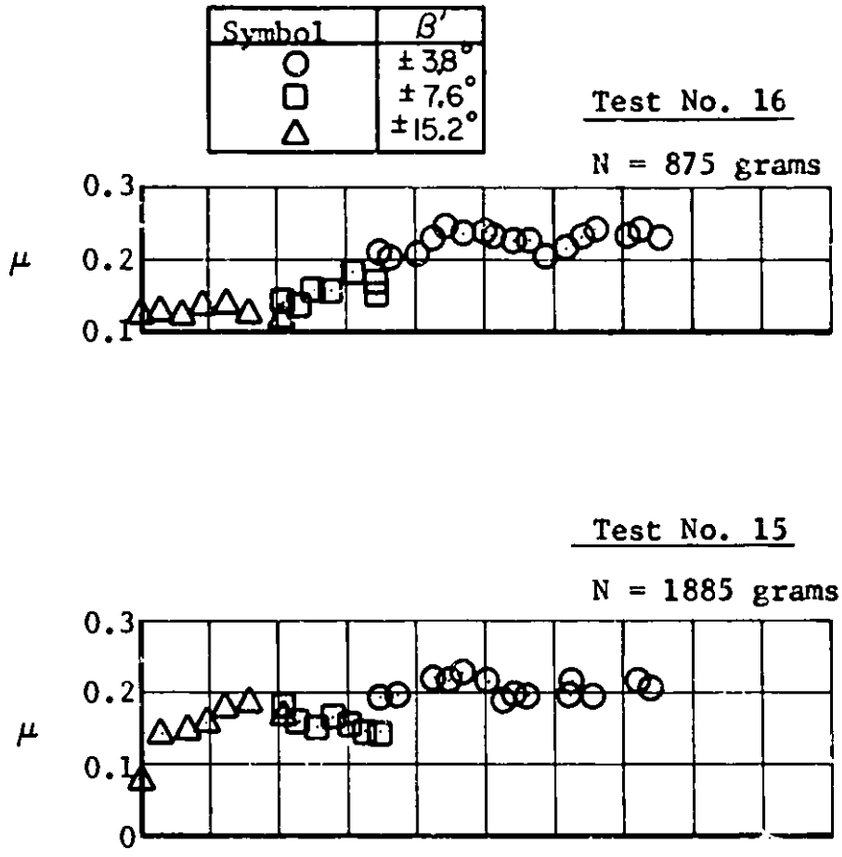

FIGURE 56. Effect of Normal Load on Friction Coefficient Time History of Nylon Rod on Oilite Track at 2000 r.p.m., 70°F.

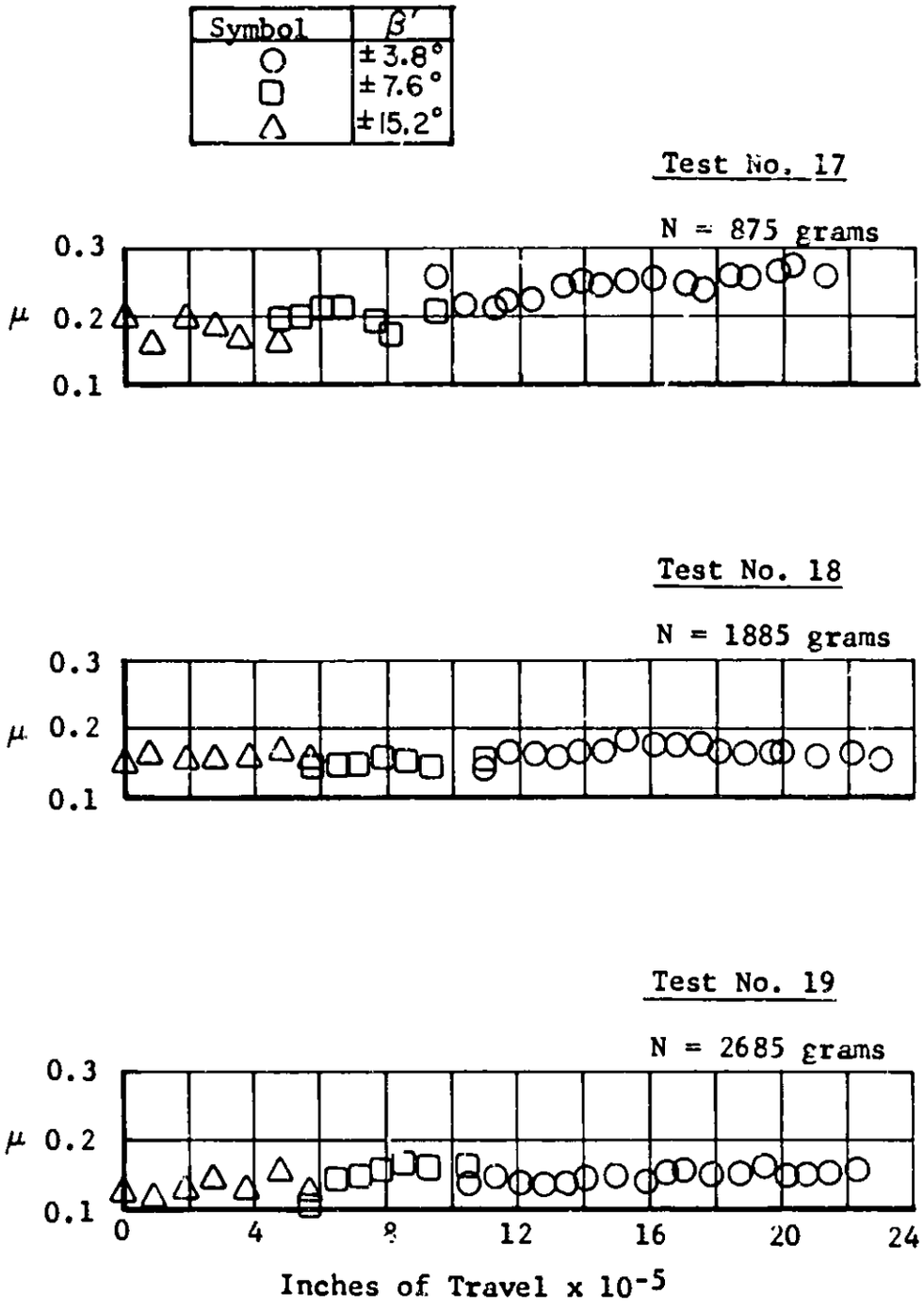

FIGURE 57. Effect of Normal Load on Friction Coefficient Time History of Nylon Rod on Oilite Track at 3000 r.p.m., 70°F.

Symbol	β'
○	±3.8°
□	±7.6°
△	±15.2°

Test No. 25

N = 1885 grams

Test No. 26

N = 2865 grams

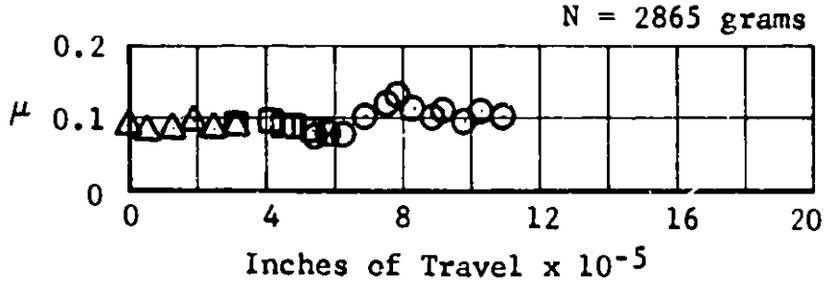

FIGURE 58. Effect of Normal Load on Friction Coefficient Time History of Nylon Rod on Oilite Track at 2000 r.p.m., 150°F.

Symbol	β'
○	±3.8°
□	±7.6°
△	±15.2°

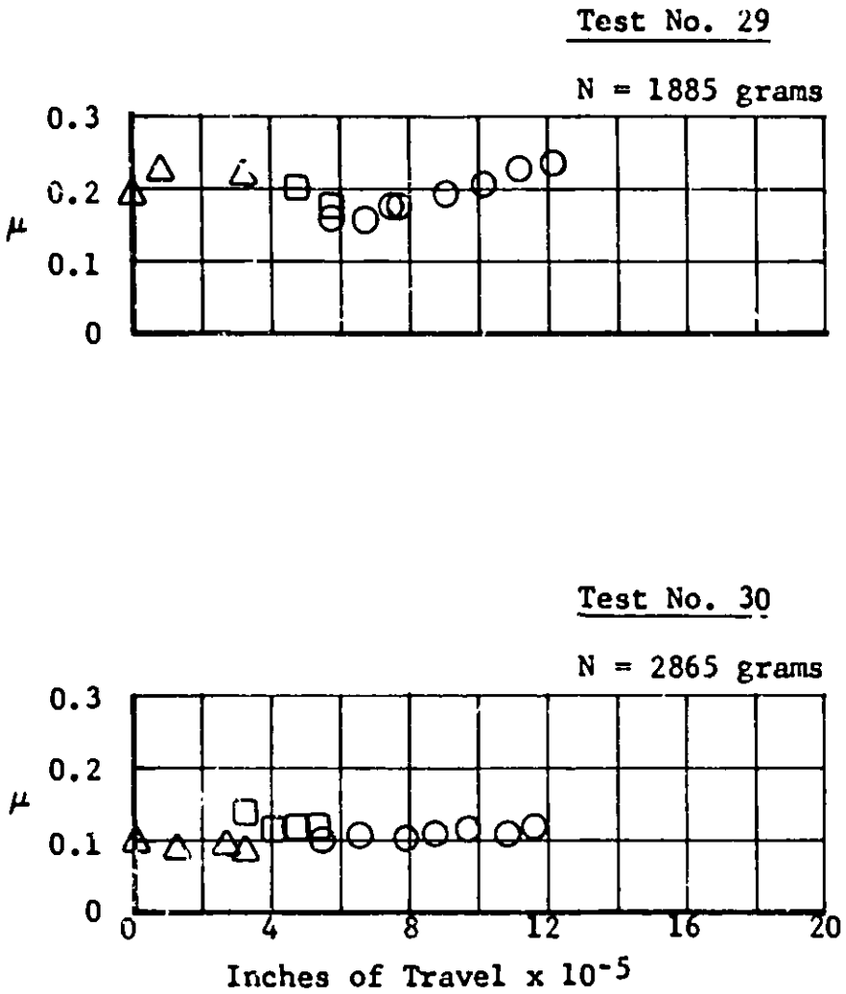

FIGURE 59. Effect of Normal Load on Friction Coefficient Time History of Nylon Rod on Oilite Track at 3000 r.p.m., 150°F.

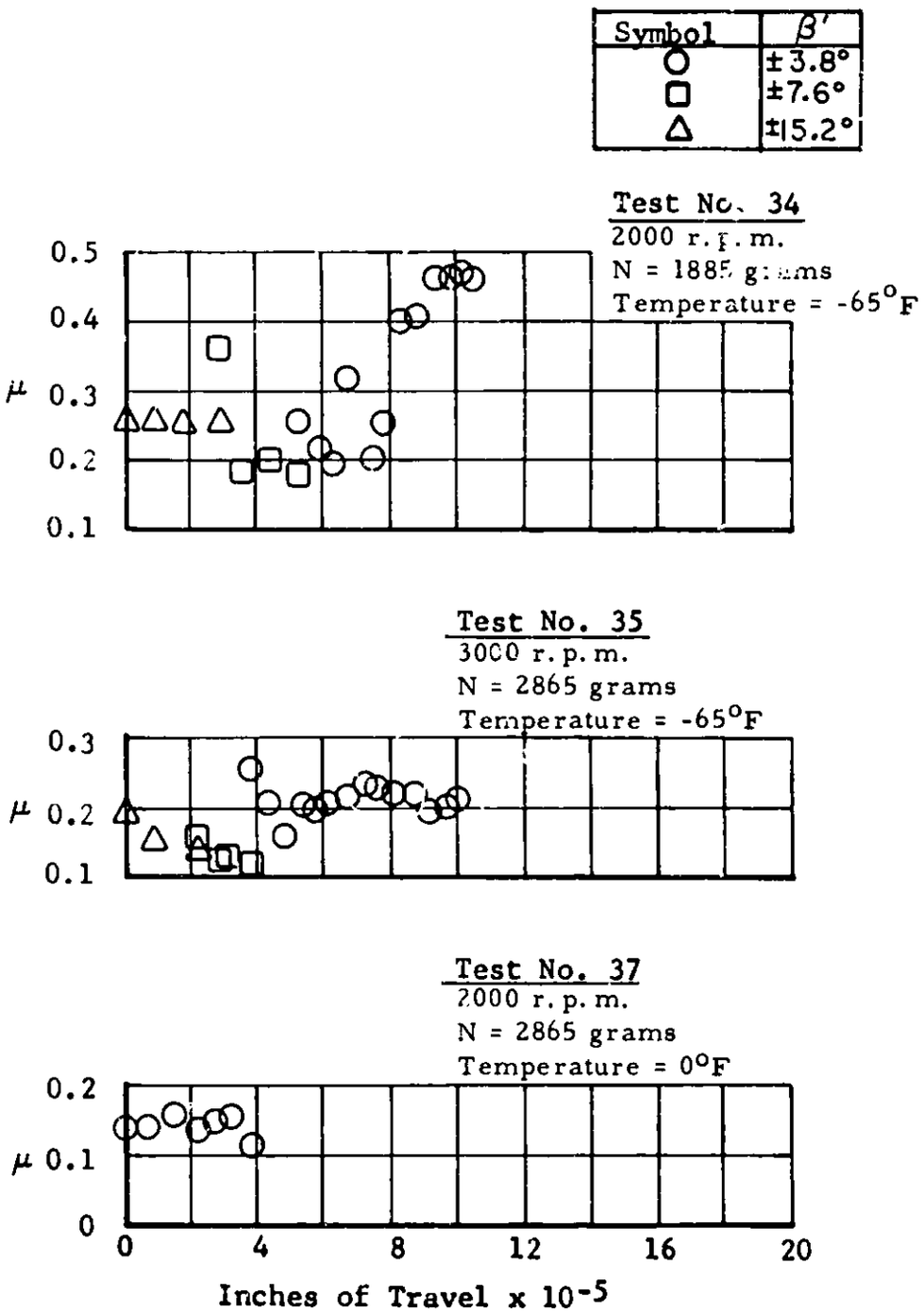

FIGURE 60. Effect of Normal Load on Friction Coefficient Time History of Nylon Rod on Oilite Track.

Symbol	β'
○	±3.2°
□	±7.6°
△	±15.2°

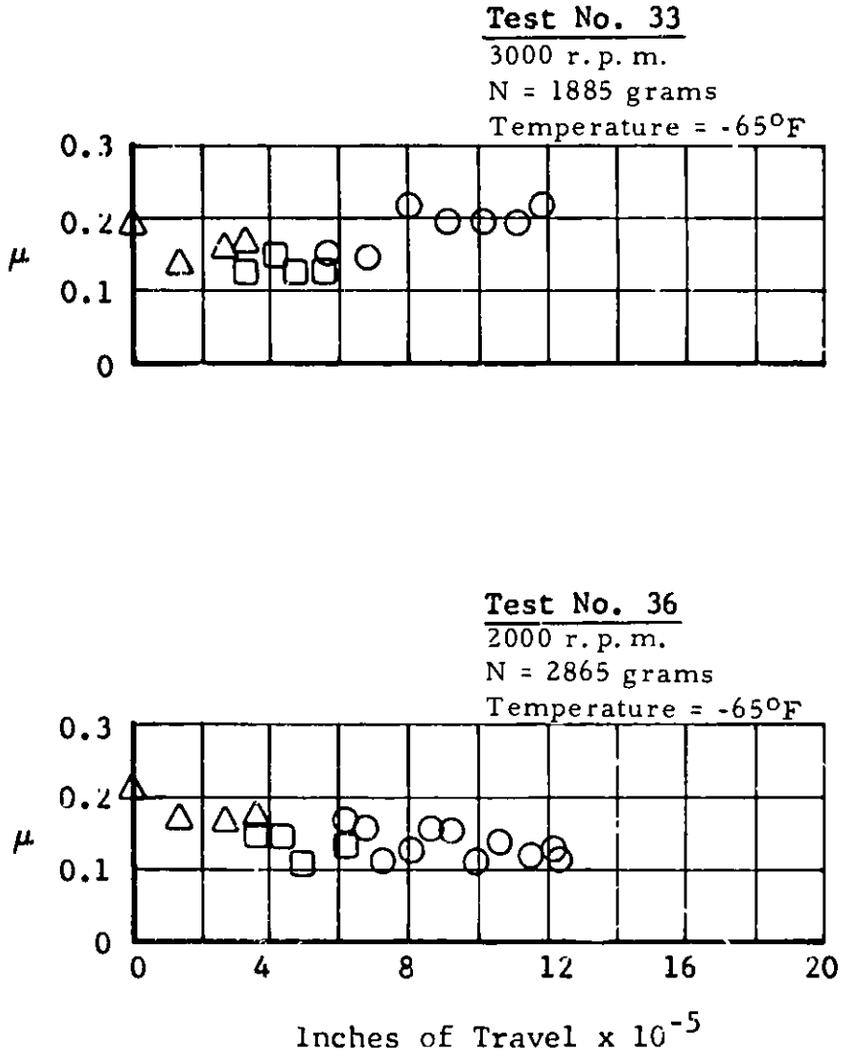

FIGURE 61. Effect of Normal Load on Friction Coefficient Time History of Nylon Rod on Oilite Track.

Unclassified

Security Classification

DOCUMENT CONTROL DATA - R&D

(Security classification of title, body of abstract and indexing annotation must be entered when the overall report is classified)

1. ORIGINATING ACTIVITY (Corporate author)
Dynasciences Corporation
Blue Bell, Pennsylvania

2a. REPORT SECURITY CLASSIFICATION
Unclassified

2b GROUP

3. REPORT TITLE
DYNAGYRO - A Mechanical Stability Augmentation System for Helicopters

4. DESCRIPTIVE NOTES (Type of report and inclusive dates)
Final Report

5. AUTHOR(S) (Last name, first name, initial)
George, M.
Kisielowski, E.
Perlmutter, A. A.

6. REPORT DATE	7a. TOTAL NO. OF PAGES	7b. NO. OF REFS
March 1967	137	8

8a. CONTRACT OR GRANT NO.	9a. ORIGINATOR'S REPORT NUMBER(S)
DA 44-177-AMC-286(T)	USAAVLABS Technical Report 67-10
b. PROJECT NO. Task 1P125901A13905	
c.	9b. OTHER REPORT NO(S) (Any other numbers that may be assigned this report)
d.	Dynasciences Report No. DCR-221

10. AVAILABILITY/LIMITATION NOTICES
Distribution of this document is unlimited.

11. SUPPLEMENTARY NOTES	12. SPONSORING MILITARY ACTIVITY
	U.S. Army Aviation Materiel Laboratories, Fort Eustis, Virginia

13. ABSTRACT

This report presents the results of an investigation of the design and performance characteristics of a compact and lightweight stability augmentation system for helicopters. This system, known as the DYNAGYRO, consists of a two-degree-of-freedom coulomb damped gyroscope which is mounted within the helicopter fuselage. The investigation includes an analog computer study, a comprehensive component test program, and a bench test performance evaluation of a laboratory test model.

The results obtained from this investigation showed that the DYNAGYRO provides stability augmentation characteristics which compare favorably with those of the much larger and heavier rotor hub-mounted devices.

DD FORM 1 JAN 64 1473

Unclassified

Security Classification

Unclassified

Security Classification

14. KEY WORDS	LINK A		LINK B		LINK C	
	ROLE	WT	ROLE	WT	ROLE	WT
Stability						
Control						
Gyroscope						
Mechanical						
DYNAGYRO						

INSTRUCTIONS

1. ORIGINATING ACTIVITY: Enter the name and address of the contractor, subcontractor, grantee, Department of Defense activity or other organization *(corporate author)* issuing the report.

2a. REPORT SECURITY CLASSIFICATION: Enter the overall security classification of the report. Indicate whether "Restricted Data" is included. Marking is to be in accordance with appropriate security regulations.

2b. GROUP: Automatic downgrading is specified in DoD Directive 5200.10 and Armed Forces Industrial Manual. Enter the group number. Also, when applicable, show that optional markings have been used for Group 3 and Group 4 as authorized.

3. REPORT TITLE: Enter the complete report title in all capital letters. Titles in all cases should be unclassified. If a meaningful title cannot be selected without classification, show title classification in all capitals in parenthesis immediately following the title.

4. DESCRIPTIVE NOTES: If appropriate, enter the type of report, e.g., interim, progress, summary, annual, or final. Give the inclusive dates when a specific reporting period is covered.

5. AUTHOR(S): Enter the name(s) of author(s) as shown on or in the report. Enter last name, first name, middle initial. If military, show rank and branch of service. The name of the principal author is an absolute minimum requirement.

6. REPORT DATE: Enter the date of the report as day, month, year, or month, year. If more than one date appears on the report, use date of publication.

7a. TOTAL NUMBER OF PAGES: The total page count should follow normal pagination procedures, i.e., enter the number of pages containing information.

7b. NUMBER OF REFERENCES: Enter the total number of references cited in the report.

8a. CONTRACT OR GRANT NUMBER: If appropriate, enter the applicable number of the contract or grant under which the report was written.

8b, 8c, & 8d. PROJECT NUMBER: Enter the appropriate military department identification, such as project number, subproject number, system numbers, task number, etc.

9a. ORIGINATOR'S REPORT NUMBER(S): Enter the official report number by which the document will be identified and controlled by the originating activity. This number must be unique to this report.

9b. OTHER REPORT NUMBER(S): If the report has been assigned any other report numbers *(either by the originator or by the sponsor)*, also enter this number(s).

10. AVAILABILITY/LIMITATION NOTICES: Enter any limitations on further dissemination of the report, other than those imposed by security classification, using standard statements such as:

(1) "Qualified requesters may obtain copies of this report from DDC."

(2) "Foreign announcement and dissemination of this report by DDC is not authorized."

(3) "U. S. Government agencies may obtain copies of this report directly from DDC. Other qualified DDC users shall request through

_____."

(4) "U. S. military agencies may obtain copies of this report directly from DDC. Other qualified users shall request through

_____."

(5) "All distribution of this report is controlled. Qualified DDC users shall request through

_____."

If the report has been furnished to the Office of Technical Services, Department of Commerce, for sale to the public, indicate this fact and enter the price, if known.

11. SUPPLEMENTARY NOTES: Use for additional explanatory notes.

12. SPONSORING MILITARY ACTIVITY: Enter the name of the departmental project office or laboratory sponsoring *(paying for)* the research and development. Include address.

13. ABSTRACT: Enter an abstract giving a brief and factual summary of the document indicative of the report, even though it may also appear elsewhere in the body of the technical report. If additional space is required, a continuation sheet shall be attached.

It is highly desirable that the abstract of classified reports be unclassified. Each paragraph of the abstract shall end with an indication of the military security classification of the information in the paragraph, represented as *(TS)*, *(S)*, *(C)*, or *(U)*.

There is no limitation on the length of the abstract. However, the suggested length is from 150 to 225 words.

14. KEY WORDS: Key words are technically meaningful terms or short phrases that characterize a report and may be used as index entries for cataloging the report. Key words must be selected so that no security classification is required. Identifiers, such as equipment model designation, trade name, military project code name, geographic location, may be used as key words but will be followed by an indication of technical context. The assignment of links, rules, and weights is optional.

Unclassified

Security Classification